Universidade de São Paulo
Faculdade de Filosofia, Ciências e Letras de Ribeirão Preto
Departamento de Química
Programa de Pós-Graduação em Química

"Estudos sobre o papel das vesículas da matriz na mineralização óssea: observações de micro à nanoescala"

"Studies on the role of matrix vesicles in bone mineralization: observations from micro to nanoscale"

Marcos Antonio Eufrásio Cruz

Tese apresentada à Faculdade de Filosofia, Ciências e Letras de Ribeirão Preto da Universidade de São Paulo, como parte das exigências para a obtenção do título de Doutor em Ciências, Área: **Química**

RIBEIRÃO PRETO -SP

2023

Universidade de São Paulo
Faculdade de Filosofia, Ciências e Letras de Ribeirão Preto
Departamento de Química
Programa de Pós-Graduação em Química

"Estudos sobre o papel das vesículas da matriz na mineralização óssea: observações de micro à nanoescala"

"Studies on the role of matrix vesicles in bone mineralization: observations from micro to nanoscale"

Marcos Antonio Eufrásio Cruz

Orientadora: Profa Dra Ana Paula Ramos

Co-orientador: Prof Dr Pietro Ciancaglini

Tese apresentada à Faculdade de Filosofia, Ciências e Letras de Ribeirão Preto da Universidade de São Paulo, como parte das exigências para a obtenção do título de Doutor em Ciências, Área: **Química**

RIBEIRÃO PRETO -SP

2023

FICHA CATALOGRÁFICA

Cruz, Marcos Antonio Eufrasio

Estudos sobre o papel das vesículas da matriz na mineralização óssea: observações em múltiplas escalas. Ribeirão Preto, 2023.

161 p. : il. ; 30cm

Tese de Doutorado, apresentada à Faculdade de Filosofia, Ciências e Letras de Ribeirão Preto da Universidade de São Paulo – Área de concentração: Química.

Orientadora: Ramos, Ana Paula.

1. Osso. 2. Biomineralização. 3. Vesículas da Matriz.

"Quando os ventos de mudança
sopram, umas pessoas levantam barreiras, outras
constroem moinhos de vento."

- Erico Verissimo

Aos meus pais, Sônia e Hélio

Vocês são meus exemplos, minha fortaleza e meu sentido

AGRADECIMENTOS

A Deus pela proteção contínua e por guiar meu caminho.

À minha família. Meus pais Sônia e Hélio, minhas irmãs Bruna e Nathália, minhas sobrinhas Alice e Julia, Beth e Wellington, meus avós e minhas tias/tios. Obrigado pelo apoio e por compartilharem minhas conquistas e sonhos. Por compreenderem os muitos momentos de ausência. Nada seria possível sem o alicerce da minha família.

À Ana Paula, pela confiança, por sempre apoiar minhas escolhas e trazer conforto quando meu pessimismo e ansiedade falam mais alto. Por ter me ensinado a ser valente e nunca desistir ou ter preguiça. Se a vida é feita de escolhas que decidem onde chegamos, sou grato por ter escolhido, lá no finalzinho de 2011, traçar minha trajetória acadêmica ao seu lado, e tenho certeza que levarei sua amizade para todo o restante da minha caminhada.

Ao Pietro, por todos os ensinamentos, que vão muito além da Bioquímica, pelo respeito, e por sempre oferecer suporte quando precisei. Obrigado pelo cafezinho diário. Sua dedicação me inspira e trabalhar ao seu lado trouxe uma nova dimensão não só ao meu doutorado, mas completamente mudou o caminho que quero seguir na ciência daqui para frente.

A todos os membros dos laboratórios da Profa Ana e do Prof Pietro, aos atuais e aos que já se foram e que de alguma forma participaram da minha trajetória. Se eu fosse citar todos os nomes, foram muitos ao longo desses anos, mas cito aqui alguns daqueles com quem compartilhei muitos dos meus dias, os períodos pandêmicos, e muita parceria e descontração: Bianca, Bruno Favarin, Claudio, Debora, Heitor, Kel, Lucas Bahia, Luiz Andrilli, Mary.

Sou grato às amizades que a USP me presenteou ao longo dessa trajetória e sei que sempre poderei contar: Camila, Claudio, Gilia, Hiskell, João, Karmel, Lucas Bahia, Lucas Urbano, Luiz Fernando, Lari Tomazela, Lari Trindade, Luiz Andrilli, Roberta Pugina, Tamires Maira. Camila obrigado pelo suporte diário e pela relação de cumplicidade e irmandade que construímos tentando cada dia nossa melhor versão, a caminhada não seria a mesma. Lucas Bahia obrigado pelo carinho, por me trazer alegria e suporte independentemente do esforço necessário. Roberta obrigado por estar presente desde os primórdios e pelo cuidado de forma tão genuína. Claudio obrigado pela amizade tão honesta e por compartilhar planos de momentos melhores. Tamires obrigado pelo carinho e por me alegrar. Gilia obrigado por sempre estar presente nessa caminhada, independente da distância. Robson obrigado por diariamente me trazer suporte, e juntos compartilhar e torcer por nossas conquistas.

Aos técnicos que apoiaram a execução desse trabalho: Lourivaldo, Ivana, Rodrigo, Janaína e Zé Augusto. Agradeço também a Roselene Camargo, pelo amizade, suporte e conversas.

À Universidade de São Paulo, que me garantiu estrutura e permanência desde o meu ingresso na graduação e me proporcionou o poder transformador da educação.

À Fapesp pelo apoio financeiro e concessão da bolsa de doutorado (Processo 17/20846-2) e da bolsa BEPE para estágio no exterior (Processo 19/26059-8).

ACKNOWLEDGEMENTS

I thank Nico Sommerdijk for having received me in his group at Radboudumc. Thank you for your trust, for allowing me to take my own decisions and for all the discussions, about bone and about life. With you, I not only expanded my vision on biomineralization, but also on how to do science in general, to see what is relevant or not, black or white. I hope to always keep learning from you.

I thank all the members of the Biochemistry of Mineralized Tissues Group.
Anat, thank you for the good humor, for the support and all the discussions.
Martijn, thank you for the many pleasant hours by your side in the cryoTEM.
Chenglong, thank you for always being there and supporting me with so much care.
Judith, thank you for all the inspiring discussions and helping me so genuinely.
Luco, thank you for the early lunchs, for the laughs and always fitting one of my samples into your analyses whenever I needed. Robin, thank you for the unwavering support and always willing to share a cup of coffee and discuss both work and life.
Rona, thank you for becoming so dear and special.

I thank to Renè Buchet and Saida Mebarek for having received me in the University of Lyon and introduced me to the world of MVs. Thank you for welcoming me to your laboratory so warmly and for all the teachings.

I thank to Massimo Bottini, at the University of Rome Tor Vergata for the participation in the autophagy project and for the so many discussions, always inspiring and fruitfull.

"*Biology is chemistry with a history.*"

- Andrew Knoll

RESUMO

Cruz, M. A. E. **Estudos sobre o papel das vesículas da matriz na mineralização óssea: observações de micro à nanoescala**. 2023. Tese (Doutorado em Ciências) - Faculdade de Filosofia, Ciências e Letras de Ribeirão Preto, Universidade de São Paulo, Ribeirão Preto, 2023.

A biomineralização óssea é um processo complexo que envolve a deposição de cristais de fosfato de cálcio em fibrilas de colágeno da matriz extracelular (MEC). Embora tenha sido proposto que as vesículas da matriz (VMs) atuem nesse processo, os mecanismos envolvidos ainda são pouco entendidos. Esta tese buscou examinar a interação entre as VMs e a formação mineral por meio de observações em três níveis: vesículas individuais, em um modelo mimético de membrana, e em cultura *in vitro* de osteoblastos. Dessa forma, VMs foram isoladas a partir de ossos de galinha embrionários e caracterizadas quanto ao seu conteúdo assim como a capacidade de iniciar a formação mineral. Caracterização por microscopia eletrônica de transmissão criogênica revelou que preparações de MVs são heterogêneas e contêm além de vesículas bilamelares, uma alta quantidade de partículas não-vesiculares, sendo essa heterogeneidade impactante na habilidade de VMs em induzir mineralização. Investigações adicionais por meio de experimentos comparativos de purificação e de mineralização demonstraram que a principal via pela qual as VMs desencadeiam a mineralização é por meio de seu maquinário enzimático, como a fosfatase alcalina, tal que a nucleação direta de mineral a partir de íons solúveis represente um processo secundário. Para acessar esse efeito secundário, a nucleação mineral induzida pela superfície das VMs foi acessada em um modelo biomimético de membrana usando monocamadas de Langmuir de lipídios sintéticos (fosfatidilcolina e fosfatidilserina) assim como lipídios nativos extraídos de VMs. O rastreamento *in-situ* da formação mineral nesse modelo revelou que nanodomínios enriquecidos em fosfatidilserina formados na superfície da membrana desencadeiam a nucleação mineral ao interagir com íons cálcio e fosfato. Tendo estabelecido a interação entre as VMs e a formação de mineral tanto ao nível de vesículas individuais quanto no modelo biomimético de membrana, o papel das VMs no controle da mineralização da MEC foi finalmente demonstrado a nível celular usando cultura primária de osteoblastos. Osteoblastos tratados com cloroquina, um bloqueador da autofagia, resultou em mineralização deficiente da MEC. Embora a mineralização dos osteoblastos seja reduzida em presença de cloroquina, como revelado pela coloração de cálcio por vermelho de Alizarina, microscopia eletrônica de transmissão revelou que VMs ainda estavam abundantemente presentes na MEC. No entanto, o isolamento de VMs e a caracterização de seu conteúdo revelaram expressão reduzida de proteínas relacionadas à mineralização, com uma diminuição notável na atividade da fosfatase alcalina. Essas observações no nível celular sugerem que a mineralização da MEC é deficiente se as MVs estiverem disfuncionais (ou seja, atividade de fosfatase reduzida), sugerindo que essas estruturas desempenham um papel predominante na mineralização óssea, sendo sua liberação controlada de maneira específica ao contexto celular. Em conclusão, os resultados coletivamente apresentados nesta tese confirmam a importância das MVs para a mineralização óssea, mas também oferecem novas perspectivas sobre a relação intricada entre as vesículas e a formação mineral.

Palavras chave: osso, biomineralização, vesículas da matriz

ABSTRACT

Cruz, M. A. E. **Studies on the role of matrix vesicles in bone mineralization: observations from micro to nanoscale**. 2023. Tese (Doutorado) - Faculdade de Filosofia, Ciências e Letras de Ribeirão Preto, Universidade de São Paulo, Ribeirão Preto, 2023.

Bone biomineralization is a complex process that involves the deposition of calcium phosphate crystals on collagen fibrils of the extracellular matrix (ECM). Although matrix vesicles (MVs) have been proposed to be responsible for the initial mineral formation, their role and mechanisms are still not fully understood. This thesis aimed to examine the interplay between MVs and forming mineral during bone mineralization at three levels: individual vesicle observation, mineralization at the interface of a membrane-like model, and *in vitro* mineralization using osteoblasts culture. To investigate the underlying factors that mediate mineralization *in vitro*, MVs were isolated from embryonic chicken bones, and their contents, as well as their ability to initiate mineral formation, were examined at a single-vesicle level using near-native cryogenic transmission electron microscopy. This approach revealed that MVs preparations contain non-vesicular particles in addition to bilayered vesicles, affecting the outcome of mineralization experiments. Further investigations using comparative purification and mineralization experiments demonstrated that the primary pathway by which MVs trigger mineralization is through their enhanced phosphatase activity, such as alkaline phosphatase, with the direct mineral nucleation from soluble ions being a secondary process driven by their membrane components. To access this secondary effect, surface-induced mineral nucleation was accessed in a biomimetic model using Langmuir monolayers of synthetic (e.g. phosphatidylcholine and phosphatidylserine) as well as native lipids extracted from MVs. *In-situ* tracking of mineral formation at Langmuir monolayers revealed that phosphatidylserine-enriched nanodomains formed at the membrane surface trigger the mineral nucleation by interacting with calcium and phosphate ions. Having established the interplay between MVs and forming mineral both at the single-vesicle level and using a membrane-like model, the role of MVs in controlling ECM mineralization was finally demonstrated in a primary osteoblast culture. Osteoblasts treated with chloroquine, a blocker of autophagy, resulted in defective ECM mineralization. Although mineralization was impaired, as revealed by alizarin red calcium staining, transmission electron microscopy revealed that MVs were still abundantly present throughout the ECM. However, isolation of MVs and characterization of their content demonstrated reduced expression of mineralization-related proteins, with a remarkable decrease in alkaline phosphatase activity. These observations at cell level suggested that ECM mineralization is impaired when MVs are dysfunctional (i.e., reduced phosphatase activity) and that these structures play a predominant role in bone mineralization, being their release controlled in a cell-context-specific manner. In conclusion, the findings presented in this thesis collectively validate the crucial role of MVs in bone mineralization while also providing valuable insights into the complex interplay between vesicles and the mineralization process.

Keywords: bone, biomineralization, matrix vesicles

CONTENTS

1
THE STRUCTURE AND FORMATION OF BONE TISSUE

1.1 | The paradox of bone mineralization 17
1.2 | Biology aspects of bone formation 18
1.3 | The stencilling principle for bone mineralization 20
1.3 | Biomineralization – nucleation and growth of mineral crystals 22
1.4 | Bone structure 27
1.4.1 | Multilevel arrangement of mineralized collagen fibrils 27
1.4.2 | The bone mineral 29
1.4.3 | From collagen molecules to fibrils 29
1.4.4 | Other components of the organic matrix 31
1.4.5 | The relationship between collagen and mineral 33
1.5 | The cell-matrix interface: the appearance of a mineralization front 36
1.6 | Matrix vesicles as players in the mineralization front 38
1.6.1 | The biogenesis of MVs 40
1.6.2 | The function of MVs 40
1.7 | Motivation and thesis outline 45
1.8 | References 46

2
THE RELATIONSHIP BETWEEN MVs AND FORMING MINERAL AT THE NANOSCALE

2.1 | Introduction 59
2.2 | Objectives 64
2.3 | Methods 64
2.3.1 | Synthetic Cartilage Lymph (SCL) preparation 64
2.3.2 | Bone tissue digestion and MVs isolation by 3-step differential ultracentrifugation 64
2.3.3 | Iodixanol density gradient fractionation of crude MVs 65
2.3.4 | Protein quantification and alkaline phosphatase activity 66
2.3.5 | SDS-PAGE and western blotting 66
2.3.6 | Nanoparticle tracking analysis (NTA) 66
2.3.7 | CryoTEM sample preparation and imaging 67
2.3.7 | Mineralization experiments 67
2.4 | Results 68
2.4.1 | Characterization of crude MVs isolated by differential ultracentrifugation 68
2.4.2 | Density-gradient fractionation separates MVs from non-vesicular particles 69
2.4.3 | Crude and low-dense MVs show different kinetics of induction of mineralization from soluble Ca^{2+} and Pi ions 72
2.4.4 | Crude and low-dense induce mineralization in presence of ATP 77
2.5 | Discussion 78
2.6 | Conclusions 84
2.7 | References 85

3
A LANGMUIR MONOLAYER MODEL FOR MINERAL NUCLEATION

3.1| Introduction 95
3.2 | Objectives 99
3.3 | Methods 99
3.3.1 | Langmuir monolayers and surface pressure (π) vs area (A) isotherms 99
3.3.2 | *In situ* mineralization of Langmuir monolayers 100
3.3.3 | Extraction of the lipid fraction from MVs 101
3.3.4 | Solution Titration 101
3.4 | Results 102

3.4.1 | Langmuir monolayers mimicking MVs lipidic composition 102
3.4.2 | Mineralization induced on Langmuir monolayers composed by lipids of selected compositions 104
3.4.3 | Mineralization induced on Langmuir monolayer composed by the lipid extract of MVs 110
3.5 | Discussion 112
3.6 | Conclusions 114
3.7 | References 114

4
AUTOPHAGY IMPAIRMENT AND THE RELEASE OF MVs

4.1 | Introduction 120
4.2 | Objectives 125
4.3 | Methods 125
4.3.1 | Chick calvaria osteoblasts *in vitro* culture 125
4.3.2 | Cell viability and apoptosis assay 126
4.3.3 | Isolation of matrix vesicles (MVs) 126
4.3.4 | Nanoparticle tracking analysis 127
4.3.5 | Atomic force microscopy and transmission electron microscopy of MVs 127
4.3.5 | Alkaline phosphatase (TNAP) assay and in vitro mineralization of MVs 127
4.3.5 | Gene Expression by RT-PCR 128
4.3.6 | SEM and TEM analysis of cells 129
4.3.7 | Proteomic analysis 129
4.5 | Discussion 131
4.5.1 | Validation of CQ treatment upon cell viability and apoptosis 131
4.5.2 | Autophagy impairment affects osteoblast mineralization 135
4.5.3 | Impairment of autophagy affect the biophysical and functional properties of MVs 140
4.5.4 | Comparative proteomics reveals difference in the proteome of MVs 142
4.6 | Discussion 144
4.7 | Conclusions 147
4.8 | References 147

5
FINAL DISCUSSION

1

THE STRUCTURE AND FORMATION OF BONE TISSUE

The zone in which tiny bone crystals grow is called the mineralization front. Use of the term "front" may be supported if one draws an analogy with a battle front, where the invading troops (mainly Ca and PO_4 with the assistance of Mg and CO_3) are brought in from elsewhere, and only survive when sufficient numbers arrive in one place at one time and enjoy the collaboration of the organic bone matrix whose territory they are about to annex.

Allan Boyde. *Metab. Bone Dis. et Rel. Res.* (**1980**), 2, 69-78

This chapter provides an introduction to the structure and the key players involved in bone formation. Additionally, the motivation and the topics to be explored in this thesis will be outlined.

1.1 | The paradox of bone mineralization

The question of how and why bones form has fascinated scientists for centuries. Bones are critical to our mobility, stature, organ protection, and homeostasis. Despite their essential role, many aspects of their formation remain a mystery. As far back as 1638, Galileo Galilei already suggested that bone structure is intimately linked to its mechanical function. He observed a correlation between bone shape, cross-sectional width, and the mechanical demands of weight-bearing. Later, Clopton Havers identified the basic components of bone as "fixed salt" (mineral) and "earth" (organic matter) in 1690. However, it was not until the mid-20th century, with the introduction of X-ray diffraction and electron microscopy, that scientific discussions about the ultrastructure of bone and the mechanisms by which this structure is assembled gained momentum. Examining bone structure revealed it to be a composite material made of constituents present all over our body. It is made by a organic matrix composed majoritarialy by fibrillar type I collagen that is impregnated by a mineral composed of calcium and phosphate (Pi) ions, with a composition similar to the hydroxyapatite (HAp).

However, mineralization of the collagenous matrix present within the extracellular matrix (ECM) is observed to occur only in hard mineralized tissues such as bone and dentin. This observation raises two major and paradoxical questions. First, why is mineralization restricted to the ECM in hard tissues? Second, how is mineralization logistically achieved? To deposit only 1 cm^3 of bone mineral, the amount of Ca^{2+} present in 30 L of blood must be concentrated, a ratio that becomes unimaginably large when the large volume of skeletal tissue is considered. Furthermore, bones reach a mineralization ratio of about 70% mineral/matrix, making it even more challenging to understand how these paradoxical requirements are achieved during bone mineralization. As it will become clearer along this introductory chapter, in order to understand bone formation, we need to consider not only biological aspects but also how organisms play with chemistry in order to control mineralization. In principle, mineralized tissues usually form by cells first elaborating an ECM and then mineral is introduced into the pre-formed matrix. Therefore, we will start presenting biological aspects of how this matrix is assembled and mineralized. Then, we will address fundamental aspects of the underlying crystallization process in order to understand the physical and chemical factors that control the formation of the mineral phase, and describe the intimate association between collagen and mineral as the basic building block of bone tissue. Finally, we will present one the players involved in the formation of a mineralization matrix: the extracellular matrix vesicles (MVs), that is the central topic of this thesis.

1.2 | Biology aspects of bone formation

Bone formation programs are highly complex, and both spatial- and temporally-regulated. Despite their inert and static appearance, bones undergo a constant cycle of remodelling in order to maintain the homeostasis and functionality of their structure. It is estimated that during an adult active years, the total mass of bone matrix is synthesized and reabsorbed every five or six years, obviously at different rates depending on the location of the bone and the individual age. Therefore, when speaking of bone formation, we refer to processes that happen *de novo*, such as in embryonic bone growth, or as a manner to substitute a bone matrix that was already present before, in a process called remodelling. In a simplistic vision, bone formation and remodelling is controlled by the action of two types of cells: osteoblasts and osteoclasts. Osteoblasts are the cells responsible for bone formation, secreting an ECM rich in type I collagen and other mineralization-related biomolecules[1]. Osteoblasts trapped within their mineralized ECM are terminally differentiated into osteocytes, the main cell type found in mature bones, and has an important function in the regulation of bone activity[2]. On the other hand, osteoclasts are the cells responsible for the resorption of the mineralized matrix. These cells are capable of creating a locally produced acidic environment for the degradation and resorption of the mineralized matrix[3]. The disturbance of the balance between bone formation and resorption leads to pathological conditions, such as osteoporosis[4].

As a tissue, bones can be formed through two mechanistically distinct histogenesis pathways: intramembranous and endochondral. Detailed aspects of these pathways are out of scope here and can be found in excellent reviews[5–7]. Importantly is that intramembranous and endochondral ossification share several aspects regarding the sequences that leads to the assembly of the ECM and its mineralization. During intramembranous ossification, responsible for the embryonic formation of flat bones such as those in the jaw and skull, occurs the condensation and differentiation of mesenchymal progenitor cells into osteoblasts. The condensation of mesenchymal cells forms a mold that predefines the location and shape of the future bone. Once the mesenchymal cells become committed to the osteoblastic phenotype, their maturation leads to the synthesis of the bone matrix, where osteoblasts express collagen and enzymes/proteins capable of controlling the nucleation and propagation of the mineral phase. The final size and shape of the bone are achieved through remodelling processes resulting from the joint action of osteoblasts and osteoclasts.

The other type of ossification, endochondral ossification, is a much more complex cellular process than the intramembranous ossification, both in terms of temporal and spatial aspects. This type of ossification is responsible for the formation of long bones, such as the femur and tibia. During the condensation of mesenchymal cells, which dictates the shape and location of the future bone (as in the case of intramembranous ossification), differentiation does not occur directly into osteoblasts, but into chondrocytes (that are cells specific to cartilage tissue), which secrete an ECM containing collagen (in this case, type II collagen, as opposed to type I collagen, which is predominant in mature bones). Therefore, what differentiates endochondral ossification from intramembranous ossification is the existence of a cartilaginous mold that precedes the final bone structure. In this mold, chondrocytes proliferate, differentiate, and alter their cellular functions when they reach a state of hypertrophy, which has a mineralizing phenotype. This events in specific region of the tissue called growth plate and results in the formation of a mineralized cartilage, which presents a poorly crystalline mineral phase dispersed in the collagen matrix. The degradation process of this matrix then begins, where osteoclasts (or more precisely chondroclasts, as they are cartilage cells) promote the removal of the mineralized cartilage, creating vacancies in the degraded matrix. These spaces become occupied by new progenitor cells that differentiate this time into osteoblasts, which laid down a new ECM that will later be mineralized and give rise to the final bone structure. It is important to note that bone formation is accompanied by a high vascularization of the growing region, thus suggesting that an ample supply of oxygen, nutrients and ions are required[8].

1.3 | The stencilling principle for bone mineralization

Simply put, the formation of mineralized tissues occurs through the ability of organisms to simultaneously construct an ECM that will serve as a foundation for the deposition of the mineral phase and to secrete a biochemical machinery capable of controlling this process. This is the genetic control of biomineralization, in which the existence of cells phenotypically capable to synthesize and control the mineralization of the ECM allowed the emergence of mineralized tissues. Obviously, the formation of mineralized tissues, such as those in the skeletal system, was fundamental to the evolution of species due to their role in protection and locomotion, for example. In addition to locomotion, bones play other important functions, such as providing support for skeletal muscles, being niche sites for blood cell synthesis, storing mineral ions, and secreting hormones.

Vertebrate organisms developed abilities during evolution to manipulate chemistry in order to form mineralized tissues. Calcium and phosphate ions are present throughout our body, circulating through the extracellular fluid. The concentration of Ca^{2+} in the extracellular medium is finely controlled by the endocrine system, which maintains its values in the narrow range of 2.2 to 2.7 mmol/L[9]. On the other hand, the concentration of Pi varies considerably with age, being higher during childhood but with values in the range of 1.12 to 1.45 mmol/L in adulthood[10]. Purely chemically speaking, a mineral will precipitate if its solubility (measured by its solubility product, Kps) is exceeded. Therefore, the circulating concentration of Ca^{2+} and Pi in the body fluid would be sufficient to explain the origin of mineralized tissues. However, despite the log(Kps) for bone mineral under physiological conditions being about 30 orders of magnitude lower than the logarithm of the ionic product of the concentration of Ca^{2+} and Pi in human plasma, direct precipitation does not occur in healthy soft tissues. When we think about biomineralization from a perspective where crystallization is controlled only by the Kps of the mineral phase, we encounter the paradox resulting from the fine control of the ionic homeostasis of the human body. Through highly sophisticated cellular mechanisms not completely understood, our body is capable of storing mineral ions and promoting the mineralization only in bones and teeth, preventing mineralization in soft tissues (except under pathological conditions). Moreover, in certain regions of the body, such as the adhesion of tendons to bone, the interface between mineralized and non-mineralized tissue must be precisely controlled to maintain anatomical functionality. This fine control of biomineralization is achieved through a cascade of spatially and temporally orchestrated events in which precursor ions are systemically prevented from precipitating as a solid mineral phase, or are stabilized as precursor phases of amorphous minerals.

The first mineralization inhibitor identified was extracellular pyrophosphate (PPi), described in the 1960s as a potent antagonist of mineralization, of which its removal was infereed to be a key step for bone formation[11]. PPi is a phosphate ester formed by two Pi monomers joined by a P-O-P bond, and it is present in the extracellular medium in concentrations of around 6 µmol/L[12]. It acts as a mineralization inhibitor by complexing with Ca^{2+}, reducing the rates of nucleation and growth of calcium phosphates. Therefore, maintaining an ideal Pi/PPi ratio is universally accepted as a necessary condition for mineral formation in the ECM[13]. As described by Garimella et al.[14], a small variation in PPi of µmol is sufficient to inhibit apatite formation, while larger variation of Pi in the range of mM is required to induce its formation, evidencing the major effect of PPi as a systemic inhibitor. In addition to PPi, phosphate esters can be found in the form of polyphosphates (-(Pi)nn-), which are another way of controlling the concentration of free Pi necessary for mineral nucleation[15].

Another potent systemic inhibitor of mineralization is fetuin-A, a circulating protein with high affinity for Ca^{2+}, which prevents the growth of mineral nuclei in the blood by mobilizing mineral ions into a colloidal complex with dimensions that can reach 150 nm, known as calciprotein particles[16,17]. A single fetuin-A molecule can sequester up to 90-120 Ca2+ and 54-72 Pi ions[18]. Additionally, it is abundant found in bone tissue, accounting for about 25% of the non-collagenous proteins therein present by mass[19]. As bone cells do not express fetuin, this observation is accordance with the fact that ossification is accompanied by intense vascularization of the developing tissue, and the calciproteins originating from the bloodstream into the forming bone matrix indicates that these structures may act as a pathway for bringing precursor ions required for mineralization[20–22].

If the nucleation of the mineral phase is systemically inhibited, the existence of mineralized tissues indicates cellular specialization to a phenotype capable of creating the microenvironment necessary for extracellular matrix mineralization. This is referred to as an *stencilling principle* of extracellular mineralization[23], a paradigm of "repressing a repressor". Osteogenic cells, such as osteoblasts, not only have a role in building the ECM that will serve as a foundation for mineral deposition, but also to express a series of enzymes capable of locally removing mineralization inhibitors. The major enzyme here is the tissue non-specific alkaline phosphatase (TNAP), a key enzyme in the osteoblast differentiation program, and has a major role in degrading PPi, removing its inhibitory effect, in order to create a microenvironment permissive for mineralization. Loss-of-function mutations in the gene encoding TNAP leads to different mineralization disorders resulted in impaired skeletal mineralization[13]. Murshed et al. demonstrated that ECM mineralization occurs only in bone because of the exclusive coexpression in osteoblasts of type I collagen and TNAP[24]. By simply ectopically expressing

TNAP in cells naturally producing fibrillar collagen (such as skin) is sufficient to induce pathological mineralization[24].

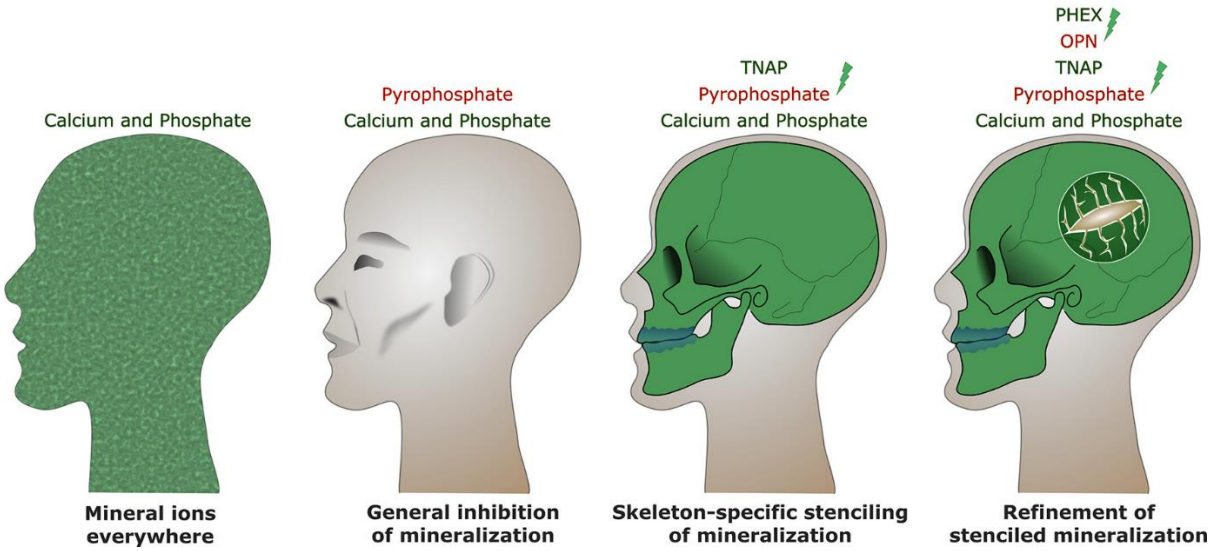

Figure 1.1 | The Stenciling Principle explains how mineralization of the skeleton occurs. Ca^{2+} and Pi ions are freely circulating throughout most tissue compartments. However, within the extracellular fluid, the abundant production of pyrophosphate PPi acts as a potent inhibitor of mineralization, preventing potential undesired mineralization events. This systemic inhibition prevents tissues intended to be "soft" from mineralizing, despite the high levels of available mineral ions. In contrast, the skeleton exhibits precise mineralization patterns, thanks to the expression of the promoter TNAP by cells in bones and teeth. This enzyme stencils mineralization at specific connective tissue sites within the pre-formed ECM, characteristic of skeletal mineralized tissues. Other promoter-inhibitor pair also exists, such as osteopontin (OPN), expressed locally by osteoblasts and which inhibit and regulate mineralization by sequestering mineral ions and possibly stabilizing an amorphous calcium-phosphate precursor phase. In contrast to the broad inhibitory action of pyrophosphate, sustained inhibitory proteins such as OPN refine mineralization patterns at specific locations. In this way, exist the enzymatic action of PHEX (phosphate-regulating endopeptidase homolog X-linked), expressed locally by bone and tooth cells, to facilitate the degradation of inhibitory OPN and thus release from mineralization inhibition. Adapted with permission from reference [23].

1.3 | Biomineralization – nucleation and growth of mineral crystals

One of the greatest challenges in current biomineralization research is to understand the relationship between physical-chemical and biochemical mechanisms that enable the extremely precise control of biomineral formation. Fundamentally, biomineralization is a process in which soluble ionic precursors undergo a phase transition from a state of high free energy (solvated state of the ionic precursors) to a state of lower free energy (the resulting biomineral crystal lattice). This phase transition is known as nucleation. The physical-chemical basis of nucleation is extensively described in the literature[25–27], so here we present only a simplified view of the process, in which some essential factors can be outlined. The basic point is that, whether for nucleation or growth, the free energy of ions in solution must be greater than the sum of the

free energies of the mineral phase and the final solution. Therefore, nucleation requires a condition of metastability, where the precursor solution exists in a supersaturated state. The supersaturation (S) of a solution is defined as the ratio of the product of the concentration of soluble precursors and their respective solubility constant (Kps), relative to the formed mineral phase. Thus, for nucleation to occur, it is necessary to accumulate precursor ions such that the condition for nucleation of the mineral phase is favoured by a minimum supersaturation (S>1).

Nucleation occurs through the migration of ions from the solution to a solid nucleus nucleated from thermodynamic fluctuations in the solution. This is accordingly to the classical nucleation theory called a homogeneous nucleation event. However, only a fraction of the particles formed through these fluctuations will become stable nuclei of the solid phase. This is due to the interfacial tension between the formed nucleus and the solution (ΔGi), which opposes the reduction in free energy generated by the transfer of ions from the solvated phase to the solid phase (ΔGv). Thus, the formation of the solid phase consists of overcoming the energy barrier of formation of the most stable nucleus (ΔG*), which then evolves into the final solid phase. While the chemical potential of the solid phase is lower than that of the solution, that is, while there is supersaturation, the nucleated particle can grow. Nucleation can also occur not in the bulk solution, but at preferential sites of surfaces, referred to as heterogeneous nucleation, showing a much lower nucleation barrier. The basic assumption is that at preferential sites, such as phase boundaries, impurities or the surface of a macromolecule, the effective surface energy is lower which decreases the activation energy. As a result, heterogeneous nucleation occurs more often than homogeneous nucleation (Figure 1.2a).

We can now visualize these concepts of nucleation during the precipitation of calcium phosphate in bone formation. As the supersaturation is the driving force for nucleation and growth, a "CaxP" value – free Ca^{2+} multiplied by the free Pi in mM can be a representation of the saturation level required to trigger mineralization. Using *in vitro* precipitation experiments, Fleisch[28] demonstrated that while homogenous nucleation occurs at CaxP values above 4 mM^2, addition of collagen fibrils to the solution lower CaxP values above 1.3 mM^2 due to heterogeneous nucleation. However, the relationship between CaxP and mineral formation is complicated composition of the serum and the free ions available. Although human serum is supersaturated with respect to apatite, with CaxP values to allow heterogeneous nucleation on some collagen, but is not high enough for spontaneous nucleation[11]. This occurs because Ca^{2+} can be present not in a bioavailable free form but bound to proteins, or complexed with small inhibitor molecules, such as PPi. This results that when collagen is incubated with human plasma, there is an inhibitory effect on mineral nucleation, and the CaxP values approach those of homogeneous nucleation (Figure 1.2c). Interestingly, mineralization occurs at a much lower

values of CaxP if the plasma is first incubated with an phosphatase enzyme that degrades the inhibitory effect of pyrophosphate bonds (Figure 1.2d).

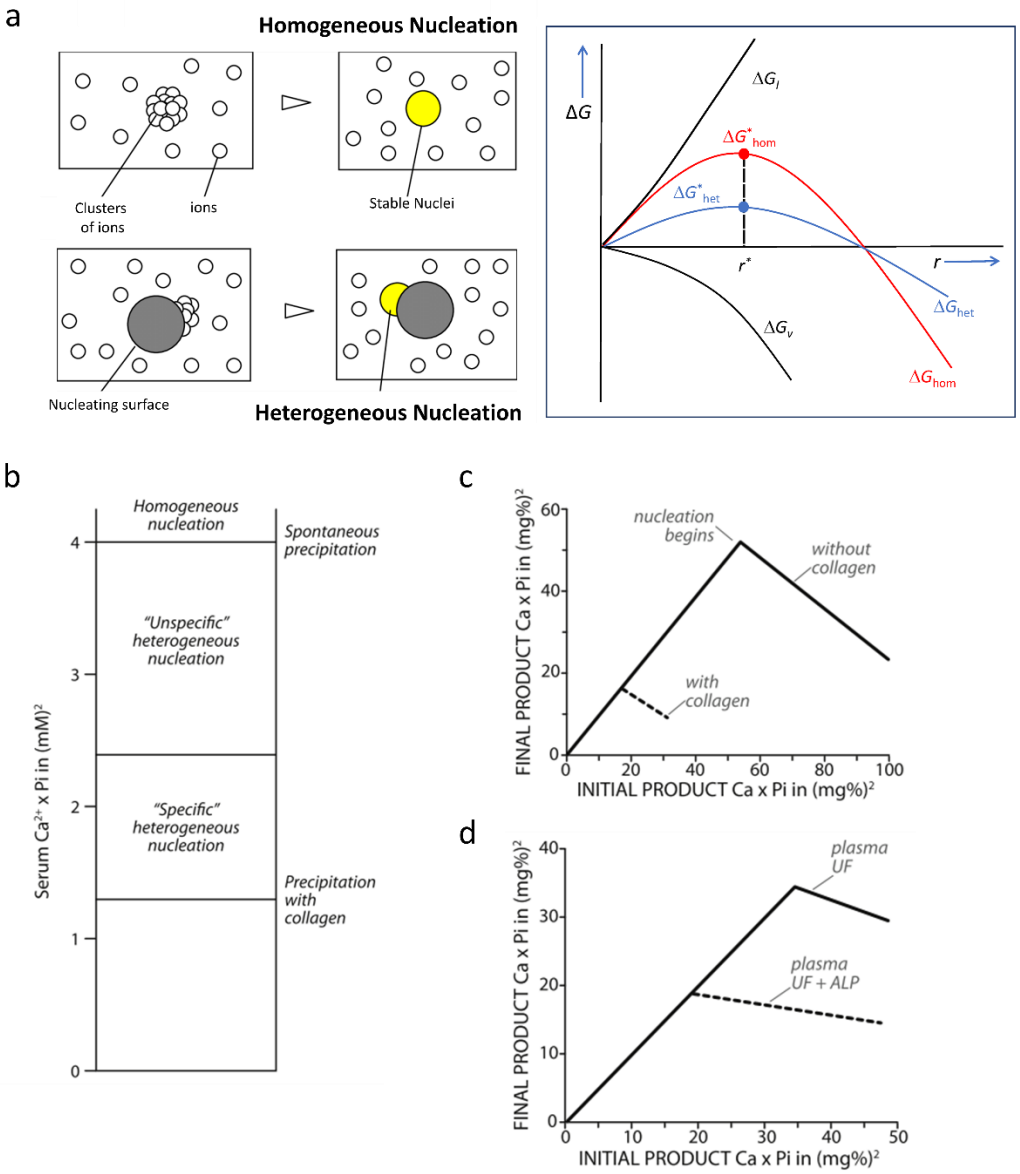

Figure 1.2 | Nucleation in biomineralization. a) Classical nucleation theory proposes two types of nucleation: homogeneous and heterogeneous. Homogeneous nucleation occurs in a solution without any foreign surfaces, while heterogeneous nucleation takes place on a pre-existing surface. The energy barrier for nucleation is defined by the interfacial energy (ΔGi) and volume energy (ΔGv) required to form a critical cluster size (rc), which represents the first stable particle or nucleus. In the right panel, we can see the relationship between ΔGi, ΔGv, and ΔG* (the nucleation energy barrier) at the critical cluster size. b) Fleisch's experiments have shown that for calcium phosphate formation, a minimum ion product of CaxP 1.3 mM^2 is required for precipitation on surfaces like collagen. However, homogeneous nucleation in a solution only occurs at a higher CaxP of 4 mM^2. The addition of collagen can reduce the minimum ion product required for nucleation (c). However, when a collagen substrate is incubated with an ultrafiltrate (UF) of human plasma, there is an inhibitory effect on mineral nucleation, and the CaxP values approach those of homogeneous nucleation. This inhibition can be removed by incubating the plasma with alkaline phosphatase (ALP) before adding it to the collagen substrate (d). Adaapted with permission from reference [29].

Throughout the evolution of vertebrates, they have developed intricate mechanisms to impose chemical constraints and overcome nucleation barriers during mineralization. By compartmentalizing and controlling the chemical environment, pH, and introducing inhibitors and catalysts, the energy barriers are lowered, resulting in smoother energy landscapes. Hence, the complexity of energy landscapes involved in biomineralization cannot always be explained by the direct nucleation of the most thermodynamically stable mineral phase[30,31]. Therefore, biomineralization generally occurs through a sequential process that involves structural and compositional modifications of amorphous precursors and crystalline intermediates, rather than a single-step pathway where the thermodynamically most stable product is promptly formed. The extent of these phase transformations depends on the solubilities of the intermediate mineral phases and the energy barriers associated with the different steps, all strongly influenced by additives, which is one of the reasons that allows for high control of the biomineral formation process by the organic matrix. *In vitro*, under conditions that mimics the physiological range of pH and ionic concentration, the formation of calcium phosphate reflects this multi-stage crystallization mechanism[32], as shown in Figure 2. This mineralization pathway from more soluble mineral have also been observed *in vivo*, where the composition of bone mineral change with age and degree of mineralization, so that the Ca/P molar ratio varies too. It increases from a mean value of 1.35 in the earliest mineral deposits to 1.60 in the fully mineralized areas[33]. Akiva et al demonstrated that a major disordered precursor mineral phase containing HPO_4^{2-} is part of the mineralization pathway in the rapidly-formed tail fin bones of zebrafish[34]. Moreover, metastable precursors to apatite were also observed in other *in vivo* studies[35,36]. While the specific ion pathways involved in bone mineralization are not yet fully understood, it is evident that organisms have evolved to take advantage of supersaturated conditions containing mineral precursors. These precursors can be stored, dissolved, and manipulated with ease, allowing for the creation of diverse shapes that can be transformed into more ordered and functional materials. We can now understand structural aspects of bone mineralization.

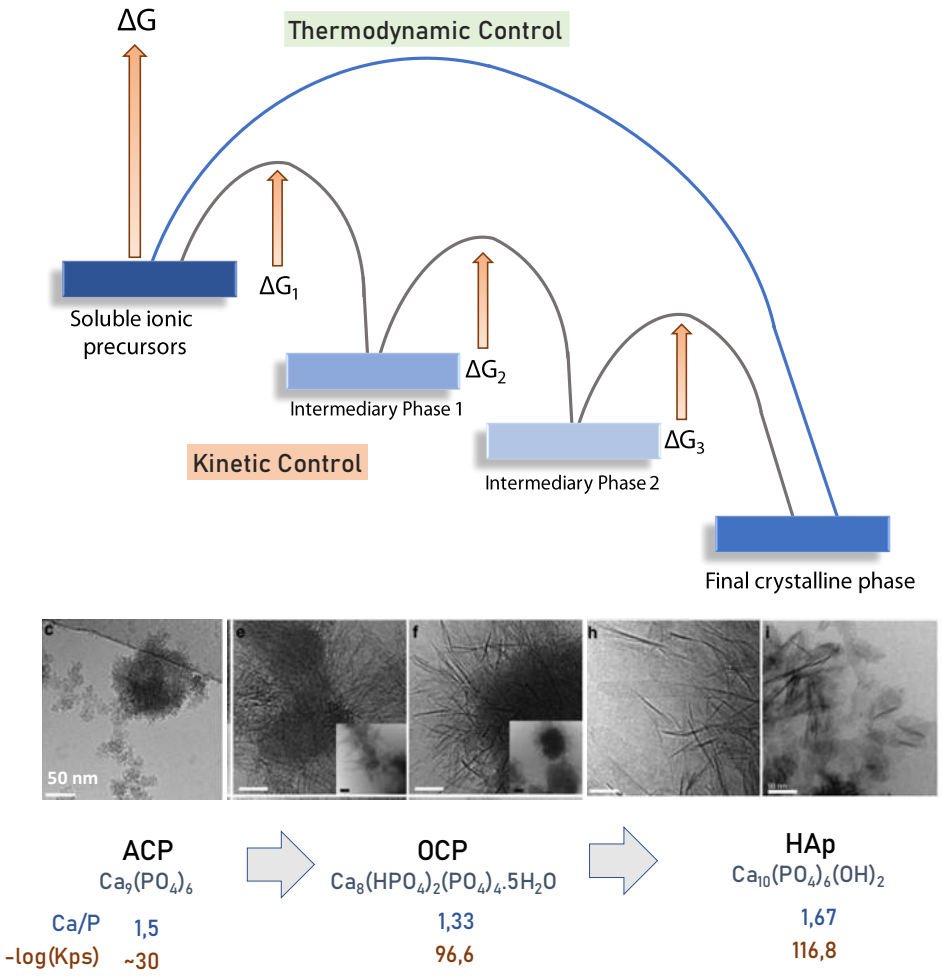

Figure 1.3 | Pathways of crystallization under thermodynamic and kinetic controls. From a thermodynamic perspective, a system containing soluble ionic precursors tends to evolve towards the direct formation of the most stable phase, provided that the energy barrier (ΔG) associated with the nucleation and growth of this phase is overcome. However, in some cases, a kinetically controlled pathway may occur, where sequential precipitation takes place from less stable precursors, controlled by energy barriers (ΔG1,2,3). The pathway adopted for mineral formation, whether it follows a single-step pathway (thermodynamic pathway) or sequential precipitation (kinetic pathway), depends on the magnitude of the energy barriers associated with nucleation, growth, and transformation of intermediate phases. This concept can be illustrated through transmission electron microscopy images of products formed from a solution containing Pi and Ca^{2+} over time. In this case, sequential precipitation occurs, in which amorphous calcium phosphate (ACP) is formed in the solution, followed by the formation of octacalcium phosphate (OCP), and finally, hydroxyapatite (HAp). As the pathway progresses, there is an increase in the Ca/P ratio and a decrease in solubility (Ksp) of the system. This demonstrates how the pathway followed by crystallization depends on the energy barriers associated with nucleation, growth, and transformation of intermediate phases, and highlights the importance of considering both thermodynamic and kinetic controls in understanding the formation of crystalline materials. Adapted with permission from reference [32].

1.4 | Bone structure

1.4.1 | Multilevel arrangement of mineralized collagen fibrils

The mechanical function of a given bone is tightly controlled by their form, which is by consequence related to their formation, where precise regulation mechanisms constrains its architecture and the extent and the pattern of mineralization within a biomechanically optimized range[37]. The bone architecture depends on several factors and varies between species, age, and location of the bone in the body. When discussing the uniqueness of bone structure, we are referring to the multi-scale and hierarchical organization between collagen fibrils and mineral crystals. The structure of bone can be disassembled into different levels, that goes from macroscopic down to the molecular level[38,39]. For conceptual reasons, it is important to give the correct dimension to the term "bone", as we can refer to it both as a tissue (the set formed by bone cells and the mineralized ECM) or as an organ (the bone as a whole, including cartilage, marrow, and blood vessels, for example).

Starting from the macroscopic level of bone as an organ, the first organizational distinction can be made even with the naked eye, where one can easily distinguish the morphology of trabecular bone tissue from cortical bone tissue, discernible at the millimetre range (Figure 1.4). While trabecular tissue has a porous structure with a disordered and interconnected arrangement of trabeculae, cortical bone tissue is dense and formed by concentric cylindrical structures called osteons. Structurally, both compact and trabecular tissues are formed by lamellae, which are three-dimensional arrangements of collagen fibres of the order of a few tens of micrometres. A fibre is a supramolecular arrangement of collagen fibrils in which all are oriented along a common axis. Lamellar arrangements of collagen fibres can be highly organized, such as in osteons, where lamellae are arranged concentrically, or arranged in a less ordered manner, such as in trabecular bone. Finally, we come to the nanometer level, where mineralized collagen fibrils emerge as the building block of bone material. We can now reconstruct the formation of bone structure from the bottom-up, starting with their mineral crystals.

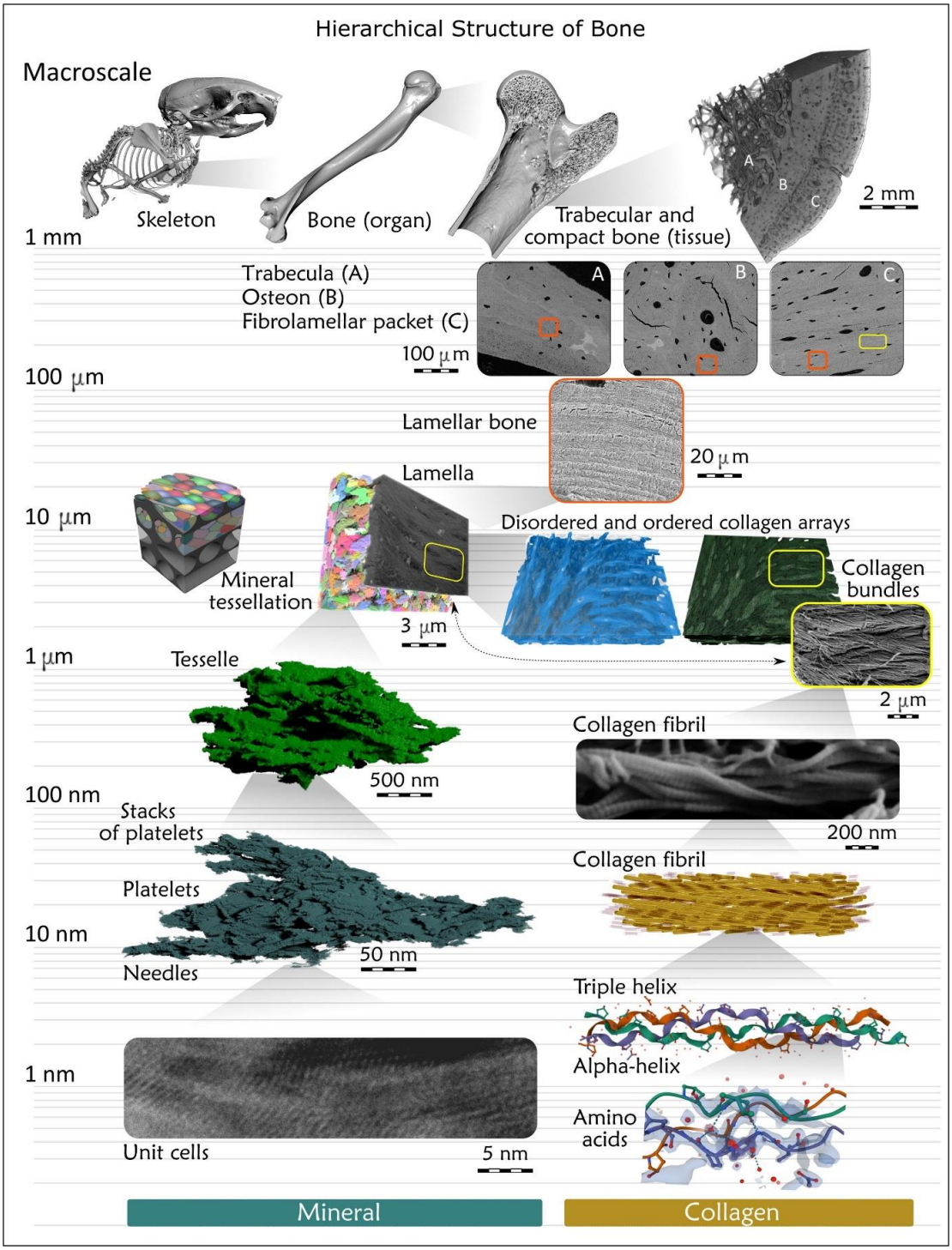

Figure 1.4 | Bone Structure. The contemporary understanding of the hierarchical structure of bone is quite intricate, consisting of around twelve levels. At the highest level, bone is composed of cortical and trabecular tissue, which are themselves composed of smaller structures such as cortical osteons, fibrolamellar bone packets, and trabecular lamellar packets that contain lamellar bone. Lamellar bone, in turn, is made up of lamellae, which consist of ordered collagen motifs forming bundles surrounded by disordered collagen. These bundles are composed of collagen fibrils, which are further made up of triple helices, alpha-helices, and ultimately amino acids. The mineral organization within bone also exhibits a hierarchical structure, starting at the level of mineralized collagen bundles that contain tessellated prolate ellipsoids of mineral, which are made up of mineral platelets, laterally merging acicular crystals, and ultimately unit cells. However, because the organic and inorganic matter split at the micrometer level and same-level mineral and collagen units have different shapes and scales, the levels are intentionally not numbered in the figure to ensure visual continuity and flow between levels.Adapted with permission from reference [39].

1.4.2 | The bone mineral

We often refer to the calcium phosphate mineral phase in bone as a hydroxyapatite (HAp), which in its pure form has a formula of $Ca_{10}(PO_4)_6(OH)_2$. But bone mineral has a composition much more complex, in form of poorly-crystalline HAp, which different ionic substitutions (mainly CO_3^{2-}, but also other ions such as Mg^{2+}, Sr^{2+}, Cl^-, F^-, HPO_4^{2-}). For example, using a specific bone type (e.g. mature cortical bone mineral from 2-year-old sheep), careful chemical analysis suggested a formula of $Ca_{7.5}(PO_4)_{2.8}(HPO_4)_{2.6}(CO_3)_{0.6}(OH)_{0.2}$ for the bone mineral[40]. In bone, studies using electron microscopy and X-ray diffraction have revealed that the mineral phase has the shape of elongated apatitic platelets with a thickness of approximately 5 nm and a width of 20-50nm[41]. These platelets are formed by needle-shaped mineral crystals that are laterally aggregated[42]. Importantly, bone mineral is neither pure crystalline nor pure inorganic. It has been demonstrated that platelets consist of a crystalline core covered by an amorphous, hydrated mineral layer[43]. Moreover, different organic anions are found associated with the hydrated layer of platelets, such as citrate[44]. Although citrate has been proposed to bridge different platelets and stabilize the amorphous hydrated layer of bone mineral[44], the factors that drives the aggregation of mineral needles into resulting platelets and how this structural organization is sustained are yet open questions.

1.4.3 | From collagen molecules to fibrils

To understand how mineral platelets assembles into 3D arrays in mature bone structure we need to consider the ultrastructure of collagen fibrils. The basic unit that characterizes collagen proteins is the existence of the collagen triple helix, formed by the intertwining of three alpha (α) chains (Figure 1.5a). The polypeptide sequence and the types of α chains that form the triple helix confer the structural diversity of different types of collagen[45]. In bone the predominant collagen is the type I, which triple helix is formed by the association of two α1(I) chains and one α2(II) chain. In contrast, in cartilage, the predominant collagen is type II, formed by the intertwining of three α2(II) chains[46]. Each α chain has its constituent amino acids arranged in a primary sequence given by the consecutive repetition of the glycine-X-Y triad, where glycine is always present in the third position, and X/Y are occupied by different amino acids. Although these positions are prone to be occupied by any amino acid, approximately 22% of non-glycine residues are proline or hydroxyproline, an amino acid derived from proline resulting from post-translational modifications (addition of hydroxyl groups in the side chain of the amino acid)[47].

The presence of glycine every third position is crucial because its side chain is the smallest among amino acids, consisting of only one hydrogen atom. This compact size facilitates the intertwining of the three α chains that form the triple helix. Specifically, the side chain of glycine residues is directed towards the center of the helix, while the side chains of other amino acids protrude outward from the helix. This unique arrangement creates essential structural motifs that allow collagen to play its biological role in the ECM by generating binding sites for various macromolecules[45]. To maintain stability, the collagen triple helix relies on weak interactions, mainly hydrogen bonds, between the amino group of glycine and the carboxylic groups of amino acids in the α chains. The importance of glycine in the third position is demonstrated by genetic pathologies that occur when this location is altered. For example, osteogenesis imperfecta, or brittle bone disease, that causes extreme bone fragility.

The collagen molecule, or tropocollagen, is composed of a triple helix that is around 300 nm in length and has a molecular mass of about 300 kDa. However, in the ECM, collagen is not present as isolated molecules. Instead, collagen has a unique ability to self-organize into supramolecular structures due to specific molecular binding sites[46]. This results in the lateral self-organization of collagen fibrils, which can form fibers on the order of tens of micrometers. This self-organization is crucial for the stability of collagen under physiological conditions[48]. Additionally, covalent bonds created by enzymatic cross-linking stabilize the extensive arrangements of laterally organized fibrils in each fiber[49]. The way in which collagen fibers associate leads to the hierarchical organization seen in tissues based on this protein, such as the lamellae found in bone tissue (see Figure 1.5).

In the ECM of bone tissue, collagen is found in the form of fibrils (with a thickness on the order of 100 nm and a length of up to 1 µm), which are supramolecular arrangements of collagen molecules aligned along an axis. The axial organization of collagen molecules was first discovered by Hodge and Petruska in 1964. Using TEM to analyze *in vitro* reconstituted collagen fibrils, they observed a repetitive pattern in which a light band alternates with a dark band every ~67 nm along the entire fibril[50]. This pattern arises from the spacing between different collagen molecules, which is referred to as the D-spacing. Hodge-Petruska proposed that the length of each collagen molecule is not an integer multiple of D, but rather around 4.46xD. Along the fibril axis, the collagen molecules are parallel but displaced from one another, resulting in regions of overlap (with a dimension of 0.46xD) and gaps (with a dimension of 0.54xD). The band coloring observed by TEM results from the contrast process with electron-dense elements that penetrate more easily into regions of lower packing of the molecules (the 'gaps'), creating dark bands, while the light bands represent overlap regions. Although this simplistic model by Hodge-Petruska is still valid today, advanced crystallography

techniques have revealed a much more complex superstructure for collagen fibrils. Orgel et al. showed that collagen molecules are not perfectly aligned but organized in a twisted and inclined arrangement[51] (Figure 1.5c).

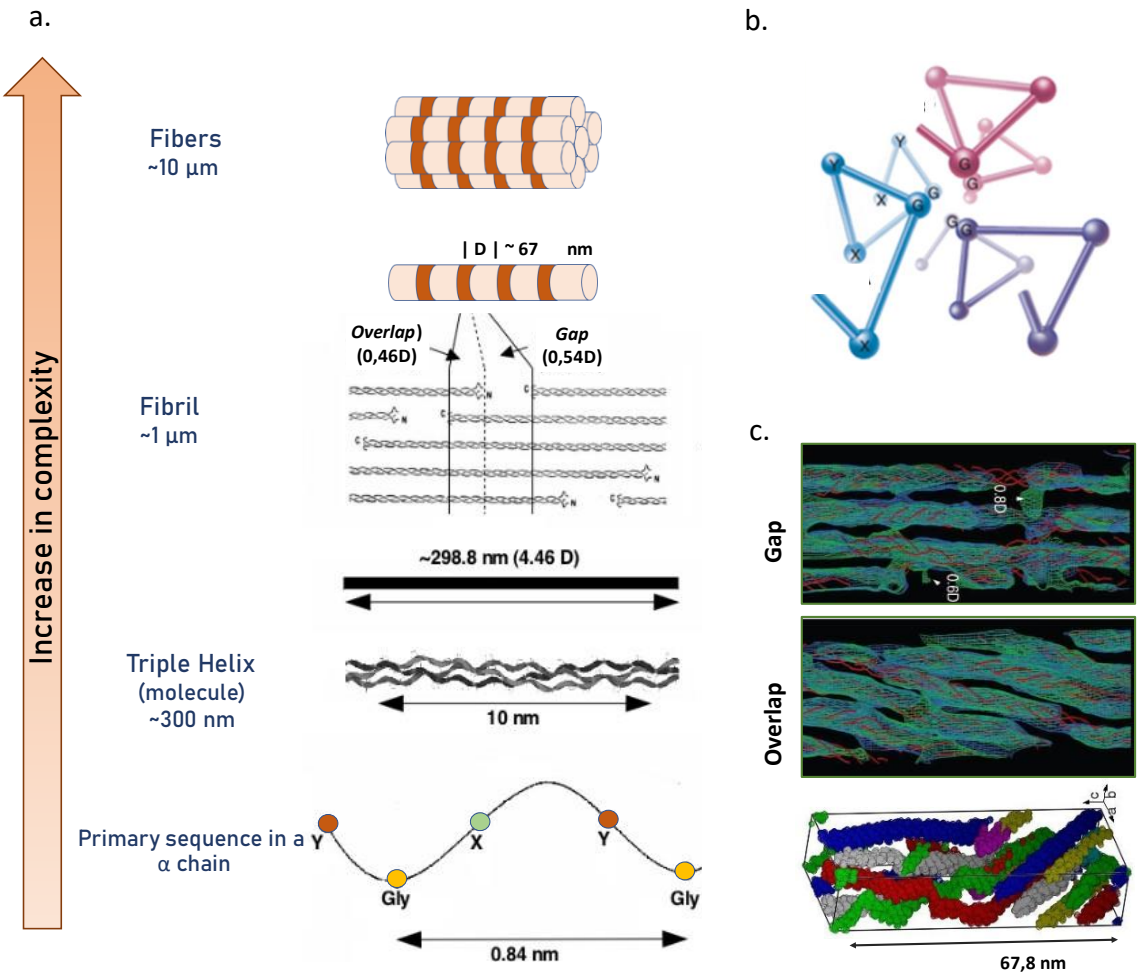

Figure 1.5 | Multi-scale organization of collagen. (a) Schematic view of the hierarchical ordering of collagen, ranging from the primary structure at the molecular scale to collagen fibers with lengths of about 10 µm. (b) In the collagen triple helix, the three polypeptide chains intertwine in such a way that their glycine residues are arranged towards the interior of the molecule, maximizing the intermolecular interactions that stabilize the structure. (c) Electron density maps of collagen fibrils obtained by crystallography. The axial arrangement between different collagen molecules gives rise to the fibril, which are alternating arrangements between overlap and gap regions. Adapted with permission from reference [51].

1.4.4 | Other components of the organic matrix

Although fibrillar collagen is the most abundant protein in terms of mass within the ECM of bone, in terms of molar quantities, other non-collagenous proteins (NCPs) and proteoglycans (PGs) are equally abundant. The local concentration of these components has a direct correlation with the speed of bone tissue formation and an indirect correlation with the packing density of collagen fibrils, demonstrating their significant contribution to bone structure and formation[52].

Non-collagenous proteins. The most studied group of NCPs in bone is the SIBLING protein family (small integrin-binding ligand N-linked glycoproteins), such as osteocalcin, osteopontin, and bone sialoprotein are proteins secreted by bone-forming cells during the maturation and mineralization of their ECM, as comprehensively reviewed elsewhere[53,54]. The main characteristics of these proteins are their high degree of phosphorylation and abundance of acidic residues such as serine, aspartic acid, and glutamic acid. They are also intrinsically disordered proteins, that is, proteins with an irregular, extended conformation and acidic character that facilitate interaction with counter ions and precursor mineral[55]. Therefore, it is believed that the presence of these proteins in the ECM may control various aspects of mineralization, specifically through mechanisms of inhibition and promotion of the process by the interaction between their charged groups and the nascent mineral phase[56]. The abundance of charged groups is thought to affect mineralization in different manners, both promoting nucleation by creating a "Ca^{2+} sponge" to increase the local supersaturation[57], or as an inhibitor, through binding to the nascent mineral phase and thus preventing its further growth[58]. One of the most studied NCP is the osteopontin, a phosphorylated glycoprotein of about 34 kDa that inhibits apatite nucleation and crystal formation[59], so that its deficiency increases mineral content and mineral crystallinity in mouse bone[60].

Proteoglycans. As indicated by their name, these molecules consist of a core protein and a variable number of glycosaminoglycan chains, with their properties depending on the composition and association between these components. Proteoglycans are abundant present in unmineralized (i.e osteoid) matrix, suggesting that they are partly lost during mineralization. This has been confirmed by the biochemical analyses of bone at different stages of mineralization, with an one-fold decrease in the level of PGs from the osteoid to the tissue at the highest degree of mineralization[61]. Although it is clear that PGs are important for bone mineralization, their precise roles remain controversial. Similar to NCPs, several *in vitro* studies have shown both inhibitory and promoter effect on PGs in mineralization[62,63]. Moreover, there are limited quantitative data regarding the distribution and composition of glycosaminoglycans in the bone matrix, that can appear in form of different species, such as chondroitin sulfate, hyaluronan, dermatan sulfate and keratan sulfate. Interestingly, *in vivo* alteration in expression of different PGs affect the mineralization of the ECM[64,65].

1.4.5 | The relationship between collagen and mineral

Despite numerous studies aimed at understanding the structural properties of bone and the relationship between mineral particles and organic matrix components, the exact mechanisms by which bone structure emerges are still a topic of debate. Early ultrastructural investigations on bone revealed that mineral platelets are periodically related to the periodic banding of collagen fibrils[66]. The mineral reinforces the collagen periodic banding due to its intrinsic electron density, acting as a 'negative stain'. In addition, during mineralization, collagen fibrils aggregate side by side in lateral register, causing their hole zones to be in register as well, resulting in transverse, electron-dense bands that cross the collagen bundles[41]. This phenomenon is due to the location of the mineral within the collagen fibrils in a process called *intrafibrillar mineralization*. Intrafibrillar mineralization occurs in which mineral platelets lie morphologically and crystallographically parallel throughout a fibril, contained within the 'holes' of the collagen gap regions[67,68].

Intrafibrillar mineralization has received significant attention in the study of bone mineralization mechanisms. However, the precise mechanisms by which collagen mediates intrafibrillar mineralization remain a topic of debate, as comprehensively reviewed[69–71]. Although some authors have proposed that aminoacids in the gap region of collagen could interact with mineral ions and initiate nucleation[72,73], the direct mineral nucleation by collagen fibrils occurs at a minor extent *in vitro*[74]. Therefore, the most prevalent hypothesis is the infiltration of mineral precursors into the collagen fibril. This hypothesis was developed after the seminal study of the Gower group, that developed an *in vitro* model using negatively charged polymers as an inhibitor to prevent bulk precipitation of calcium phosphate and recreating intrafibrillar mineralization of collagen fibrils in supersaturated solutions[75]. In this model, negatively charged polymers, such as polyaspartic acid, is thought to mimic the effect of NCPs, where its interaction with mineral ions results in the formation of a negatively charged liquid-like mineral precursor[75]. This mineral precursor can then electrostatically interact with the gap region of collagen, which contains positively charged domains, facilitating infiltration of ACP into the fibril, that later transforms into crystalline apatite[74]. Mineral infiltration is the result of a balance between electrostatic interactions and osmotic equilibrium within the collagen fibril[76]. Moreover, the ultrastructure of the gap region provides intermolecular channels that control and define the size and orientation of the apatite crystals formed inside the fibril[42]. The importance of intrafibrillar mineralization for bone has been recently demonstrated at the functional level, with the mineral grown inside collagen fibrils creating contractile stresses, thereby significantly contributing to the mechanical properties of bone[77].

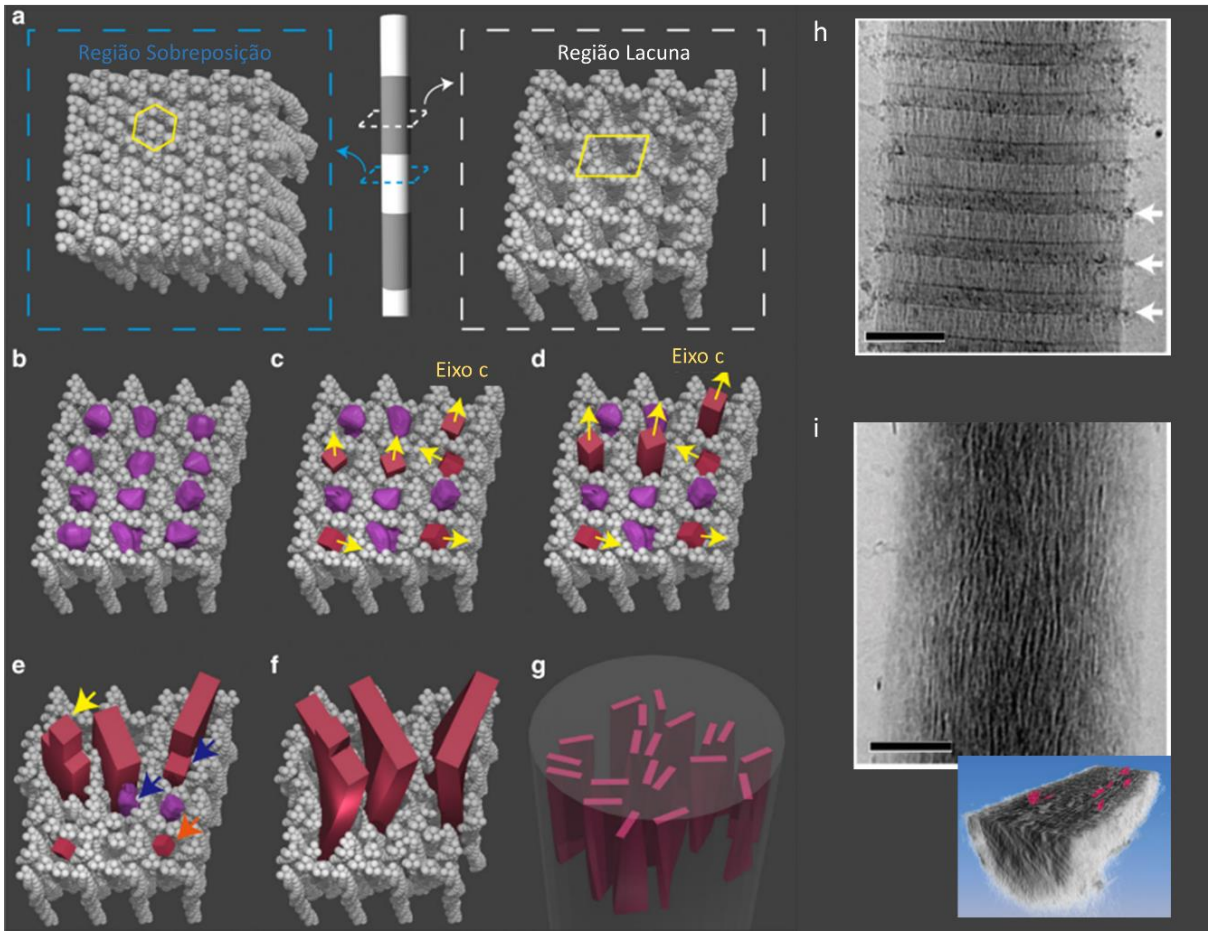

Figure 1.6 | Mineralization of collagen fibrils. The collagen fibril is formed by overlapping and gap regions that intercalate along the fibril axis (a). Calcium phosphate precursor infiltrates from the gap regions of the fibril (b). The ultrastructure of the collagen fibril creates a confined environment where apatite crystals are formed from the infiltrated ACP, giving rise to oriented nanocrystals with their c-axis parallel to the long axis of the collagen fibril (c-g). Transmission electron microscopy image of in vitro mineralized collagen fibrils (h). The dark spots show ACP infiltrating the gap region of the fibril, giving rise to the apatite crystals inside the fibril (i). Image adapted with permission from references 7 and 71.

However, electron microscope studies have shown that the bone mineral is only partly intrafibrillar, while it is mostly located in the extrafibrillar space, in a ratio of about 75% extrafibrillar as identified in one study[78]. While some authors have proposed that extrafibrillar mineral is the result of an overgrowth of intrafibrillar minerals, others have challenged this idea by proposing that mineral is located mainly between collagen fibrils[79,80]. In fact, as bone has a 3D structure, it is now clear that in 2D projections the observed mineral organization will depend on the orientation of the analysed section. In a comprehensive paper, Reznikov and colleagues demonstrated that bone mineral organization is more more complex than simply classified as intra or extrafibrillar mineralization[81]. Bone mineral organization is a fractal-like assembly, where needle-shaped mineral units merge laterally to form platelets, and these are further organized into stacks of roughly parallel platelets. These stacks coalesce into aggregates

that exceed the lateral dimensions of the collagen fibrils and span adjacent fibrils as continuous, cross-fibrillar mineralization[81]. Although much is know about the ultrastrucural features of collagen (the intermolecular channels within a single collagen fibril) that shape the crystals formed intrafibrillary[42], much less is know about the factors that drives cross-fibrillar mineralization. Most evidence points for the participation of different proteins present within the ECM (such as NCPs and proteoglycans) as the key players in the process[82–84].

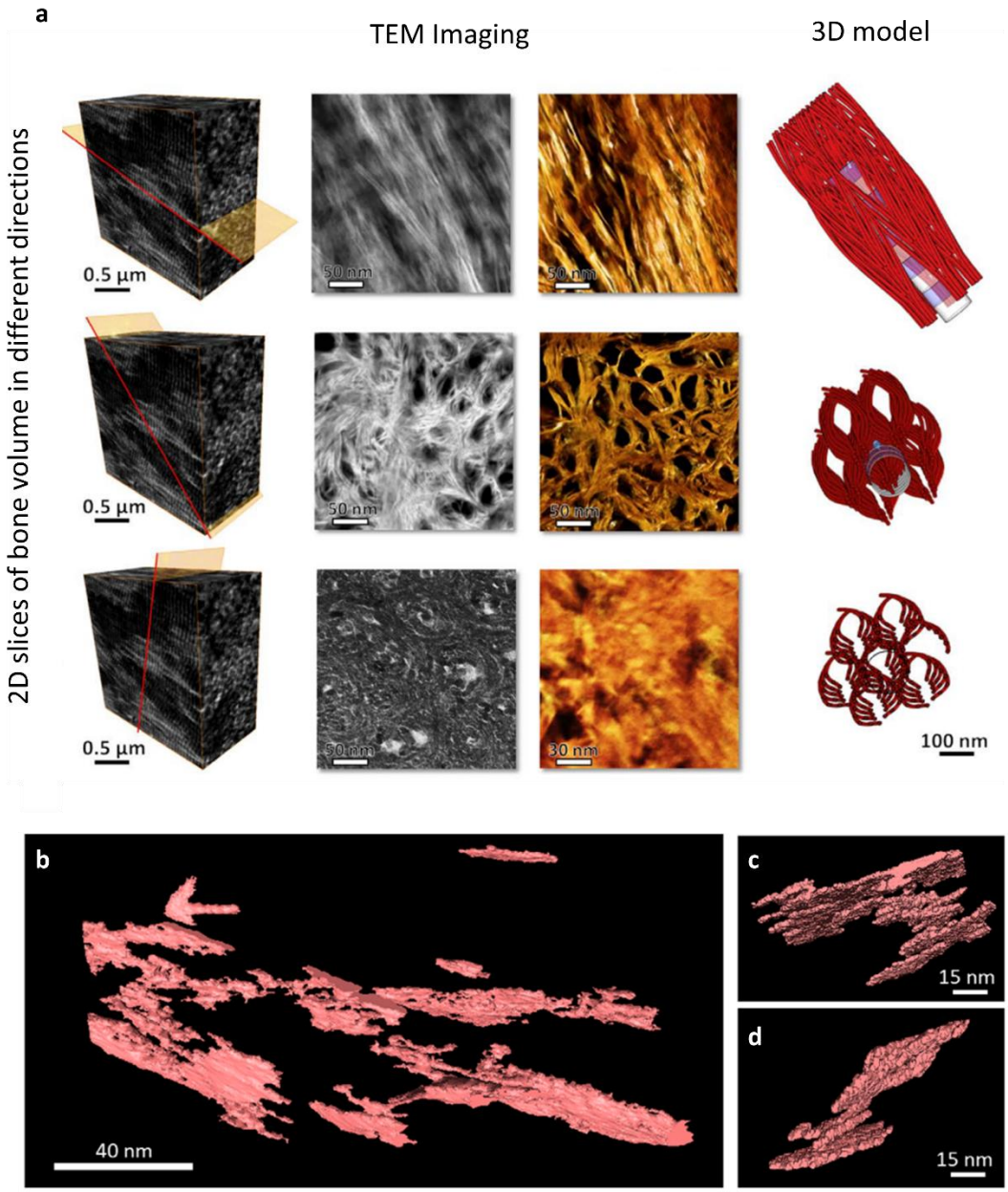

Figure 1.7 | Fractal-like organization of mineral in bone. A) 2D projections obtained from TEM of a thin specimen with respect to the ordered array of mineralized collagen fibrils in lamellar bone. The first column in the panel shows the orientation regarding the 3D bone volume that the thin specimen was retrieved. The last column of panels features a simplified 3D model of bone apatite crystals (in red) viewed in three different projections: in-plane, out-of-plane, and edge-on views. Panels B-D shows different 3D reconstructions of the apatite crystals observed in bone. Notice the confluence of mineral from the assembly of different individual platelet-shaped crystals, and that in three dimensions almost all mineral aggregates shows a twist. Adapted with permission from reference [81].

1.5 | The cell-matrix interface: the appearance of a mineralization front

Independently of the type of bone being formed, the sequence of events usually involves cells (either an osteoblast or and chondrocyte) first elaborating an ECM and the mineral then being introduced into the matrix. In bone the preformed organic matrix is often referred to as osteoid, and since the early days of electron microscopy examinations of bone mineralization, the boundary between the unmineralized collagen fibrils of the osteoid tissue and the mineralized matrix is called *mineralization front*[85]. This interface is therefore a key location for understanding mineralization processes (Figure 1.8a). Under the electron microscope at this site, the prevalent image corresponds to the presence of roundish or elongated aggregates referred to as "calcification nodules" or "calcification islands" (Figure 1.8b). Calcification nodules are found in the interfibrillar spaces, and their size varies. As the degree of mineralization increases, the number of crystals within the calcification nodules also increases until they eventually coalesce. The calcification islands, on the other hand, are often seen running to the axis of the collagen fibrils, indicating a possible relationship between their formation and the fibril surface. In the literature, different names have been used to describe these mineralization patterns observed in the mineralization front, as comprehensively recently reviewed[86,87]. The appearance of these mineralization pattherns seems to be intimately related with different components, such as proteoglycans, non-collagenous proteins and membrane vesicles (Figure 1.8d). Recently, using 3D imaging approaches, these mineralization patterns have been collectively termed as a mineral tessellations (Figure 1.8e), demonstrated to be ubiquitously present in mineralizing tissues[86]. Here, a commonly observed phenomenon is mineralization that begins as discreet and evenly dispersed mineral foci within the unmineralized extracellular matrix (ECM). Various observations across different types of bones have shown that the distance between the smallest mineral foci and the mature mineralized ECM in the most recently deposited collagen is approximately 2-3 μm[88–90]. As mineralization progresses, crystals grow, propagate, and increase in number from the initial mineral foci in radial manner within the osteoid, resulting in a recurrent crossfibrillar mineralization tessellation pattern. Once the initial mineral focci is nucleated, it follows a sperulitic-like growth to form each individual ellipsoid with average dimensions of about 1.6 × 0.8 × 0.8 μm[39,83,87].

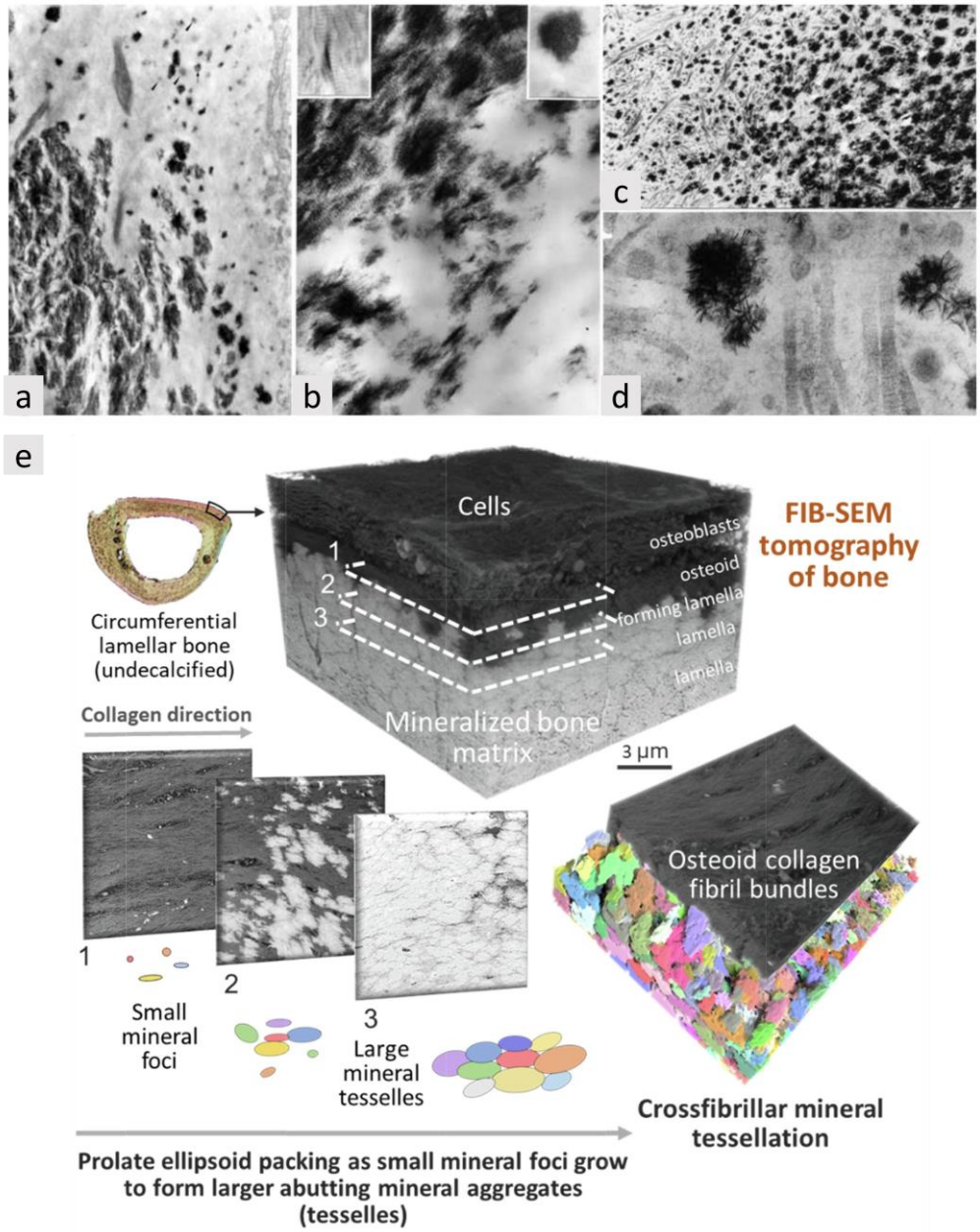

Figure 1.8 | The mineralizing front. a) Typical electron microscopy observation of a mineralization front, where the degree of mineralization increases going from right to left, as isolated calcification nodules increase in size and coalesce. Part of an osteoblast in shown in right side of the image. b) Detail of a mineralization front where can be identified calcification islands (one shown at the upper left corner) and calcification nodules (one shown at the upper right corner). c) Another example of a mineralization front consisting of numbers of calcification nodules that increase in size and coalesce (right) as the degree of mineralization increases, showing that it represents a repetitive patthern among different species and bone types. d) Detail of calcification nodules and uncalcified matrix vesicles (that will be defined later) at the mineralization front, where a few unmineralized collagen fibrils are also evident Panels a-d were adapted with permission from reference [91]. e) Current understanding of mineralization front described as a mineral tessellation pattern. 3D maps of the mineralization front were reconstructed using FIB-SEM tomography. Small mineral foci located within the collagen fibril bundles of the osteoid grow and enlarge into elipsoids (tesselles) that abut against one another to form a crossfibrillar mineral tessellation pattern. Different slices obtained from the tissue related to the cell-osteoid interface (1) up to the fully mineralized matrix (3) reveals the evolution in the crossfibrillar mineralization. To a rough geometric approximation, bone mineral tesselles are generally discrete ellipsoids with average dimensions of about 1.6 × 0.8 × 0.8 µm, but they do not merge together, leaving intervening gaps up to 100–200 nm between adjacent tesseles. Image adapted with permission from reference [86].

An intriguing observation is that individual mineral elipsoids do not merge together, leaving intervening gaps up to 100–200 nm of unmineralized matrix. In fact, the existence of these discreet mineral elipsoids within the bone matrix is now recongnized as an mesoscale hierarchical level within the bone structure (see Figure 1.4). The limited size variation of mineral ellipsoids can be understood from a time-resolved sequence of their initiation as small foci of more-or-less simultaneous and generally evenly dispersed heterogeneous nucleation events within the osteoid. Mckee and colleagues recently proposed that the transition from initial foci evenly dispersed in the matrix to mature mineral elipsoids within a range of just few micrometers might reflect that mineralization occurs within a relatively narrow window near the mineralization front, where conditions are just optimal enough[86]. These conditions seems to be related the disponibility of mineral ions and balance of promoters and inhibitors of mineralization within the ECM. Therefore, the existence of boundaries of unmineralized matrix between mineral elipsoids could be due to the local peripheral accumulation of mineral-bound inhibitors and lack of access to additional mineral ions and promoters[86].

However, little is known about the logistics by which Ca^{2+} and Pi ions are concentrated within the mineralization front, nor the factors that trigger initial nucleation. Several observations have been made in this direction, but a comprehensive picture remains to be obtained. These pathways might include the translocation of intracellular mineral precursors to the ECM[92], a direct connection between bone and the vasculature to transport mineral precursors from the blood[20,22], or the involvment of extracellular vesicles. As bone mineralization is a highly complex physiological process, it is expected that there are certain redundancies, and these different pathways might coexist depending on the specific requirements of the tissue type and its developmental stage.

1.6 | Matrix vesicles as players in the mineralization front

In 1967, two seminal studies used electron microscopy to examine the mineralizing front in endochondral bone and discovered membrane-bound vesicles embedded within the collagenous matrix just before the onset of mineralization[93,94]. These structures were later coined as matrix vesicles (MVs) due to their specific interaction within the ECM of bone tissue. When inspecting the mineralization front, many MVs can be found coinciding with the earliest crystals within the ECM (Figure 1.9a). These crystals appear to be associated in an out the membrane of MVs (Figure 1.9b-d), suggesting that these structures play a major role in the process. A breakthrough came with the confirmation that these vesicles showed enriched alkaline phosphatase on their membranes[95,96], as was extensively confirmed in different studies

(Figure 1.9e). Therefore, these initial observations led to the hypothesis that MVs provide an appropriate microenvironment for the onset of mineralization. Although an extensive body of work has been accumulated over the years attempting to delineate the molecular mechanism by which MVs operate, many aspects of their mode of action remain to be determined. Comprehensive reviews can be found in the literature about MVs[97–99].

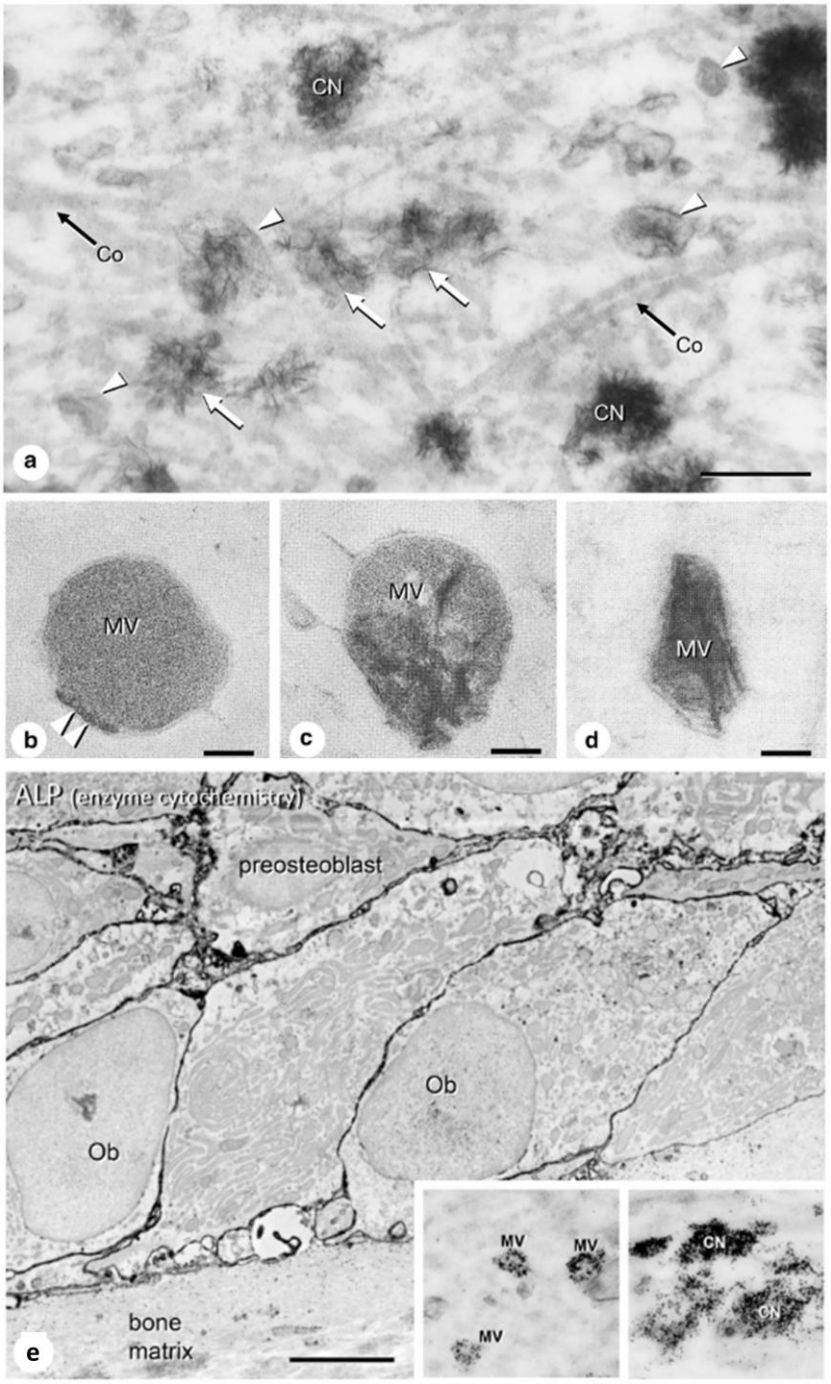

Figure 1.9 | Ultrastructural observation of MVs. a) Electron microscopy image of MVs (white arrowheads), incipient calcifying nodules (white arrows) and collage fibrils (Co) in osteoid. The initial stage of calcifying nodules (white arrows) includes growing assemblies of mineral crystals and vesicles. Mineral can be observed interacting with the membrane of MVs (b), inside (c) and also with ruptured vesicles (d). Bars, a 500 nm, b–d 30 nm. e) Enzyme cytochemistry at an electron microscopic level demonstrate an intense reactivity for alkaline phosphatase (black deposits) on the cell membranes as well as on MVs and calcifying nodules (CN). Bar, 2 µm. Adapted with permission from reference [100].

1.6.1 | The biogenesis of MVs

MVs are a class of extracellular vesicles secreted by mature mineralizing cells coincidently with the first observation of ECM mineralization[101,102]. MVs are currently described to be originated from the polarized apical side of the plasma membrane of mature mineralizing cells[98]. There is morphological evidence for this, as using freeze-fracture studies, where some vesicles could be observed to be forming by budding and then pinching off from the membrane of cells mediating mineralization[103,104]. Moreover, isolated MVs were demonstrated to display a similar protein and lipid composition compared to the microvilli of osteoblasts[105]. Further proteomic analysis of isolated MVs also demonstrated the presence of several markers for plasma microvilli, including TNAP, 5′-nucleotidase, annexins (AnxA2, AnxA5, AnxA6), transporters (e.g., Na^+/K^+ ATPase, monocarboxylate transporter 1, transient receptor potential channel V member 4), and receptors (e.g., scavenger receptor class B, integrin alpha-V, glycoprotein HT7, CD9)[106,107]. Furthermore, lipidomic analysis of MVs isolated from chondrocytes also confirmed a similar composition of fatty acids in microvilli-like membranes and MVs[108]. Although these studies strongly suggest the plasma membrane of MVs as a biogenesis route, the precise pathways remain to be defined.

1.6.2 | The function of MVs

The proposed role of MVs in bone mineralization is to act as a nanoreactor that accumulates Ca^{2+} and Pi ions, resulting in the precipitation of HAp crystals once a certain threshold is reached. To perform this function, MVs are described to be enriched with proteins and lipids that are involved in mineralization. These include various Ca^{2+}-binding molecules, such as annexins and phosphatidylserine, as well as different phosphatases, which will be discussed in detail below.

The recurrent observation of minerals associated with both the inner and outer membrane of MVs at the ultrastructural level (as shown in Figure 1.9b-d) has led to the postulation of a biphasic model to explain MV-mediated mineralization[109,110]. According to this model, HAp is first formed within the lumen of MVs, and only after membrane rupture, the crystals are released into the extravesicular medium. This model is based on a combination of observations of MVs at the ultrastructural level and the dissection of the content (proteins and lipids), and the functionality (i.e., ability to trigger mineralization) of isolated MVs. The study of MV-mediated mineralization *in vitro* will be detailed in Chapter 2. For now, we will present

the current understanding of the proteins involved and how they are proposed within MVs (as shown in Figure 1.10).

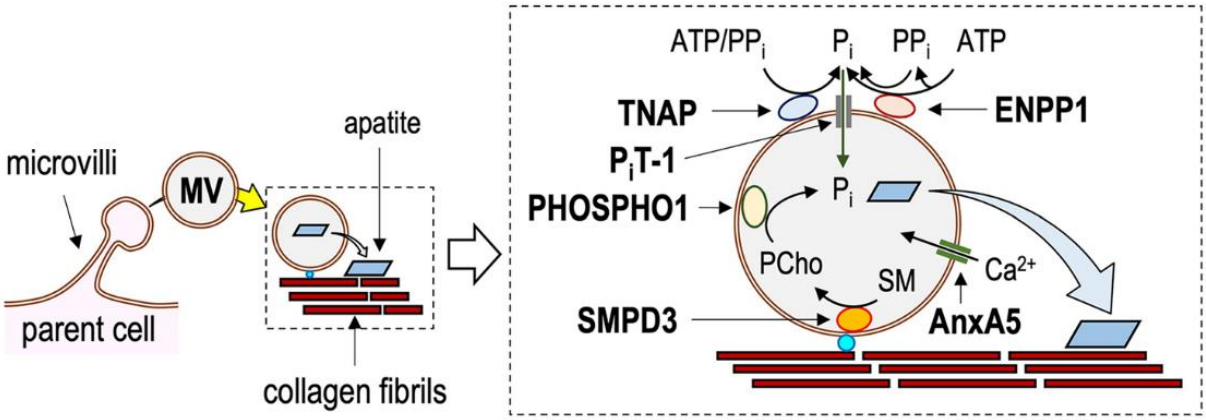

Figure 1.10 | The biochemical machinery of MVs. MVs are proposed to be released by outward budding from the apical microvilli of mineralization-competent cells and are equipped with the biochemical machinery necessary to bind to collagen fibrils and to allow the intraluminal accumulation of Pi and Ca^{2+} to trigger apatite formation. Different enzymes and proteins are present within MVs that can operate both to locally control the Pi/PPi ratio permissive for mineralization, as well as to accumulate Ca^{2+} and Pi necessary for the mineralization. Pi/PPi ratio are orchestrated by the concerted action of three phosphatases: alkaline phosphatase (TNAP), nucleotide pyrophosphatase (ENPP1) and Phospho1. In addition, MVs are enriched in annexins (such as AnxA5) as well as phosphatidylserine, both molecules with Ca^{2+}-binding properties. Intraluminal Pi accumulation is also thought to occur though the action of a Pi transporter (PiT-1). Imaged adapted with permission from reference [111].

In order to start mineralization within the lumen of MVs, Ca^{2+} and Pi ions must be transported from the extravesicular medium across the bilayer. As there is until now no evidence of any voltage-gated Ca^{2+} channel operating in MVs[97], the transport of Ca^{2+} are proposed to be mediated by annexins, a family of ubiquitous proteins (~35 kDa; exceptionally ~70 kDa for A6), which bind Ca^{2+} and interact with phospholipids (e.g. phosphatidylserine) in a Ca^{2+}-dependent manner[112]. Early biochemical dissection revealed these proteins to be dominant within MVs isolated from embryonic chicken bones[113]. Proteomic analysis of various MVs preparations further confirmed the presence of several annexins, with A5, A6, and A2 being particularly abundant[106,107]. However, the precise mechanisms by which annexins acquire Ca^{2+} within MVs are not yet fully understood. While some studies proposed that annexins could insert themselves into the lipid bilayer and function as Ca^{2+} channels within MVs[114,115], their abundance in these structures surpasses what would be necessary for this role alone[97]. Thus, the role of annexins in Ca^{2+} acquisition may encompass diverse mechanisms beyond Ca^{2+}-channelling. Interestingly, Veschi et al.[116] recently demonstrated that AnxA6 has the ability to translocate across the membrane of MVs, providing an intriguing avenue for further research.

The most in depth exploited functionality of MVs is their enrichment on phosphatase enzymes, remarkable TNAP, ENPP1 and Phospho1[117]. The major player in this phosphatase

system is the enzyme TNAP, that was already introduced along this chapter, and operate in the outer surface of MVs. TNAP is an enzyme that has phosphomonoesterase activity, meaning it produces Pi from the hydrolysis of any phosphorylated substrate, such as adenosine triphosphate (ATP) or pyrophosphate (PPi), or even can dephosphorylate proteins, such as osteopontin[118]. TNAP is a member of a protein family that includes different isoforms of this enzyme distributed in almost all tissues[119]. Encoded by the ALPL gene, TNAP is expressed at higher levels in the liver, bone, and kidney, earning it the name tissue-nonspecific. The other three isoforms are tissue-specific: placental alkaline phosphatase (PLAP, *ALPP* gene), germ cell alkaline phosphatase (GCAP, *ALPP2* gene), and intestinal alkaline phosphatase (IAP, *ALPI* gene). As we discussed in section 1.3, mineralization is a physiological process limited to cartilage and bone, since it necessitates a specific extracellular matrix (collagen) as a template for mineral deposition, and the concurrent expression of TNAP and fibrillar collagens only takes place in areas of bone formation[24]. Activation of TNAP expression have been associated to different pathological vascular calcifications[120,121]. TNAP is situated in the outer surface of MVs attached by a glycosylphosphatidylinositol (GPI) anchor[118]. There, it has a major role to degrade PPi, removing its inhibitory effect to create a microenvironment permissive for mineralization. Loss-of-function mutation in TNAP is associated with different mineralization disorders[13]. Interestingly, Anderson and colleagues investigated the growth plate cartilage at the ultrastructural level from patients with perinatal (lethal) hypophosphatasia and found that MVs were normally present in the ECM and containing luminal apatite-like mineral but failed to vectorially spread throughout the matrix[122].

In concerted action to TNAP, a second phosphatase enzyme, the nucleoside pyrophosphatase/phosphodiesterase 1 (NPP1) work to control controls the Pi/PPi ratio within the extracellular environment[123]. This enzyme stands out for its ability to hydrolyse ATP to generate PPi, creating another level of regulation in the Pi/PPi ratio permissive for mineralization[124]. Failures in NPP1 expression result in abnormalities related to bone hypermineralization and pathological mineralization of soft tissues, including arterial calcification[123]. Moreover, not only producing PPi, NPP1 can also operate as a phosphatase enzyme to directly produce Pi[125].

Pi generated in the extravesicular space by the concerted action of TNAP and NPP1 is thought to reach the lumen of MVs through the action of a Pi transporter, the type III Na/Pi co-transporter (PiT-1), encoded by the *Slc20a1* gene[126]. The presence of Na/Pi co-transporters in MVs was inferred from the importance of these transporters in mineralizing cells[126,127]. However, several proteomic studies have been unable to detect PiT-1, PiT-2, nor any other sodium-coupled phosphate transporter within MV[106,107,128]. Furthermore, no sodium gradient

exists within MVs[129] and there are controversial results regarding the dependence on Na^+ for *in vitro* mineralization of MVs[130,131]. Therefore, there is still much work to be done in order to determine the transporter(s) involved in Pi influx on MVs.

The most compelling evidence for an intraluminal production of Pi is through the action a third phosphatase, the orphan phosphatase 1 (Phospho1), demonstrated to be specifically located in mineralizing regions of skeletal tissue[132]. The presence of Phospho1 in MVs was extensively demonstrated[102,133]. Phospho1 is proposed to operate within MVs by generating Pi from the hydrolysis of phosphocholine (PC) and phosphoethanolamine (PE)[134]. A recent study employing spatial metabolomics in mice growth plate confirmed the involvement of lipid metabolites related to PC and PE in mineralizing regions[135]. An intriguing discovery from a spectroscopic study is that choline can be integrated into the bone mineral, providing further evidence for their involvement in bone mienralization[136]. However, the mechanisms underlying the production of Phospho1 substrates within MVs are yet to be fully elucidated, and may entail the involvement of various enzymes co-existing in MVs, including sphingomyelinases and other phospholipases[137,138].

Although these different phosphatases in MVs operate to control Pi homeostasis within the ECM, their non-redundant role was demonstrated by analysing the phenotype in mice where these enzymes are single or double knocked-out[117]. In these animal models, it was demonstrated the recurrent phenotype where the ablation of one enzyme results in defective skeletal mineralization, implying that the concerted action among them is important for proper ECM mineralization. Interestingly, at the ultrastructural level, it appears that crystals can still be found in and out of the membrane of MVs but fail to propagate towards a fully mineralized ECM (Figure 1.11), in a manner that resembles a defective mineral crossfibrillar tessellation, as described in the section 1.5. An outstanding observation is that the absence of both TNAP and Phospho1 completely blocks the formation of a mineralized skeleton, indicating that the ability of MVs to enzymatically control the availability of Pi within the ECM is a fundamental requirement for bone mineralization[139].

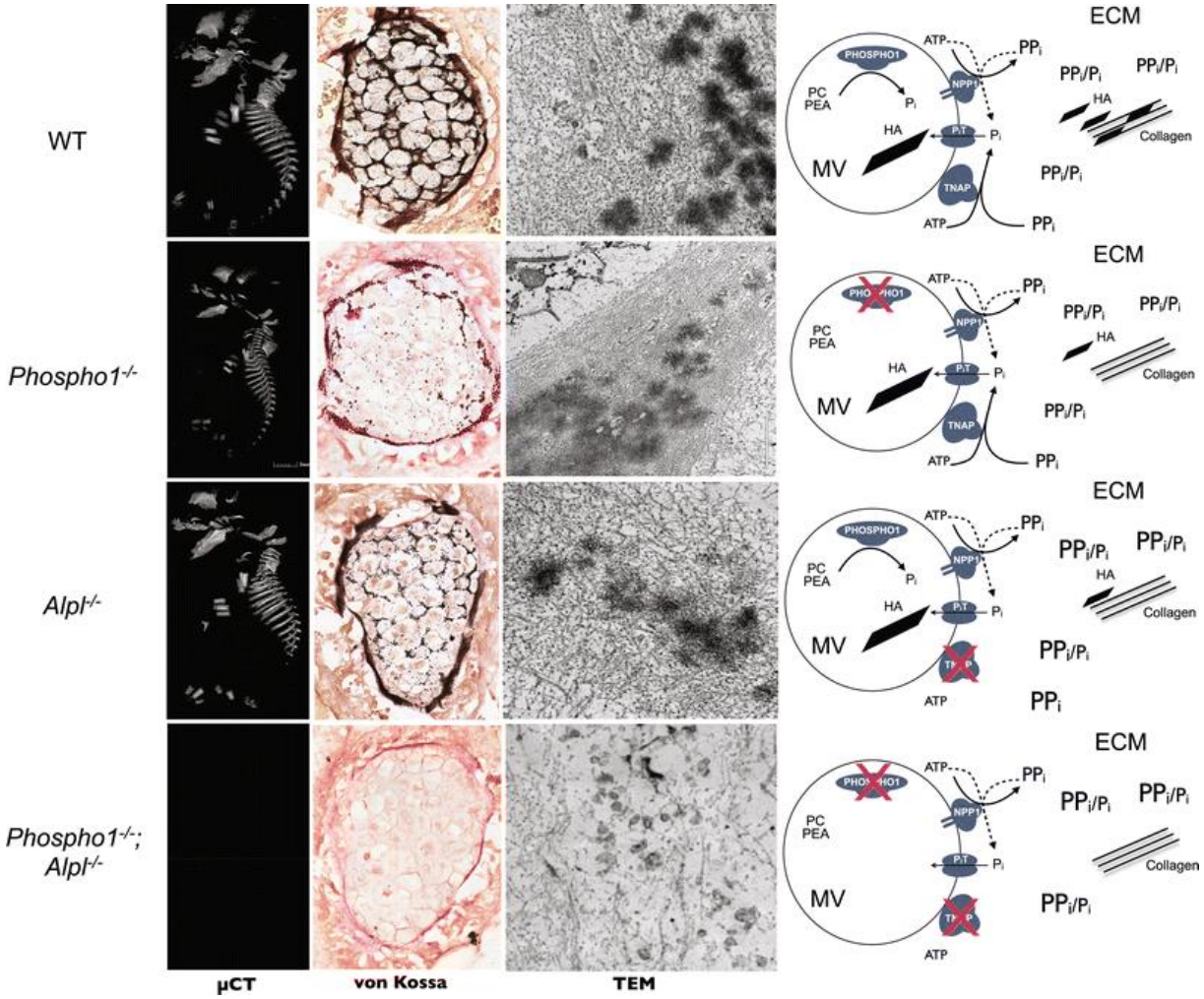

Figure 1.11 | The role of phosphatases in the initiation of skeletal mineralization. Pi concentration can be manipulated by phosphatases operating in the outer membrane of MVs (TNAP and NPP1) or within the lumen (Phospho1). Mineralization in different animal models was assessed at the skeletal level by tomography (µCT), at the histological level by mineral staining (von Kossa), and at the ultrastructural level by electron microscopy (TEM). In wild-type (WT) mice, mineralization is normal and involves intravesicular Pi generation by Phospho1 and influx of Pi, generated extravesicularly by TNAP and NPP1. Extravesicular propagation occurs on collagen scaffolds facilitated by the pyrophosphatase function of TNAP and NPP1. Ablation of TNAP and Phospho1 results in defective mineralization, while in double knocked-out [Phospho1 –/–; Alpl –/–] mice, complete absence of skeletal mineralization is observed. In the right panel, the underlying biochemical pathways involved are schematized. See the reference for a detailed explanation. The image is adapted with permission from the reference [117].

1.7 | Motivation and thesis outline

Since their seminal discovery in the late 1960s, a large body of evidence has accrued for the participation of MVs in the initiation of bone mineralization. MVs are hypothesized to facilitate mineralization by transporting and targeting cargo to the preformed collagenous matrix, where they act as a compartmentalized environment within which Ca^{2+} and Pi may accumulate to trigger the formation of mineral that further propagate into the ECM. However, we still have many questions, and several aspects of the underlying mechanism regarding both the origin and function of MVs remain to be determined. The difficulty in studying MVs is that it requires a multidisciplinary approach, where not only biochemical aspects must be taken into account, but also the use of physical-chemistry approaches to understand the product of their functionality: the mineral phase. Moreover, any proposed model for the mechanism by which MVs trigger mineralization needs to realize that, in fact, it is operating on the nanoscale level of a single vesicle. Therefore, the challenge is to properly translate bulk observations when analyzing a pool of isolated MVs or the phenotype in an *in vitro*/*in vivo* model to the underlying mechanisms.

This thesis aimed to examine the interplay between MVs and forming mineral during bone mineralization at three levels: individual vesicle observation, mineralization at the interface of a membrane-like model, and *in vitro* mineralization using osteoblasts culture.

In Chapter 2, our aim was **to identify the primary factors driving MVs mineralization**. To achieve this, we combined bulk characterizations of isolated MVs with single-vesicle nanoscale imaging. This allowed us to examine the relationship between vesicles and forming mineral.

Moving to Chapter 3, we set out **to recreate the ability of lipids within the membrane of MVs to mediate mineral nucleation**. To accomplish this, we developed a biomimetic model of the MV membrane and used it to examine mineralization at an interfacial level.

Finally, in Chapter 4, the goal was **to investigate the requirement for mineralization-competent MVs to mediate mineralization** at a tissue culture level. For this, we isolated and characterized MVs from an in vitro osteoblast culture where mineralization is impaired due to treatment of cells with an autophagy inhibitor.

1.8 | References

1. Long, F. Building strong bones: Molecular regulation of the osteoblast lineage. *Nat. Rev. Mol. Cell Biol.* **13**, 27–38 (2012).

2. Robling, A. G. & Bonewald, L. F. The Osteocyte: New Insights. *Annu. Rev. Physiol.* **82**, 485–506 (2020).

3. Xu, F. & Teitelbaum, S. L. Osteoclasts: New Insights. *Bone Res.* **1**, 11–26 (2013).

4. Yin, X. *et al.* Autophagy in bone homeostasis and the onset of osteoporosis. *Bone Res.* **7**, (2019).

5. Hartmann, C. & Yang, Y. Molecular and cellular regulation of intramembranous and endochondral bone formation during embryogenesis. in *Principles of Bone Biology* 5–44 (Elsevier, 2020).

6. Maes, C. & Kronenberg, H. M. Bone Development and Remodeling. in *Endocrinology: Adult and Pediatric* 1038–1062.e8 (Elsevier, 2016).

7. Kovacs, C. S. *et al.* The role of biomineralization in disorders of skeletal development and tooth formation. *Nat. Rev. Endocrinol.* **17**, 336–349 (2021).

8. Sivaraj, K. K. & Adams, R. H. Blood vessel formation and function in bone. *Dev.* **143**, 2706–2715 (2016).

9. Goldstein, D. A. Serum Calcium. In: *Clinical Methods: The History, Physical, and Laboratory Examinations*. **3rd**, 677–679 (1990).

10. Chande, S. & Bergwitz, C. Role of phosphate sensing in bone and mineral metabolism. *Nat. Rev. Endocrinol.* **14**, 637–655 (2018).

11. Fleish, H. & Neuman, W. F. Mechanisms of calcification: role of collagen, polyphosphates, and phosphatase. *Am. J. Physiol. Content* **200**, 1296–1300 (1961).

12. Orriss, I. R. Extracellular pyrophosphate: The body's "water softener". *Bone* **134**, 115243–115252 (2020).

13. Collins, M. T. *et al.* Skeletal and extraskeletal disorders of biomineralization. *Nat. Rev. Endocrinol.* **18**, 473–489 (2022).

14. Garimella, R., Bi, X., Anderson, H. C. & Camacho, N. P. Nature of phosphate substrate as a major determinant of mineral type formed in matrix vesicle-mediated in vitro

mineralization: An FTIR imaging study. *Bone* **38**, 811–817 (2006).

15. Omelon, S., Ariganello, M., Bonucci, E., Grynpas, M. & Nanci, A. A review of phosphate mineral nucleation in biology and geobiology. *Calcif. Tissue Int.* **93**, 382–396 (2013).

16. Heiss, A., Pipich, V., Jahnen-Dechent, W. & Schwahn, D. Fetuin-A Is a Mineral Carrier Protein: Small Angle Neutron Scattering Provides New Insight on Fetuin-A Controlled Calcification Inhibition. *Biophys. J.* **99**, 3986–3995 (2010).

17. Jahnen-Dechent, W. *et al.* Mud in the blood: the role of protein-mineral complexes and extracellular vesicles in biomineralisation and calcification. *J. Struct. Biol.* **212**, 107577–107589 (2020).

18. Jahnen-Dechent, W., Schäfer, C., Ketteler, M. & McKee, M. D. Mineral chaperones: a role for fetuin-A and osteopontin in the inhibition and regression of pathologic calcification. *J. Mol. Med.* **86**, 379–389 (2008).

19. Jahnen-Dechent, W., Heiss, A., Schäfer, C. & Ketteler, M. Fetuin-A regulation of calcified matrix metabolism. *Circ. Res.* **108**, 1494–1509 (2011).

20. Kerschnitzki, M. *et al.* Transport of membrane-bound mineral particles in blood vessels during chicken embryonic bone development. *Bone* **83**, 65–72 (2016).

21. Haimov, H. *et al.* Mineralization pathways in the active murine epiphyseal growth plate. *Bone* **130**, 115086–115095 (2020).

22. Akiva, A. *et al.* Intercellular pathways from the vasculature to the forming bone in the zebrafish larval caudal fin: Possible role in bone formation. *J. Struct. Biol.* **206**, 139–148 (2019).

23. Reznikov, N. *et al.* Biological stenciling of mineralization in the skeleton: Local enzymatic removal of inhibitors in the extracellular matrix. *Bone* **138**, 115447–115461 (2020).

24. Murshed, M., Harmey, D., Millán, J. L., McKee, M. D. & Karsenty, G. Unique coexpression in osteoblasts of broadly expressed genes accounts for the spatial restriction of ECM mineralization to bone. *Genes Dev.* **19**, 1093–1104 (2005).

25. Meldrum, F. C. & Cölfen, H. Controlling mineral morphologies and structures in biological and synthetic systems. *Chem. Rev.* **108**, 4332–432 (2008).

26. Gebauer, D. & Wolf, S. E. Designing Solid Materials from Their Solute State: A Shift in Paradigms toward a Holistic Approach in Functional Materials Chemistry. *J. Am. Chem. Soc.* **141**, 4490–4504 (2019).

27. De Yoreo, J. J. *et al.* Crystallization by particle attachment in synthetic, biogenic, and geologic environments. *Science.* **349**, aaa6760–aaa6769 (2015).

28. Fleisch, H. Role of Nucleation and Inhibition in Calcification. *Clin. Orthop. Relat. Res.* **32**, 170–182 (1964).

29. Dean, M. N. *et al.* Mineral homeostasis and regulation of mineralization processes in the skeletons of sharks, rays and relatives (Elasmobranchii). *Semin. Cell Dev. Biol.* **46**, 51–67 (2015).

30. Meldrum, F. C. & Cölfen, H. Controlling mineral morphologies and structures in biological and synthetic systems. *Chem. Rev.* **108**, 4332–4432 (2008).

31. Kahil, K., Weiner, S., Addadi, L. & Gal, A. Ion Pathways in Biomineralization: Perspectives on Uptake, Transport, and Deposition of Calcium, Carbonate, and Phosphate. *J. Am. Chem. Soc.* **143**, 21100–21112 (2021).

32. Habraken, W. J. E. M. *et al.* Ion-association complexes unite classical and non-classical theories for the biomimetic nucleation of calcium phosphate. *Nat. Commun.* **4**, 1507–1519 (2013).

33. Wergedal, J. E. & Baylink, D. J. Electron microprobe measurements of bone mineralization rate in vivo. *Am. J. Physiol.* **226**, 345–352 (1974).

34. Akiva, A. *et al.* Mineral Formation in the Larval Zebrafish Tail Bone Occurs via an Acidic Disordered Calcium Phosphate Phase. *J. Am. Chem. Soc.* **138**, 14481–14487 (2016).

35. Crane, N. J., Popescu, V., Morris, M. D., Steenhuis, P. & Ignelzi, M. A. Raman spectroscopic evidence for octacalcium phosphate and other transient mineral species deposited during intramembranous mineralization. *Bone* **39**, 434–442 (2006).

36. Mahamid, J., Sharir, A., Addadi, L. & Weiner, S. Amorphous calcium phosphate is a major component of the forming fin bones of zebrafish: Indications for an amorphous precursor phase. *Proc. Nat. Acad. Sci. USA* **105**, 12748–12753 (2008).

37. Currey, J. D. The structure and mechanics of bone. *J. Mater. Sci.* **47**, 41–54 (2012).

38. Reznikov, N., Shahar, R. & Weiner, S. Bone hierarchical structure in three dimensions. *Acta Biomater.* **10**, 3815–3826 (2014).

39. Buss, D. J., Kröger, R., McKee, M. D. & Reznikov, N. Hierarchical organization of bone in three dimensions: A twist of twists. *J. Struct. Biol. X* **6**, 100057– 100067 (2022).

40. Von Euw, S. *et al*. Bone mineral: new insights into its chemical composition. *Sci. Rep.* **9**, 1–11 (2019).

41. Glimcher, M. J. Bone: Nature of the Calcium Phosphate Crystals and Cellular, Structural, and Physical Chemical Mechanisms in Their Formation. *Rev. Mineral. Geochemistry* **64**, 223–282 (2006).

42. Xu, Y. *et al.* Intermolecular channels direct crystal orientation in mineralized collagen. *Nat. Commun.* **11**, 5068–5080 (2020).

43. Wang, Y. *et al*. Water-mediated structuring of bone apatite. *Nat. Mater.* **12**, 1144–53 (2013).

44. Davies, E. *et al.* Citrate bridges between mineral platelets in bone. *Proc. Natl. Acad. Sci.* **111**, E1354–E1363 (2014).

45. Fidler, A. L., Boudko, S. P., Rokas, A. & Hudson, B. G. The triple helix of collagens – an ancient protein structure that enabled animal multicellularity and tissue evolution. *J. Cell Sci.* **131**, jcs203950– jcs203965 (2018).

46. Kadler, K. E. Fell Muir Lecture: Collagen fibril formation in vitro and in vivo. *Int. J. Exp. Pathol.* **98**, 4–16 (2017).

47. Shoulders, M. D. & Raines, R. T. Collagen Structure and Stability. *Annu Rev Biochem* **78**, 929–958 (2010).

48. Leikina, E., Mertts, M. V, Kuznetsova, N., Leikin, S. & Caspar, D. L. D. Type I collagen is thermally unstable at body temperature. *Proceedings of the National Academy of Sciences* **99**, 1314–1318 (2002).

49. Eyre, D. R., Dickson, I. R. & Van Ness, K. Collagen cross-linking in human bone and articular cartilage. Age-related changes in the content of mature hydroxypyridinium residues. *Biochem. J.* **252**, 495–500 (1988).

50. Petruska, J. A. & Hodge, A. J. A subunit model for the tropocollagen macromolecule.

Proc. Natl. Acad. Sci. **51**, 871–876 (1964).

51. Orgel, J. P. R. O., Irving, T. C., Miller, A. & Wess, T. J. Microfibrillar structure of type I collagen in situ. *Proc. Natl. Acad. Sci. U. S. A.* **103**, 9001– 9005 (2006).

52. Nanci, A. Content and distribution of noncollagenous matrix proteins in bone and cementum: Relationship to speed of formation and collagen packing density. *J. Struct. Biol.* **126**, 256–269 (1999).

53. George, A. & Veis, A. Phosphorylated proteins and control over apatite nucleation, crystal growth, and inhibition. *Chem. Rev.* **108**, 4670–4693 (2008).

54. Staines, K. A., MacRae, V. E. & Farquharson, C. The importance of the SIBLING family of proteins on skeletal mineralisation and bone remodelling. *J. Endocrinol.* **214**, 241–255 (2012).

55. Boskey, A. L. & Villarreal-Ramirez, E. Intrinsically disordered proteins and biomineralization. *Matrix Biol.* **52**–**54**, 43–59 (2016).

56. Mckee, M. D. & Nanci, A. Osteopontin: An Interfacial Extracellular Matrix Protein in Mineralized Tissues. *Connect. Tissue Res.* **35**, 197–205 (1996).

57. Chen, L., Jacquet, R., Lowder, E. & Landis, W. J. Refinement of collagen-mineral interaction: A possible role for osteocalcin in apatite crystal nucleation, growth and development. *Bone* **71**, 7–16 (2015).

58. Gorski, J. P. Biomineralization of bone: a fresh view of the roles of non-collagenous proteins. *Front. Biosci.* **16**, 2598–2639 (2011).

59. Boskey, A. L. *et al.* Osteopontin-hydroxyapatite interactions in vitro: inhibition of hydroxyapatite formation and growth in a gelatin-gel. *Bone Miner.* **22**, 147–159 (1993).

60. Boskey, A. L., Spevak, L., Paschalis, E., Doty, S. B. & McKee, M. D. Osteopontin deficiency increases mineral content and mineral crystallinity in mouse bone. *Calcif. Tissue Int.* **71**, 145–154 (2002).

61. Pugliarello, M. C., Vittur, F., de Bernard, B., Bonucci, E. & Ascenzi, A. Chemical modifications in osteones during calcification. *Calcif. Tissue Res.* **5**, 108–114 (1970).

62. Wojtas, M., Lausch, A. J. & Sone, E. D. Glycosaminoglycans accelerate biomimetic collagen mineralization in a tissue-based in vitro model. *Proc. Natl. Acad. Sci. U. S. A.* **117**, 12636–12642 (2020).

63. Chen, C. C., Boskey, A. L. & Rosenberg, L. C. The inhibitory effect of cartilage proteoglycans on hydroxyapatite growth. *Calcif. Tissue Int.* **36**, 285–290 (1984).

64. Goldberg, M. *et al*. Targeted disruption of two small leucine-rich proteoglycans, biglycan and decorin, excerpts divergent effects on enamel and dentin formation. *Calcif. Tissue Int.* **77**, 297–310 (2005).

65. Goldberg, M., Septier, D., Oldberg, Å., Young, M. F. & Ameye, L. G. Fibromodulin-deficient mice display impaired collagen fibrilloqenesis in predentin as well as altered dentin mineralization and enamel formation. *J. Histochem. Cytochem.* **54**, 525–537 (2006).

66. Robinson, R. A. & Watson, M. L. Collagen-crystal relationships in bone as seen in the electron microscope. *Anat. Rec.* **114**, 383–409 (1952).

67. Landis, W. J., Hodgens, K. J., Arena, J., Song, M. J. & McEwen, B. F. Structural relations between collagen and mineral in bone as determined by high voltage electron microscopic tomography. *Microsc. Res. Tech.* **33**, 192–202 (1996).

68. Weiner, S. & Traub, W. Organization of hydroxyapatite crystals within collagen fibrils. *FEBS Lett*. **206**, 262–266 (1986).

69. Oosterlaken, B. M., Vena, M. P. & With, G. In Vitro Mineralization of Collagen. *Adv. Mater*. **33**, 2004418–2004445 (2021).

70. Nudelman, F., Lausch, A. J., Sommerdijk, N. A. J. M. & Sone, E. D. In vitro models of collagen biomineralization. *J. Struct. Biol.* **183**, 258–269 (2013).

71. Jiao, K. *et al*. Complementarity and Uncertainty in Intrafibrillar Mineralization of Collagen. *Adv. Funct. Mater*. **26**, 6858–6875 (2016).

72. Silver, F. H. & Landis, W. J. Deposition of apatite in mineralizing vertebrate extracellular matrices: A model of possible nucleation sites on type I collagen. *Connect. Tissue Res.* **52**, 242–254 (2011).

73. Xu, Z. *et al*. Molecular mechanisms for intrafibrillar collagen mineralization in skeletal tissues. *Biomaterials* **39**, 59–66 (2015).

74. Nudelman, F. *et al*. The role of collagen in bone apatite formation in the presence of hydroxyapatite nucleation inhibitors. *Nat. Mater*. **9**, 1004–1009 (2010).

75. Olszta, M. J. *et al*. Bone structure and formation: A new perspective. *Mater. Sci. Eng.*

R Reports **58**, 77–116 (2007).

76. Niu, L. *et al*. Collagen intrafibrillar mineralization as a result of the balance between osmotic equilibrium and electroneutrality. *Nat. Mater.* **1**, 1–9 (2016).

77. Ping, H. *et al*. Mineralization generates megapascal contractile stresses in collagen fibrils. *Science (80-.).* **376**, 188–192 (2022).

78. Pidaparti, R. M. V., Chandran, A., Takano, Y. & Turner, C. H. Bone mineral lies mainly outside collagen fibrils: Predictions of a composite model for osteonal bone. *J. Biomech.* **29**, 909–916 (1996).

79. McNally, E. A., Schwarcz, H. P., Botton, G. A. & Arsenault, A. L. A model for the ultrastructure of bone based on electron microscopy of ion-milled sections. *PLoS One* **7**, 1–12 (2012).

80. Schwarcz, H. P., McNally, E. A. & Botton, G. A. Dark-field transmission electron microscopy of cortical bone reveals details of extrafibrillar crystals. *J. Struct. Biol.* **188**, 240–248 (2014).

81. Reznikov, N., Bilton, M., Lari, L., Stevens, M. M. & Kröger, R. Fractal-like hierarchical organization of bone begins at the nanoscale. *Science.* **360**, 507–5018 (2018).

82. Bonucci, E. Fine structure and histochemistry of 'calcifying globules' in epiphyseal cartilage. *Zeitschrift für Zellforsch. und Mikroskopische Anat.* **103**, 192–217 (1970).

83. Macías-Sánchez, E. *et al*. Spherulitic Crystal Growth Drives Mineral Deposition Patterns in Collagen-Based Materials. *Adv. Funct. Mater.* 2200504–2200516 (2022).

84. Bonucci, E. Crystal ghosts and biological mineralization: Fancy spectres in an old castle, or neglected structures worthy of belief? *J. Bone Miner. Metab.* **20**, 249–265 (2002).

85. Boyde, A. Electron Microscopy of the Mineralizing Front. *Metab. Bone Dis. Rel. Res.* **2**, 69–78 (1980).

86. McKee, M. D., Buss, D. J. & Reznikov, N. Mineral tessellation in bone and the stenciling principle for extracellular matrix mineralization. *J. Struct. Biol.* **214**, 107823–107830 (2022).

87. Micheletti, C. *et al*. Bone Mineral Organization at the Mesoscale: A Review of Mineral

Ellipsoids in Bone and at Bone Interfaces. *Acta Biomater.* **142**, 1–13 (2022).

88. Ayoubi, M. *et al.* 3D Interrelationship between Osteocyte Network and Forming Mineral during Human Bone Remodeling. *Adv. Healthc. Mater.* **10**, 2100113–2100124 (2021).

89. Varsano, N. *et al.* Characterization of the growth plate-bone interphase region using cryo-FIB SEM 3D volume imaging. *J. Struct. Biol.* **213**, 107781–107796 (2021).

90. Buss, D. J., Reznikov, N. & McKee, M. D. Crossfibrillar mineral tessellation in normal and Hyp mouse bone as revealed by 3D FIB-SEM microscopy. *J. Struct. Biol.* **212**, 107603–107618 (2020).

91. Bonucci, E. Bone mineralization. *Front. Biosci.* **17**, 100–128 (2012).

92. Mahamid, J. *et al.* Mapping amorphous calcium phosphate transformation into crystalline mineral from the cell to the bone in zebrafish fin rays. *Proc. Natl. Acad. Sci.* **107**, 6316–6321 (2010).

93. Bonucci, E. Fine structure of early cartilage calcification. *J. Ultrastruct. Res.* **20**, 33–50 (1967).

94. Anderson, H. C. Electron microscopic studies of induced cartilage development and calcification. *J. Cell Biol.* **35**, 81–101 (1967).

95. Ali, S. Y., Sajdera, S. W. & Anderson, H. C. Isolation and characterization of calcifying matrix vesicles from epiphyseal cartilage. *Proc. Natl. Acad. Sci. U. S. A.* **67**, 1513–1520 (1970).

96. Matsuzawa, T. & Anderson, H. C. Phosphatases of epiphyseal cartilage studied by electron microscopic cytochemical methods. *J. Histochem. Cytochem.* **19**, 801–808 (1971).

97. Wuthier, R. E. Matrix vesicles: structure, composition, formation and function in calcification. *Front. Biosci.* **16**, 2812–2902 (2011).

98. Bottini, M. *et al.* Matrix vesicles from chondrocytes and osteoblasts: Their biogenesis, properties, functions and biomimetic models. *Biochim. Biophys. Acta - Gen. Subj.* **1862**, 532–546 (2018).

99. Cui, L., Houston, D. A., Farquharson, C. & MacRae, V. E. Characterisation of matrix vesicles in skeletal and soft tissue mineralisation. *Bone* **87**, 147–158 (2016).

100. Hasegawa, T. Ultrastructure and biological function of matrix vesicles in bone mineralization. *Histochem. Cell Biol.* **149**, 289–304 (2018).

101. Kirsch, T. & Wuthier, R. E. Stimulation of calcification of growth plate cartilage matrix vesicles by binding to type II and X collagens. *J. Biol. Chem.* **269**, 11462–11469 (1994).

102. Chaudhary, S. C. *et al.* Phosphate induces formation of matrix vesicles during odontoblast-initiated mineralization in vitro. *Matrix Biol.* **52**–**54**, 284–300 (2016).

103. Borg, T. K., Runyan, R. B. & Wuthier, R. E. Correlation of freeze-fracture and scanning electron microscopy of epiphyseal chondrocytes. *Calcif. Tissue Res.* **26**, 237–241 (1978).

104. Wuthier, R. E., Linder, R. E., Warner, G. P., Gore, S. T. & Borg, T. K. Non-enzymatic isolation of matrix vesicles : characterization and initial studies on 45Ca and 32P-orthophosphate metabolism. *Metab. Bone Dis. Relat. Res.* **1**, 125–136 (1978).

105. Thouverey, C., Strzelecka-Kiliszek, A., Balcerzak, M., Buchet, R. & Pikula, S. Matrix vesicles originate from apical membrane microvilli of mineralizing osteoblast-like saos-2 cells. *J. Cell. Biochem.* **106**, 127–138 (2009).

106. Balcerzak, M. *et al.* Proteome analysis of matrix vesicles isolated from femurs of chicken embryo. *Proteomics* **8**, 192–205 (2008).

107. Thouverey, C. *et al.* Proteomic characterization of biogenesis and functions of matrix vesicles released from mineralizing human osteoblast-like cells. *J. Proteomics* **74**, 1123–1134 (2011).

108. Abdallah, D. *et al.* Fatty acid composition in matrix vesicles and in microvilli from femurs of chicken embryos revealed selective recruitment of fatty acids. *Biochem. Biophys. Res. Commun.* **446**, 1161–1164 (2014).

109. Anderson, H. C., Garimella, R. & Tague, S. E. The role of matrix vesicles in growth plate development and biomineralization. *Front. Biosci.* **10**, 822–837 (2005).

110. Wuthier, R. E. Mechanism of De Novo Mineral Formation by Matrix Vesicles. *Connect. Tissue Res.* **22**, 653–659 (1989).

111. Ramos, A. P. *et al.* The functional role of soluble proteins acquired by extracellular vesicles. *J. Extracell. Biol.* **1**, e34–e55 (2022).

112. Gerke, V., Creutz, C. E. & Moss, S. E. Annexins: Linking Ca2+ signalling to membrane dynamics. *Nat. Rev. Mol. Cell Biol.* **6**, 449–461 (2005).

113. Genge, B. R., Wu, L. N. Y. & Wuthier, R. E. Identification of phospholipid-dependent calcium-binding proteins as constituents of matrix vesicles. *J. Biol. Chem.* **264**, 10917–10921 (1989).

114. Arispe, N., Rojas, E., Genge, B. R., Wu, L. N. Y. & Wuthier, R. E. Similarity in calcium channel activity of annexin V and matrix vesicles in planar lipid bilayers. *Biophys. J.* **71**, 1764–1775 (1996).

115. Huber, R., Romisch, J. & Paques, E. P. The crystal and molecular structure of human annexin V, an anticoagulant protein that binds to calcium and membranes. *EMBO J.* **9**, 3867–3874 (1990).

116. Veschi, E. A. *et al*. Localization of Annexin A6 in Matrix Vesicles during Physiological Mineralization. *Int. J. Mol. Sci.* **21**, 1367–1383 (2020).

117. Millán, J. L. The role of phosphatases in the initiation of skeletal mineralization. *Calcif. Tissue Int.* **93**, 299–306 (2013).

118. Goettsch, C. *et al*. TNAP as a therapeutic target for cardiovascular calcification: a discussion of its pleiotropic functions in the body. *Cardiovasc. Res.* **118**, 84–96 (2022).

119. Millán, J. L. *Mammalian Alkaline Phosphatases*. (Wiley, 2006).

120. Aikawa, E. & Blaser, M. C. 2020 Jeffrey M. Hoeg Award Lecture; Calcifying Extracellular Vesicles as Building Blocks of Microcalcifications in Cardiovascular Disorders. *Arteriosclerosis, Thrombosis, and Vascular Biology*. **41**, 117–127 (2021).

121. Sheen, C. R. *et al*. Pathophysiological role of vascular smooth muscle alkaline phosphatase in medial artery calcification. *J. Bone Miner. Res.* **30**, 824–836 (2015).

122. Anderson, H. C., Hsu, H. H., Morris, D. C., Fedde, K. N. & Whyte, M. P. Matrix vesicles in osteomalacic hypophosphatasia bone contain apatite-like mineral crystals. *Am. J. Pathol.* **151**, 1555–1561 (1997).

123. Hessle, L. *et al*. Tissue-nonspecific alkaline phosphatase and plasma cell membrane glycoprotein-1 are central antagonistic regulators of bone mineralization. *Proc. Natl. Acad. Sci.* **99**, 9445–9449 (2002).

124. Simão, A. M. S. *et al*. Proteoliposomes harboring alkaline phosphatase and nucleotide

pyrophosphatase as matrix vesicle biomimetics. *J. Biol. Chem.* **285**, 7598–7609 (2010).

125. Andrilli, L. H. S. *et al.* NPP1 and TNAP hydrolyze ATP synergistically during biomineralization. *Purinergic Signal.* **1**, 1–14 (2022).

126. Yadav, M. C. *et al.* Skeletal Mineralization Deficits and Impaired Biogenesis and Function of Chondrocyte-Derived Matrix Vesicles in Phospho1-/- and Phospho1/Pit1 Double-Knockout Mice. *J. Bone Miner. Res.* **31**, 1275–1286 (2016).

127. Montessuit, C., Bonjour, J. P. & Caverzasio, J. P(i) transport regulation by chicken growth plate chondrocytes. *Am. J. Physiol. - Endocrinol. Metab.* **267**, 24–31 (1994).

128. Xiao, Z., Blonder, J., Zhou, M. & Veenstra, T. D. Proteomic analysis of extracellular matrix and vesicles. *J. Proteomics* **72**, 34–45 (2009).

129. Wuthier, R. E. Electrolytes of isolated epiphyseal chondrocytes, matrix vesicles, and extracellular fluid. *Calcif. Tissue Res.* **23**, 125–133 (1977).

130. Wu, L. N. Y., Sauer, G. R., Genge, B. R., Valhmu, W. B. & Wuthier, R. E. Effects of analogues of inorganic phosphate and sodium ion on mineralization of matrix vesicles isolated from growth plate cartilage of normal rapidly growing chickens. *J. Inorg. Biochem.* **94**, 221–235 (2003).

131. Montessuit, C., Caverzasio, J. & Bonjour, J. P. Characterization of a P(i) transport system in cartilage matrix vesicles: Potential role in the calcification process. *J. Biol. Chem.* **266**, 17791–17797 (1991).

132. Houston, B., Stewart, A. J. & Farquharson, C. PHOSPHO1 - A novel phosphatase specifically expressed at sites of mineralisation in bone and cartilage. *Bone* **34**, 629–637 (2004).

133. Stewart, A. J. *et al.* The presence of PHOSPHO1 in matrix vesicles and its developmental expression prior to skeletal mineralization. *Bone* **39**, 1000–1007 (2006).

134. Roberts, S. J., Stewart, A. J., Sadler, P. J. & Farquharson, C. Human PHOSPHO1 exhibits high specific phosphoethanolamine and phosphocholine phosphatase activities. *Biochem. J.* **382**, 59–65 (2004).

135. Tzvetkov, J. *et al.* Spatial Lipidomic Profiling of Mouse Joint Tissue Demonstrates the Essential Role of PHOSPHO1 in Growth Plate Homeostasis. *J. Bone Miner. Res.* **00**, 1–16 (2023).

136. Goldberga, I. *et al.* Detection of nucleic acids and other low abundance components in native bone and osteosarcoma extracellular matrix by isotope enrichment and DNP-enhanced NMR. *RSC Adv.* **9**, 26686–26690 (2019).

137. Dillon, S., Staines, K. A., Millán, J. L. & Farquharson, C. How To Build a Bone: PHOSPHO1, Biomineralization, and Beyond. *JBMR Plus* **3**, e10202–e10214 (2019).

138. Dillon, S. *et al.* Ablation of Enpp6 Results in Transient Bone Hypomineralization. *JBMR Plus* **5**, 1–11 (2020).

139. Yadav, M. C. *et al.* Loss of skeletal mineralization by the simultaneous ablation of PHOSPHO1 and alkaline phosphatase function: A unified model of the mechanisms of initiation of skeletal calcification. *J. Bone Miner. Res.* **26**, 286–297 (2011).

2

THE RELATIONSHIP BETWEEN MVs AND FORMING MINERAL AT THE NANOSCALE

Matrix vesicles (MVs) are involved in the initial deposition of hydroxyapatite (HAp) during bone mineralization, but their mechanism of action is not yet fully understood. *In vitro* studies propose two pathways by which MVs can trigger HAp precipitation: the first is mediated by their enhanced phosphatase activity, and the second suggested to depend on structural components present in MVs to mediate nucleation directly from soluble ions without the involvement of any phosphatase. However, the relevance of these two pathways for bone mineralization and the relationship between MVs and forming mineral in such *in vitro* experiments remains unclear. Here, we used near-native cryoTEM nanoscale imaging in combination with bulk characterizations to disentangle the content and action of MVs during *in vitro* mineralization. We show that MVs isolation by conventional ultracentrifugation results in heterogeneous dispersions containing non-vesicular particles, including collagens and proteoglycans, in addition to bilayered vesicles. The separation of phosphatase-enriched MVs from non-vesicular particles and comparative mineralization experiments demonstrated that the ability of MVs to induce fast mineralization, independently of phosphatase activity, depends on the presence of non-vesicular particles. Therefore, we conclude that the primary pathway by which MVs trigger mineralization is through the action of their resident phosphatase enzymes, with the direct mineral nucleation to be a secondary event consequential of their membrane components. Lastly, we observed mineral formation restricted to the extravesicular space or in close proximity to the membrane interface, suggesting that the relationship between MVs and forming mineral is more intricate than previously understood.

2.1 | Introduction

Bone biomineralization is the process by which calcium phosphate in the form of carbonated hydroxyapatite (HAp) is deposited in and on collagen fibrils within the extracellular matrix[1]. Despite its significance, the mechanisms behind the initiation of HAp mineralization within the collagen matrix are still not fully understood. MVs were first imaged in the late 1960s[2,3], when examining cartilage mineralization during endochondral bone formation. At the ultrastructural level, MVs are membrane-enclosed 100-300 nm nanostructures containing mineral associated to the lipid bilayer both internally and externally, always identified where HAp is initially deposited within the ECM[4]. However, the precise visualization of MVs within tissues depends on the methodology applied for sample preparation and imaging[5]. Furthermore, 2D electron microscopy images of tissue sections are limited in providing accurate 3D positioning between vesicles and minerals[6]. Despite the controversies imposed by these technical limitations, MVs have been extensively demonstrated to be present in different tissues undergoing mineralization, such as calvarial osteoid[7] and dentin[8]. They have also been observed in pathological mineralization[9], and it is now widely recognized that MVs play a role in the initiation of mineralization. However, the mechanism of action remains largely unknown.

The controversy surrounding the function of MVs is partly due to the difficulties in investigating them in detail. Their size in the nanometer scale and their presence in the densely packed ECM make reliable characterization challenging. Therefore, the main approach to study MVs is by isolating them from native tissues and reconstituting their content and functionality (i.e. mineralization) *in vitro*. A seminal approach used enzymatic digestion of epiphyseal cartilage, along with differential ultracentrifugation steps, to extract a vesicle pellet containing MVs[10]. Application of this approach revealed one of the main features of MVs, that is their increased alkaline phosphatase activity when compared to the mother cells[10]. However, the enzymatic digestion using proteases caused significant harm to the proteins in the vesicles. In an attempt to overcome this drawback, other researchers homogenized epiphyseal cartilage in absence of proteases, using differential ultracentrifugation in conjunction with sucrose gradient fractionation[11,12]. Although this technique led to a significant increase in alkaline phosphatase activity of the resulting sample, it also resulted in contamination of the samples by intracellular membrane fragments precipitated in the pellet. In an effort to preserve MVs functionality

after enzymatic digestion, low-protease collagenases were utilized in subsequent studies. These more refined techniques ultimately succeeded in isolating a MVs fraction that was both reproducible and capable of inducing fast mineralization in solution[13]. This methodology is now the gold-standard to study the *in vitro* functionality of MVs and has been extensively applied for chicken and mouse embryonic bones.

The ultimate goal of isolating MVs from tissues is to retrieve their ability to induce mineralization *in vitro*. Inspired by their enrichment in alkaline phosphatase and adenosine triphosphatase (ATPase) activity, these experiments started by exposing MVs to a medium containing organophosphate compounds, such as ATP[14]. The ability to degrade organophosphates compounds has for long being implicated in the bone formation[15]. This enzymatic control has a dual effect, not only removing the inhibitory effect of the pyrophosphate (PPi) , that strongly interacts with Ca^{2+} and supresses mineral formation and growth[16], but also by the ability to produce free phosphate ion (Pi) to trigger mineralization. Exposure of MVs to a medium containing organophosphates induced the precipitation of calcium phosphate mineral[17,18]. It is now recognized that the enzyme tissue non-specific alkaline phosphatase (TNAP) responds as the more important phosphatase operating in MVs. Enzymatic cleavage of TNAP from the outer membrane of MVs resulted in 80% reduction in mineral deposition[19]. The action of TNAP evidences a major role of MVs by fine-tunning the promotor/inhibitor molar ratio, Pi/PPi, permissive for mineralization[1,20]. Failure in the control of inhibitors' concentration is related to the development of several mineralization disorders and skeletal abnormalities[21]. Moreover, in cooperation with TNAP, other phosphatases have also been demonstrated to be operational within MVs, such as the nucleoside pyrophosphohydrolase-1 (NPP1)[22] and the orphan phosphatase (PHOSPHO1)[23]. Alterations in the function of these phosphatases lead to softening of bone, spontaneous fractures, loss of teeth, as well as pathological calcification of soft tissues[20,22,24]. Remarkably, MVs isolated from wild-type and TNAP-, NPP1- and PHOSPHO1-knockout animals showed different ability to degrade organophosphate substrates and thereby to trigger *in vitro* mineralization[25].

In spite of their intrinsic phosphatase activity, MVs have also been demonstrated to induce mineral precipitation *in vitro* without the need of any organophosphate degradation[26]. In this case, mineralization is described to occur by simply uptaking Ca^{2+} and Pi ions from the medium into the newly formed mineral through a nucleation process driven by MVs structural components. These components, referred to as a "nucleational

core" are hypothesized to be composed of a membranous component formed between phosphatidylserine and annexins[27,28], and a pool of bound Ca^{2+} and Pi ions[29]. Isolated MVs are described to contain a large amount of Ca^{2+} and Pi, with the majority of the Ca^{2+} (>90%) initially present in an bound form, but only about 8-10% of the Ca^{2+} complexed with acidic phospholipids, as revealed by biphasic solvent partition of electrolytes[30]. This pool of bound Ca^{2+} and Pi ions was demonstrated to be a primordial component for the ability of MVs to trigger mineralization in a phosphatase-independent manner, since their removal upon treatments with slightly acidic buffer, calcium chelating agents or through sucrose fractionation hindered the functionality[31,32].

Historically, *in vitro* mineralization of MVs were termed "uptake" assays, in which the amount of Ca^{2+} and Pi ions incorporated into the newly precipitated mineral over time in the presence of the vesicles were radiometrically measured. These experiments aided to demonstrate the rate, type, and amount of mineral formed *in vitro*, as extensively reviewed by Wuthier[33]. However, a major challenge is the translation from bulk observations of *in vitro* mineralization to the underlying mechanisms by which enzymes and proteins operate within MVs, which occurs at a nanometric scale. Moreover, the relation between vesicles and forming mineral in such experiments is yet poorly understood. So far, visualization of mineral associated with MVs have been obtained with aid of conventional electron microscopy, but very few reports combined bulk assessments of mineral formation with imaging. Moreover, it is required to sediment MVs and mineral prior to the deposition of the collected material in TEM grids. This approach has allowed to follow the formation of mineral particles during in vitro mineralization (Figure 2.1). However, conventional TEM have the disadvantage of not faithfully preserve the imaged material in a fully hydrated state. This is of particular importance when handling biological samples like MVs, that include membranes and mineral particles, to prevent the collapse of the three-dimensional volume and extraction or mixture of the contents upon dehydration.

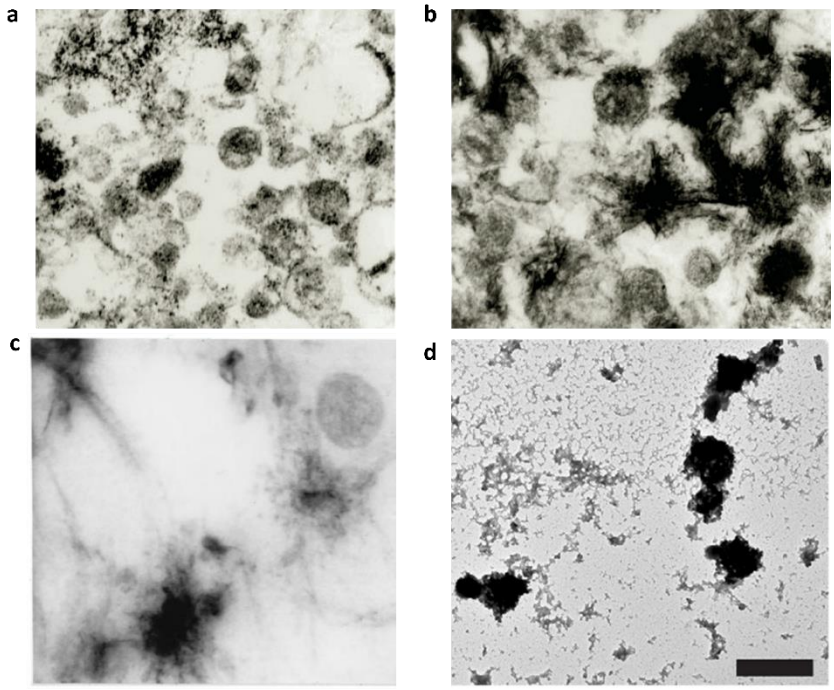

Figure 2.1 | Conventional TEM images reveal formation of mineral by MVs. (a) TEM images of MVs collected after 5 h of exposure to mineralizing solution in the presence of 1 mM ATP. Several dense particles can be observed closely associated to MV´s surfaces. (b) After 24 h, mineral with needle-like morphology typical of apatite can be observed. Images a and b were obtained after sedimentation of MVs, resin-embedding of pellets and sectioning with the aid of a microtome. Scales bars were not provided in the original reference[17]. c) Image obtained from a thin section of a resin-embedded pellet of MVs mineralized in presence of Ca^{2+} and Pi ions for 5 h, without ATP, where mineral particles associated with fibrils and intact vesicles can be identified. The scale bar was not provided in the original reference[34]. d) Pellet collected after *in vitro* mineralization of MVs and dropped on a TEM grid showing the formation of aggregated particles, scale bar 500 nm[35]. The images were adapted with permission from the references [17], [34] and [35].

Here, in order to overcome these challenges and to solve in depth the relation between MVs and forming minerals, we used cryogenic transmission electron microscopy (cryoTEM) to image vesicles and mineral in a near-native state. CryoTEM involves the investigation of a thin vitrified film of a solution containing the particle of interest (Figure 2.2). During vitrification, all processes happening at bulk level are arrested and the particles under investigation become embedded in an amorphous film of the solvent[36]. Therefore, this imaging approach brings an unprecedent advantage of visualizing processes in a near-native state by keeping the whole material in a fully hydrated state. Application of cryoTEM was fundamental to uncover different aspects of bone biomineralization, such as the mechanism of collagen mineralization[37,38] and the phase transitions observed during HAp formation[39]. Therefore, cryoTEM can be explored as a powerful approach to investigate the content and functionality of MVs *in vitro*.

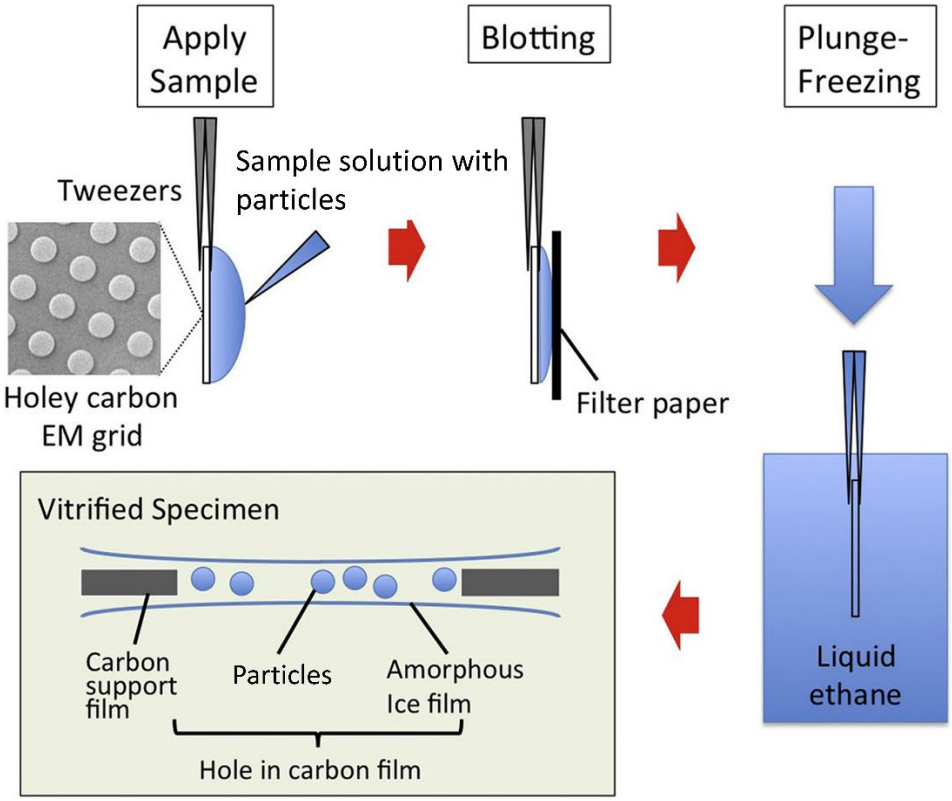

Figure 2.2 | CryoTEM captures near-native snapshots of particles through rapid freezing of the sample. A droplet of the sample (typically ~3 µL) is deposited on a holey carbon TEM grid. The excess of fluid is then blotted with a filter paper. This process leads to the formation of a thin film of the fluid with a thickness of typically ~100 nm. Since the TEM grid has holes on its carbon supporting film, the liquid will be trapped within these holes. The formed thin film is then rapidly vitrified by plunging the TEM grid into liquid ethane (−183 °C), what assure the formation of an amorphous ice with embedded particles within. Then, the particles can be observed in a fully hydrated state using a TEM microscope operating at cryogenic temperature. Image adapted with permission from reference [40].

2.2 | Objectives

General objective

To investigate the composition and mechanism of action of MVs during *in vitro* mineralization by cryoTEM to understand the role of vesicles in mineral formation.

Specific aims

(i) To compare the composition of MVs isolated from embryonic chicken bones by differential ultracentrifugation and after density-gradient fractionation;
(ii) To compare the *in vitro* mineralization of MVs using different purification approaches to probe the phosphatase dependent and independent mechanisms of mineralization;
(iii) To determine the relation between vesicles and forming mineral during *in vitro* mineralization;

2.3 | Methods

2.3.1 | Synthetic Cartilage Lymph (SCL) preparation

Synthetic cartilage lymph (SCL) is a solution that mimics the composition of the cartilage fluid[41]. It was prepared by mixing the required salts in ultrapure water (MilliQ®) to achieve the following final concentrations: 1.42 mM Na_2HPO_4, 1.83 mM $NaHCO_3$, 12.7 mM KCl, 0.57 mM $MgCl_2$, 100 mM NaCl, 0.57 mM Na_2SO_4, 5.55 mM glucose, 63.5 mM sucrose, and 16.5 mM 2-([2-hydroxy-1,1-bis (hydroxymethyl) ethyl]amino)–propanesulfonic acid. The pH of the solution was adjusted to 7.5, at 37°C. SCL was initially prepared without $CaCl_2$ and added only just before use to achieve the final concentration required for a given experiment.

2.3.2 | Bone tissue digestion and MVs isolation by 3-step differential ultracentrifugation

Leg bones were dissected from chick embryos (17-days post fertilization), characterized to be between developmental stages 42–44 accordingly to Hamburger and Hamilton[42]. In The Netherlands, chick embryos are considered as non-licensed animal use and full animal ethics committee approval was not required for this purpose. The embryos were killed by decapitation, leg bones dissected, and growth plates and epiphyseal cartilages

carefully sliced in pieces of approximately 1 mm. The tissue was never frozen and always freshly processed for MVs isolation. MVs were isolated following the protocol described by Buchet et al.[41] Tissue slices (approximately 4 g) were extensively washed in ice-cold SCL buffer, then digested for 3.5 h, at 37°C, under mild stirring in 16 mL of SCL containing 100 U/mL of collagenase (type II, from *Clostridium histolyticum*, Sigma C6885) and 1 mM $CaCl_2$. After digestion, the suspension was filtered through a nylon membrane (100 µm) and consecutively centrifuged at 600 × g_{av} for 15 min to sediment cells and large debris. The supernatant was then centrifuged at 20 000 x g_{av} for 20 min using a Ti 70 fixed-angle rotor (Beckman Coulter). Finally, the collected supernatant was centrifuged at 80 000 x g_{av} for 60 min (Ti 70 fixed-angle rotor). The pellet obtained was suspended in SCL and this preparation we will refer to as crude MVs. Characterizations herein reported were always obtained with freshly isolated MVs that were never subjected to freezing and thawing and stored for no longer than 5 days in ice. We define as a biological replicate the preparation of MVs obtained from bones dissected from 25 animals.

2.3.3 | Iodixanol density gradient fractionation of crude MVs

In this approach, a tube is filled with layers of liquid having a density that increases in density from the top to the bottom of the tube. Frequently used substances to create layers of different density are sucrose and iodixanol. During centrifugation in this density gradient, sufficient time is allowed for all particles in the sample to reach the part of the gradient with a density equivalent to their own. This allows the particles to be separated based on their buoyant density. The buoyant density of a particle is its apparent density in a given liquid medium. In an iodixanol gradient, bilayer-enclosed vesicles float in a density range of 1.025-1.125 g/mL, while non-vesicular components such as protein aggregates float at higher densities[43]. This difference in flotation densities enables the precise separation of membranous vesicles from non-vesicular components.

Iodixanol (Optiprep™ 60 vol.% in water, Serumwerk Bernburg, Germany) was prepared diluted in ice-cold SCL to achieve a final concentration 48 vol.%. This working-solution was then mixed with a dispersion of crude MVs in SCL to achieve a final concentration of 45 vol.%. 4 mL of the iodixanol solution containing the crude MVs was loaded in the bottom of an ultra-clear tube and then solutions of descending densities (35, 30, 28, 26, 24, 22, 20 and 10 %) were carefully layered on top. All solutions with different densities

were prepared in SCL containing 1 mM $CaCl_2$, to prevent dissolution of any labile Ca^{2+} and Pi initially present[12]. The bottom-loaded 45-10% gradient was then centrifuged at 120 000 x g_{av} for 16 h in a SW40 Ti Swinging Bucket rotor (Beckman Coulter). After ultracentrifugation, fractions were carefully collected from the top of the gradient, and 12-fold diluted in ice-cold SCL and subjected to ultracentrifugation at 100 000 x g_{av} for 2 h in a Ti 70 fixed-angle rotor (Beckman Coulter). The resulting pellets were resuspended in SCL and freshly used for downstream analysis and never subjected to freezing and thawing.

2.3.4 | Protein quantification and alkaline phosphatase activity

Total protein concentration was quantified using the Bradford protein assay (Biorad), using bovine serum albumin as standard. Alkaline phosphatase activity was determined by the hydrolysis of p-nitrophenyl phosphate (p-NPP, Sigma-Aldrich) in a reaction medium containing 10 mM p-NPP and 1 mM $MgCl_2$ in AMPOL buffer (2-amino-2-methyl-1- propanol), pH 10.3, at 37°C. The reaction was monitored by changes in the absorbance at 405 nm related to the formation of the yellowish product p-nitrophenolate ($p\text{-}NP^-$) and the specific activity expressed as U/mg of total protein, where U = µmol pNP^-/min.

2.3.5 | SDS-PAGE and western blotting

Samples were prepared in Laemmli buffer and heated at 95°C for 10 min before being loaded on gels[44]. The samples were separated on 4%–15% Mini-PROTEAN® TGX™ Precast Gels (Biorad) under reducing conditions before being transferred to PVDF membranes (Biorad) using a Trans-Blot® Turbo Blotting System. All procedures were done using manufacturers protocols. Membranes were blocked for 1 h in Odyssey TBS Blocking Buffer (LI-COR Biosciences, Lincoln, NE, USA), and incubated with anti-ALPL primary antibody (Proteintech, 11187-1-AP), diluted 1:1000, overnight. For fluorescence detection of proteins, IRDye 800CW anti-rabbit IgG (H+L) secondary antibody (LI-COR) was used. Detection was with an Odyssey Imaging System (LI-COR).

2.3.6 | Nanoparticle tracking analysis (NTA)

MVs size distribution and concentration were estimated in a NanoSight NS300 equipped with a syringe pump (Malvern Panalytics, Malvern, UK). Concentrations were calculated

using Nanoparticle Tracking Analysis 3.2 software (Nanosight Ltd, Amesbury, UK). Vesicles were diluted in PBS until a suitable concentration for analysis was reached (20-60 particles per frame). Each sample was measured for 30 s, using the following software settings: flow rate 50, camera level 10, and detection threshold 5.

2.3.7 | CryoTEM sample preparation and imaging

3 µL of sample was applied on glow-discharged Au200 R2/1 grids (Quantifoil), and the excess liquid was removed by blotting for 4 s (blot force 3) using filter paper followed by plunge freezing in liquid ethane using a FEI Vitrobot Mark IV, at 100% humidity and 25°C. A JEOL JEM-2100 microscope (Jeol Ltd., Tokyo, Japan) equipped with a Gatan 914 high tilt cryo holder and a LaB6 filament was used for cryogenic imaging at 200 kV. Images were recorded with a Gatan 833 Orius camera (Pleasanton, CA, USA).

2.3.7 | Mineralization experiments

Crude and low-dense MVs were exposed to SCL medium supplemented with $CaCl_2$ (2 mM) and either 2 mM Na_2HPO_4 or 1 mM adenosine triphosphate (Sigma-Aldrich). Mineralization was carried out at 37°C and using samples with fixed 50 µg of total protein/mL concentration. Turbidity was measured as absorbance at 350 nm, in 200 µL of solution in 96-well plate using a Biorad model 680 microplate reader. Dynamic light scattering (DLS) was carried out in a NanoZS equipament (Malvern, UK).

For on-grid mineralization experiments, 10 µL of samples were placed on top of a glow-discharged Au200 R2/1 grids (Quantifoil) and incubated in a 100%-humidity controlled environment, at 37°C. After incubation for a desired time, samples were processed for vitrification and imaging as described above.

2.4 | Results

2.4.1 | Characterization of crude MVs isolated by differential ultracentrifugation

After enzymatic digestion of epiphysial cartilage slices with collagenase to release extracellular matrix-trapped vesicles, MVs were isolated using a standard three-step differential ultracentrifugation protocol (Figure 2.3a). Crude MVs (the pellet obtained at 80 000 *x g*) display all the characteristic features described in the literature[13]. A population of small vesicles with a diameter in the range of 100 – 300 nm was identified by nanoparticle tracking analysis (NTA) (Figure 2.3b), displaying high alkaline phosphatase (TNAP) activity (Figure 2.3c) and a typical electrophoretic protein profile (Figure 2.3d). From the SDS-page electrophoresis, we can discern 4 intense bands at apparent molecular weight of ~ 30, 39, 42 and 45 kDa. The presence of these intense bands within this molecular weight range are characteristic of MVs isolated from chicken bones[13,33]. The 30- and 33-kDa proteins are now known to be annexin A5 (AnxA5); the 36-kDa protein is annexin A2 (AnxA2); and the 68-kDa protein is annexin A6 (AnxA6), but usually yielding a more faint band[33]. The presence of these proteins within chicken-derived MVs was confirmed by proteomic analysis[45]. TNAP appear as a faint and broad band at ~ 70-76 kDa[26], as also confirmed by western blotting analysis (Figure 2.3c). Other less intense bands appear migrating at higher apparent molecular weight (~ 100, 150 kDa), previously assigned to collagen from the extracellular matrix[46]. Finally, cryoTEM imaging (Figure 2.3e) allowed visualization of the crude MVs preparations in a near-native state, indeed revealing a population of bilayered vesicles, with diameters in the range of 100-200 nm, corroborating NTA results. However, alongside the vesicles, a large amount of non-vesicular material was observed, most likely extracellular matrix components, including collagen fibrils (Figure 2.3f), and mineral particles with needle-like morphology typical for calcium phosphates. These mineral particles were either associated to the vesicles (arrows, Figure 2.3f), or in aggregates associate to proteinaceous materials (Figure 2.3g). The nature of these mineral particles is uncertain. They might come from either mineralization triggered by MVs during the digestion step or endogenous mineral particles.

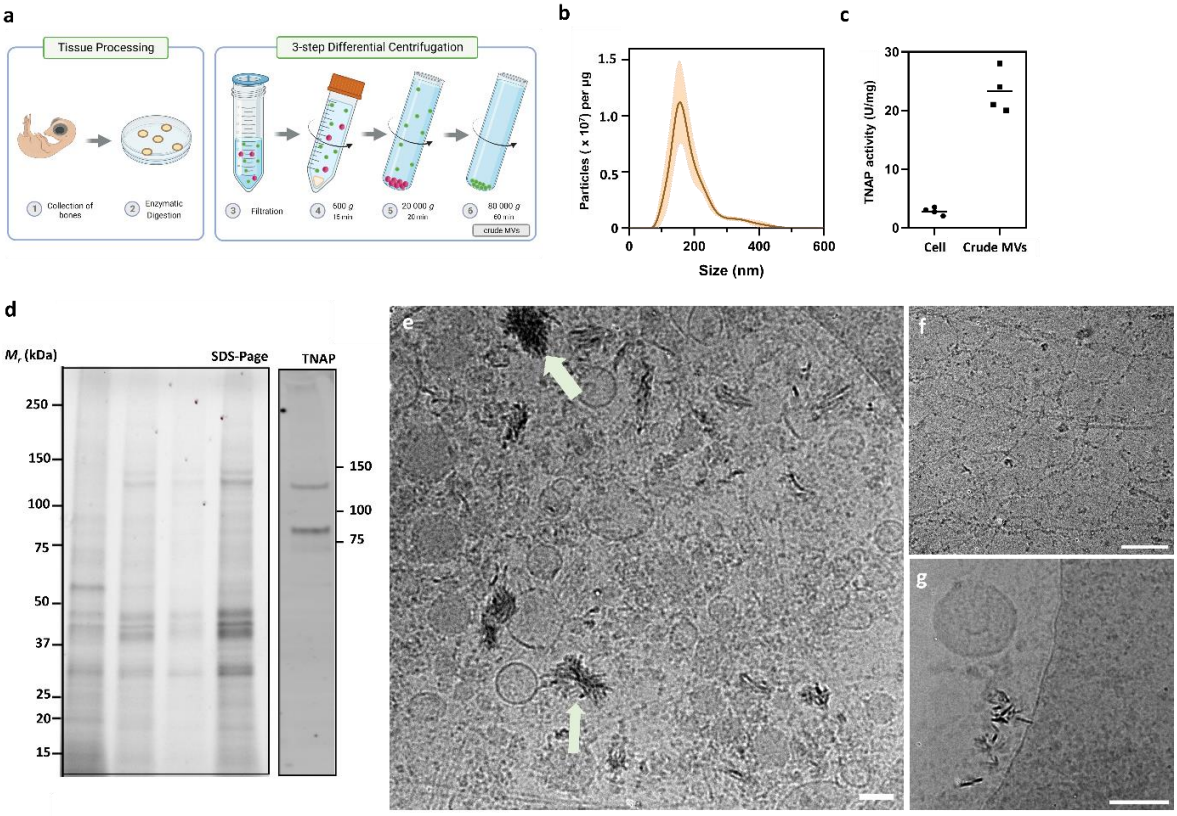

Figure 2.3 | Characterization of crude MVs preparations. a) Crude MVs were isolated after enzymatically digestion of bone slices and collected through differential ultracentrifugation. b) Distribution of particles size measured by NTA. Data presented as number of particles per µg of total protein, obtained for 3 individual experiments. c) TNAP activity (U/mg) of crude MVs compared to cell pellet (step 4 in the scheme presented in the panel a). d) SDS-PAGE migration pattern of crude MVs for 4 independent experiments (3 µg of protein per lane). The overall migration profile observed for MVs is in accordance with the expected from the literature. Notice the reproducibility in the protein profile observed for 4 different crude MVs preparations. Western Blotting against alkaline phosphatase (TNAP) revealed the presence of a broad band migrating ~ 75 kDa, and a band at ~ 130 kDa. The broad band is related to the high glycosylation of TNAP, while the band at ~130 kDa is assigned to the dimeric form of the enzyme, that is the active conformation[47]. e) cryoTEM imaging reveal the heterogeneity of crude MVs. A mixture of bilayered vesicles with non-vesicular particles is clearly discernible. f) non-vesicular particles are dominated by fibrillar proteins. While some mineral particles appear to be associated to vesicles (white arrow, panel e), mineral particles are also observed associated to non-vesicular material (X arrow, panel f). Scale bars, 100 nm.

2.4.2 | Density-gradient fractionation separates MVs from non-vesicular particles

To further separate bilayered vesicles from non-vesicular components, we used a density gradient centrifugation. Crude MVs were bottom-loaded into an iodixanol density-gradient column (10-45%), to separate MVs from co-sedimented non-vesicular particles (Figure 2.4a). Iodixanol was chosen for being isosmotic in all density ranges used. Moreover, bottom-loading is advantageous since membranous vesicles will float upwards, leaving denser components downwards. After centrifugation at 120 000 *x g* for 16 h to assure the isopycnic separation, low-dense fractions were characterized by high

TNAP activity (Figure 2.4b) and high number of particles detected with NTA per µg of protein (Figure 2.4c), when compared to crude MVs. High number of particles per µg of protein is an indicative of vesicles´ purity, since the presence of high amounts non-vesicular associated proteins will decrease the number of particles normalized per protein amount[48]. However, high density fractions were characterized by low TNAP activity and reduced number of particles/µg of protein. Therefore, low-dense MVs with high TNAP activity represents functional vesicles implicated in bone biomineralization. SDS-PAGE comparison of the protein profile of crude and low-dense MVs revealed remarkable differences (Figure 2.4d). Low-dense MVs lack bands at high molecular weight range (100-150 kDa) and some major bands at 38 and 46 kDa compared to crude MVs. Previous studies described that treatment of crude MVs with hypertonic salt solutions selectively removed bands on SDS-PAGE analysis at an apparent molecular weight of 130-150 kDa, identified to be related to type II collagen and its fragments, as confirmed by antibody recognition[46,49]. Further extraction with low ionic strength solutions removed two major bands on SDS-PAGE analysis of MVs, at an apparent molecular weight of 40-48 kDa, identified as proteoglycan-related proteins[49]. The main changes in the SDS-PAGE profile of low dense MVs were found close to these apparent molecular weight range, thus suggesting that collagens, proteoglycans, and associated proteins correspond for the majority of non-vesicular particles present in crude MVs.

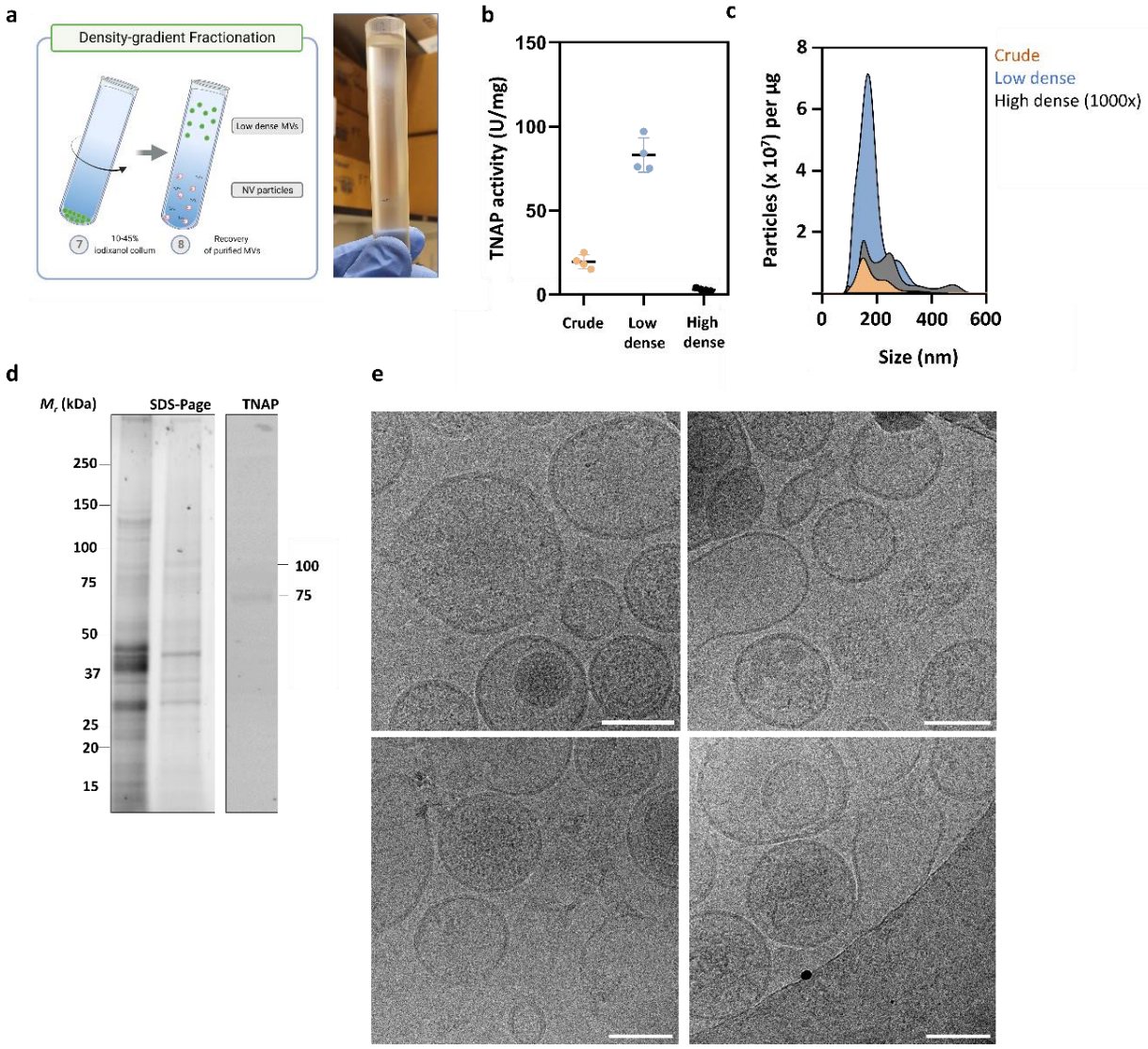

Figure 2.4 | Iodixanol density-gradient was able to separate low dense MVs from non-vesicular components. a) Crude MVs were bottom-loaded in a 10-45% iodixanol column, that after centrifugation for 16 h separated low-dense MVs from non-vesicular components. Photography of the gradient column after the centrifugation showing a broad band containing the low-dense MVs at the interface of 20-22% solutions. b) TNAP activity (U/mg) for low dense MVs compared to crude MVs. d) SDS-Page electrophoresis gel comparing crude MVs with low dense MVs. e) cryoTEM images of low dense MVs showing a distribution of bilayered MVs with almost absence of non-vesicular particles. Notice that the morphology of vesicles are heterogenous, with some vesicles appearing electron-lucent, others electron-dense, and some minor extent of multi-layered, that might be associate to the fusion upon ultracentrifugation[50]. Scale bar, 100 nm.

Finally, we imaged low dense MVs with the aid of cryoTEM, confirming the presence of single-membrane bilayered vesicles with diameters in the range of 100-200 nm. CryoTEM images also confirmed that low dense MVs are devoid of any large macromolecular aggregates and fibrillar proteins, corroborating NTA and SDS-PAGE data. Moreover, we also observe that all mineral particles observed in crude MVs (Figure

2.3e) were removed after density fractionation, and no evidence of calcium phosphate mineral presence was find neither in the inner nor at outside of the vesicles.

2.4.3 | Crude and low-dense MVs show different kinetics of induction of mineralization from soluble Ca^{2+} and Pi ions

Crude and low-dense MVs were exposed to SCL containing Ca^{2+} and Pi ions, reproducing conditions where fast induction of mineralization without the requirement of phosphatase activity is described to occur[13,26]. Then, we used cryoTEM to examine mineral formation in the presence of both the MVs preparations. To minimize bias from disturbance of the samples, we avoided the need of centrifugation to collect MVs and minerals at specific time points by conducting an on-grid mineralization experiment. In this approach we incubated MVs in solutions dropped directly on a TEM grid, in a humidity-controlled environment, and further processed for vitrification at a desired time point.

After 24 h, cryoTEM images confirmed the formation of crystalline mineral in crude MVs exposed to the SCL medium containing Ca^{2+} and Pi ions (Figure 2.5a-b). The crystals appeared as large aggregates around the vesicles, and many intact vesicles that had no sign of any associated mineral were also observed (Figure 2.5b). In contrast, for low-dense MVs at same conditions, after 24 h, we observed the majority of vesicles devoid of any associated mineral (Figure 2.5c) and some of them associated to an amorphous-like mineral at their membranes´ surface (Figure 2.5d). Note the presence of calcium phosphate clusters with approximately 20 nm, typical of metastable solutions still present in the samples containing low dense MVs even after 24 h (white arrows, Figure 2.5d). These observations were confirmed throughout the entire volume analysed, as demonstrated by the low magnification images (Figure 2.6).

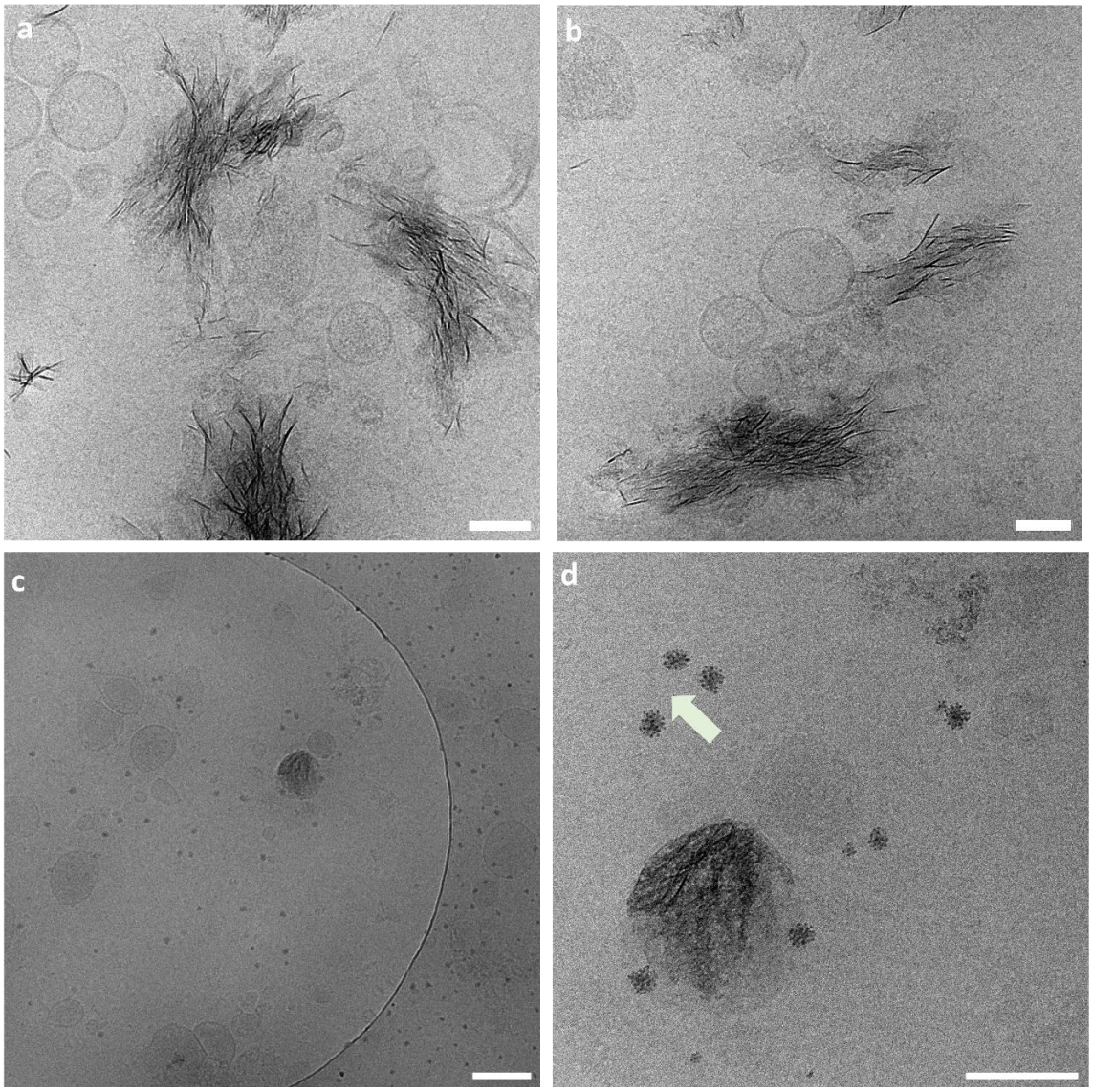

Figure 2.5 | CryoTEM reveals the relationship between MVs and forming mineral. CryoTEM images of crude (a,b) and low-dense MVs (c,d) incubated in SCL containing Ca^{2+} and Pi ions for 24 h. Arrow in panel d points to calcium phosphate clusters. Scale bars, 100 nm.

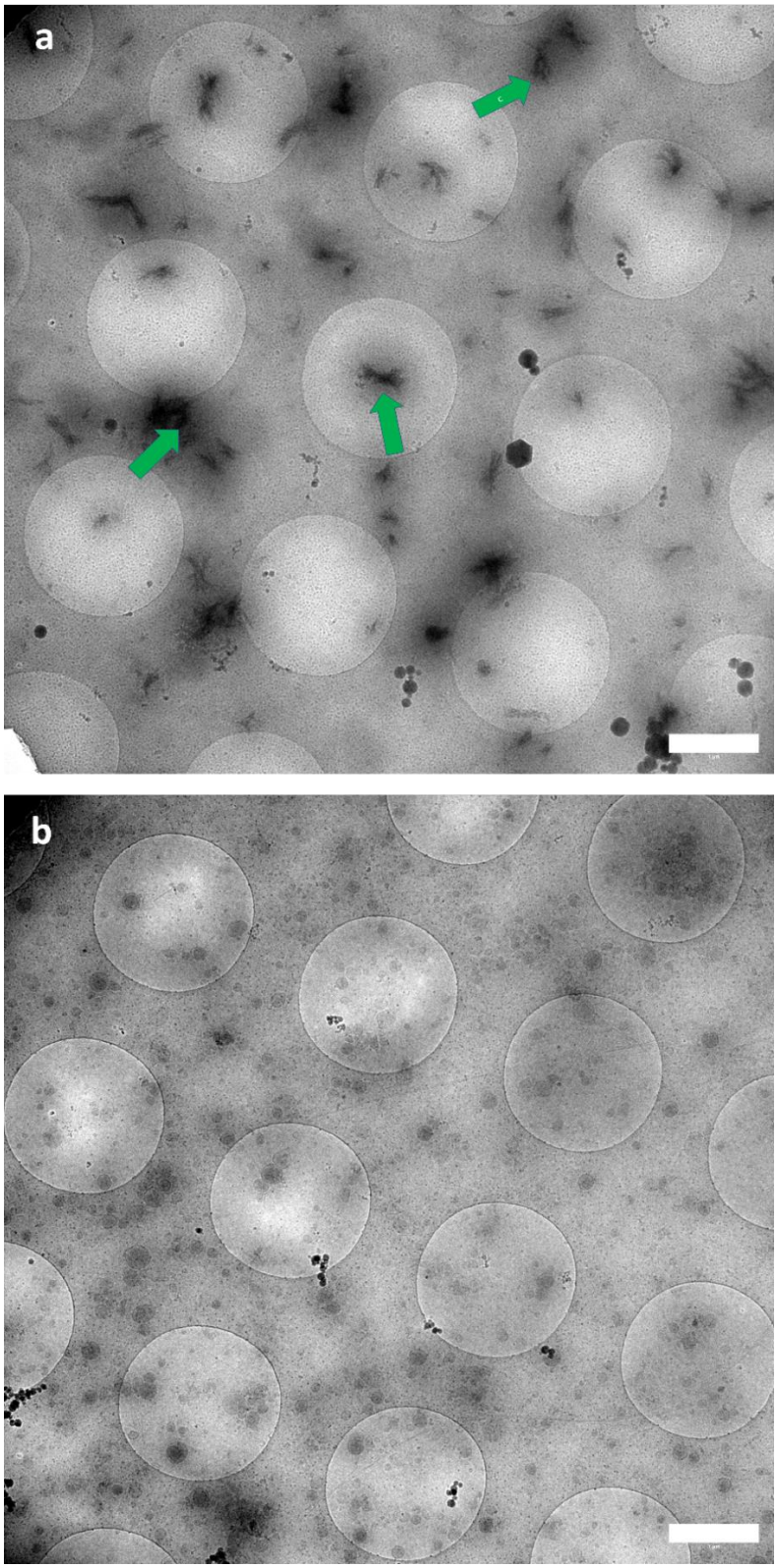

Figure 2.6 | Low magnification images of crude (a) and low-dense MVs (b) induced for mineralization for 24 h. Green arrows in image a points the large mineral aggregates. Notice the remarkable difference in the number of vesicles, at same protein concentration, for crude and low dense MVs. Scale bar, 1 μm.

To improve the knowledge about the origin of the crystalline mineral present in the samples after 24 hours of mineralization, we conducted the experiments also in an earlier time point. We found that after only 8 hours of mineralization, crude MVs already showed evidence of crystalline mineral formation. These crystals were found to be associated with vesicles (Figure 2.7a) but were also dispersed freely in the medium along with intact vesicles that did not have associated mineral (Figure 2.7b). In a small fraction of the analysed sample, some vesicles were found to be intimately associated with mineral at their membranes (white arrow, Figure 2.7c). Similar results were observed for low-dense MVs, with vesicles without any signs of associated mineral dominating the sample (Figure 2.7d). Some amorphous-like mineral particles associated to the vesicles´ membranes were also observed (Figure 2.7d), similar to the result found after 24 hours. Due to the high concentration of vesicles in low-dense MVs, we could often observe vesicles clustered together (Figure 2.7f).

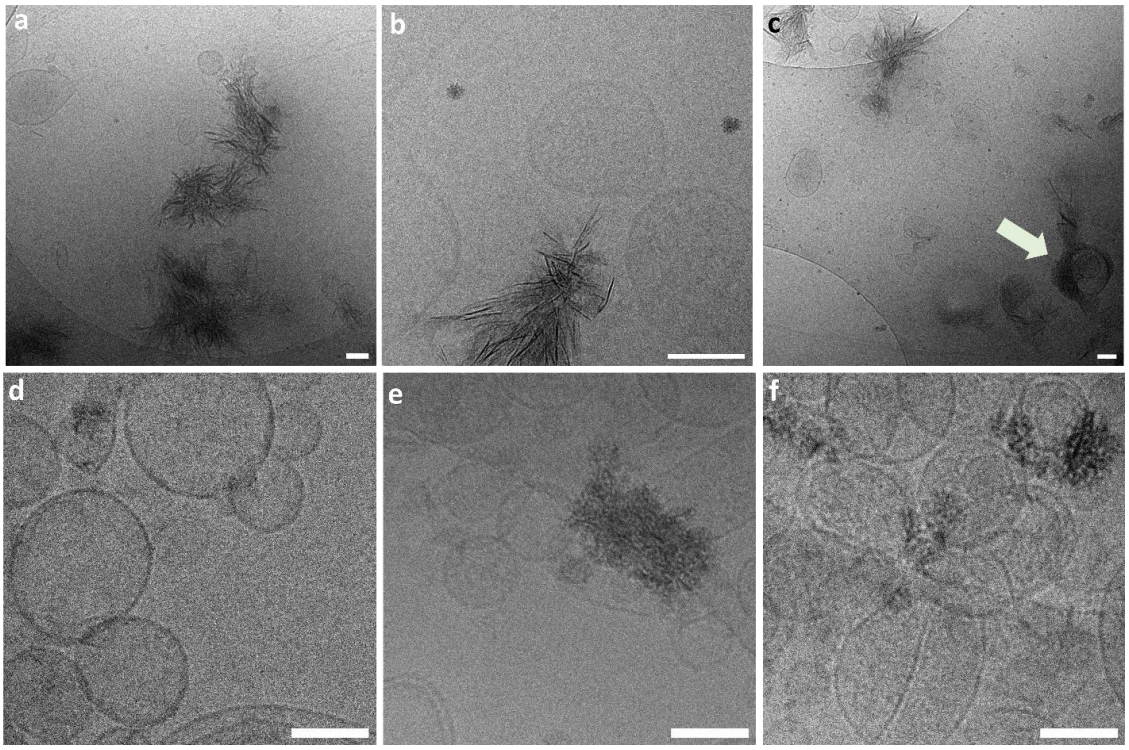

Figure 2.7 | Relationship between MVs and forming mineral at early stage. CryoTEM images of crude (a-c) and low-dense (d-f) MVs incubated in SCL containing Ca^{2+} and Pi ions for 8 h. Arrow in panel d points to mineral associated to the membrane of vesicles. Scale bars, 100 nm.

To validate the findings by cryoTEM at the nanoscale, we also examined the differences in the ability of crude and low-dense MVs to trigger mineralization at the bulk scale. For this, we first used turbidimetry, since this approach has been extensively applied to probe mineralization of MVs *in vitro*. Tracking changes in the turbidimetry

(absorbance at 350 nm) of the solution containing crude MVs (Figure 2.8a), we observed an initial increase in the turbidimetry after a lag time of 3 h, and an increase of 0.3 absorbance units after 8 h of incubation. However, low-dense MVs, at same protein concentration, induced slower changes in the turbidimetry of the solution, with an increase of only 0.1 absorbance units after 8 h of incubation. Turbidimetry is based on the measurement of the loss of intensity of transmitted light in a solution due to the scattering effect of particles in suspension. Therefore, an increase in the turbidimetry will be sensitive to changes in the diameter of scattering centres already present in the dispersion, or to the formation of new scattering particles in the medium. The turbidimetry measurements confirmed the cryoTEM findings, i.e., the formation of sub-micrometric clusters of particles in presence of crude MVs is responsible for the increase in the intensity of scattered light after incubation into SCL containing Ca^{2+} and Pi.

To get a more quantitative data, we sought to use dynamic light scattering (DLS) to investigate the size distribution of particles in solution at the beginning of the mineralization experiment and after 24 hours of incubation. By DLS we measured the intensity of light scattered by particles dispersed in liquid. Fluctuations in the intensity of the scattered light as a function of time can be recorded and used to calculate de translation diffusion coefficient of the particles from a correlation function. Then, the diffusion coefficient is converted into hydrodynamic diameter of the particles by using the Stokes-Einstein equation[51].

DLS data (Figure 2.8b) show that both crude and low-dense MVs exhibited one distribution of diameter centred at 250 nm in the initial time. However, after 24 hours of mineralization two distributions can be observed for crude MVs- one centred at 150 nm and another, much more intense, shifted towards particles with higher diameters. However, no significant changes were observed in low-dense MVs (Figure 2.8b), corroborating the cryoTEM observations, i.e., the formation of large mineral aggregates only for crude MVs after 24 hours of mineralization. Since the intensity of light scattering is proportional do the diameter[6], bigger particles scatter more light than smaller ones, explaining why the distribution of particles was dominated by the bigger particles in the DLS intensity data for crude MVs after 24 hours. The differences observed in the size distributions become clearer when we analyse the raw correlation function (Figure 2.8d). The raw correlation data shows the correlation function plotted as a function of the correlation time. The exponential function reaches zero (loss of correlation) faster in samples containing smaller particles than larger particles[51]. Therefore, we can definitively

conclude from the exponential curves in Figure 2.8d that crude MVs trigger the formation of larger particles after 24 hours of mineralization, while low-dense MVs remain almost unchanged corroborating at a bulk level our examination of mineral formation by cryoTEM. These observations were further confirmed by the polydispersity (Pdi) indexes obtained from the DLS data, which increased considerably for crude MVs samples after 24 hours due to the presence of large mineral particles (Figure 2.8e).

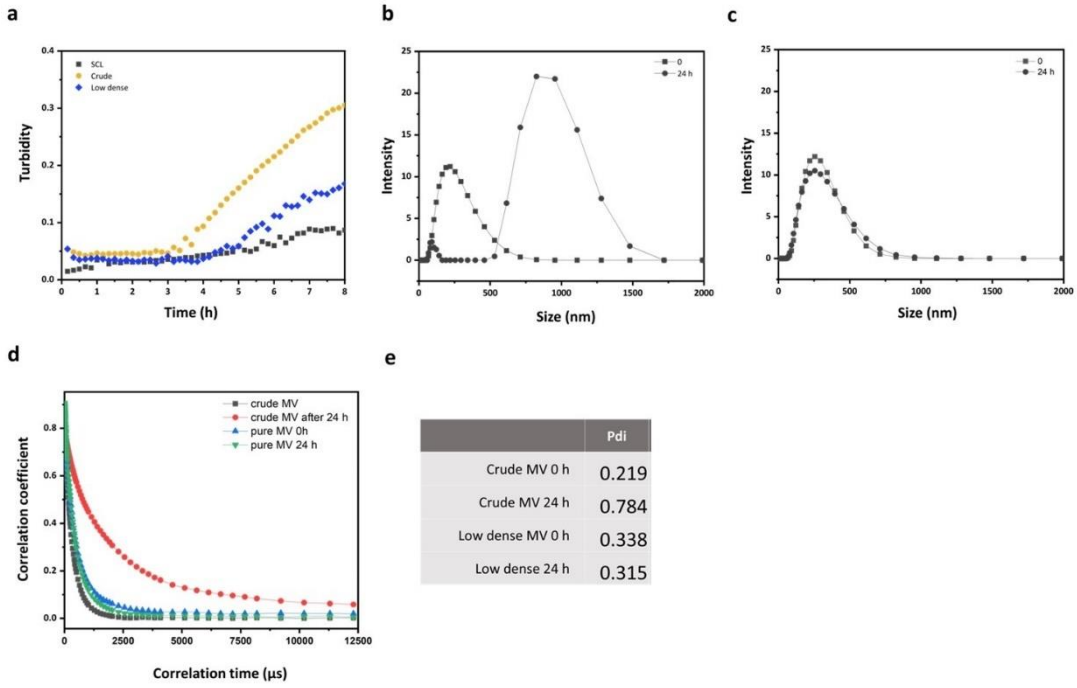

Figure 2.8 | Examination of mineral formation at bulk level. a) Turbidity (absorbance at 350 nm) over time for crude and low-dense MVs in SCL containing Ca^{2+} and Pi, at 37°C. Distribution of particles measured with DLS at time 0, and after 24 h of mineralization, for crude (b) and low-dense MVs (c). d) Correlation coefficient versus correlation time (µs). e) Pdi values obtained for the different measurements.

2.4.4 | Crude and low-dense induce mineralization in presence of ATP

Finally, we tested the ability of the crude and low-dense MVs to induce mineral formation through by the hydrolysis of ATP by TNAP present in the MVs´ structure, to generate Pi. Since ATP is a strong mineralization inhibitor, no mineralization is induced without its degradation[52]. Both crude and low-dense MVs were able to hydrolyse ATP as revealed by the increased Pi concentration as a function of time (Figure 2.9a). However, the conversion rate is faster for low-dense MVs due to their increased TNAP activity compared to crude MVs. CryoTEM images of crude (Figure 2.9b-c) and low-dense MVs (Figure 2.9d-e**)** after 24 h of incubation in SCL in the presence of ATP revealed the

formation of mineral precipitates around the vesicles, in accordance with previous reports[53,54].

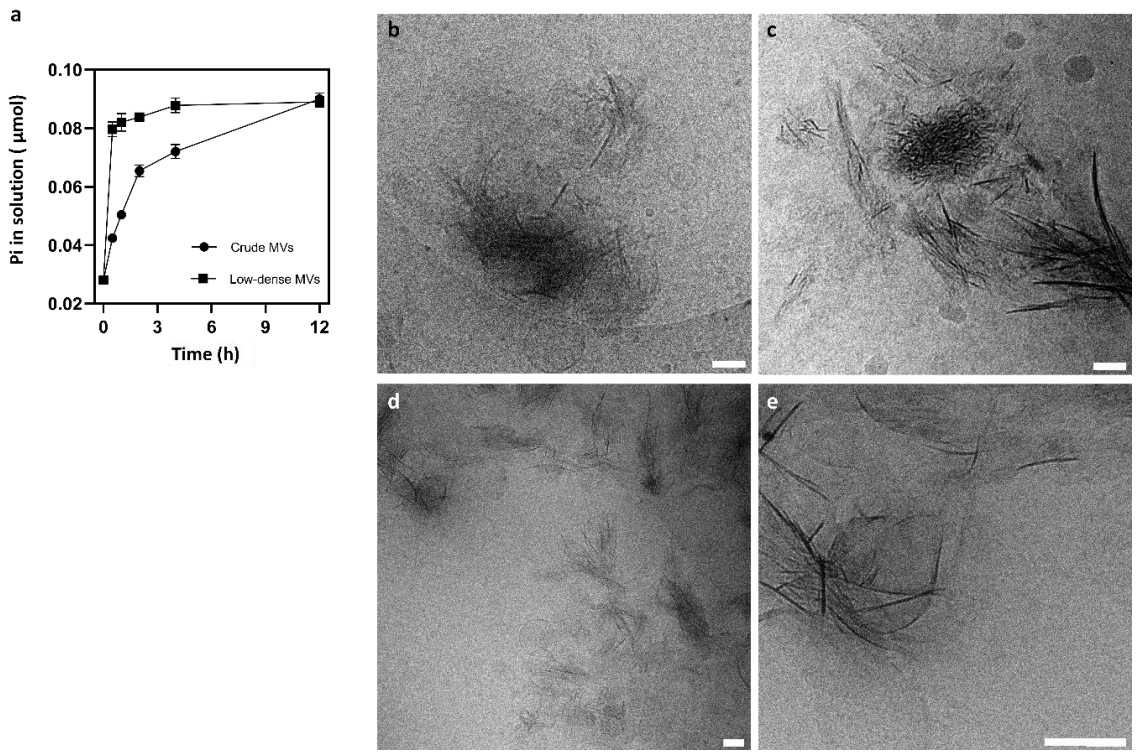

Figure 2.9 | Mineralization induced by hydrolysis of ATP. a) Changes in the concetration of Pi formed as a function of time for crude and low-dense MVs exposed to SCL containing 1 mM ATP, at 37°C and measured in a reaction volume of 20 µL. CryoTEM images mineral formed when crude (b,c) and low-dense (d,e) MVs were incubated for 24 h in the SCL containing ATP.

2.5 | Discussion

The coexistence of MVs along with apatite crystals within different tissues undergoing mineralization has been extensively demonstrated[33,55]. However, understanding the mechanisms of MVs action is challenging due to the changes at nanoscale that takes place during bone mineralization. Furthermore, the formation of products resultant of MV action, i.e., HAp crystals, follows general physicochemical rules, thus requiring a multidisciplinary approach to fully appreciate all underlying mechanisms. The interpretation of the mineralization rate, type, and amount of mineral formed after exposure of MVs to mineralizing solutions has led to the proposal of two major pathways for HAp precipitation. These mechanisms involve either the direct nucleation from soluble ions, or through an increase in Pi concentration due to phosphatase enzymes able to hydrolyze organophosphate compounds. In this thesis studies, we presented new insights into these two mechanisms, thanks to our

unprecedented capability to integrate bulk measurements with near-native cryoTEM imaging at a single vesicle scale.

First, we demonstrated that crude MVs preparations are heterogenous and contains a large amount of non-vesicular particles in addition to bilayered vesicles, based on cryoTEM images. Conventional TEM imaging of dried and stained vesicles revealed also the presence of fibrillar proteins in the samples but it was difficult to discern the relationship between the different components of the material (Supplementary Figure S2.1). By keeping the samples in hydrated state using cryoTEM, we observed that, in general, the fibrillar proteins are not intimately associated with the vesicles, but rather dispersed in the medium. Upon fractionation with the iodixanol-density gradient, we dissected a population of bilayered low-dense MVs absent of any non-vesicular structure. By comparing the mineralization ability of crude and low-dense MVs, we observed that removing these non-vesicular particles had a major impact in the onset of mineral formation in presence of soluble Ca^{2+} and Pi ions. Crude MVs induced fast formation of crystalline mineral after 8 h, however low-dense MVs promoted the formation of a small amount of mineral associated to their lipid membranes after 24 h, as observed by cryoTEM. This result is in accordance with previous studies in which fractionation of crude MVs in sucrose gradients yield a less-dense fraction of vesicles with high TNAP activity, but reduced ability to induce fast mineralization in the presence of Ca^{2+} and Pi ions[56,57]. In those studies, it was demonstrated that Ca^{2+} and Pi ions migrated to denser sucrose fractions, not coexisting anymore with the TNAP-rich less-dense fractions. Since sucrose solutions are hyperosmotic at high concentrations, its use for MVs fractionation is thought to destabilize a luminal pool of Ca^{2+} and Pi ions due to the osmotic pressure imposed by high concentration of sucrose. Therefore, this pool of bound Ca^{2+} and Pi ions has been hypothesized to be a major component responsible for the ability of MVs to trigger mineral nucleation[29]. This hypothesis was supported by other treatments of crude MVs, such as citrate buffer, or with calcium-chelating agents, that also removed most of the associated mineral ions and as a consequence the ability of MVs to trigger mineral nucleation[12,29,31]. In our experiments we used a isosmotic medium (iodixanol) and added Ca^{2+} ions to prevent dissolution of labile ions[12]. Upon fractionation in the iodixanol gradient, analysis of cryoTEM images and the changes in the SDS-Page protein profile led us to the conclusion that this purification step removed most of the associated fibrillar collagens and proteoglycans from the samples. Therefore, our results suggest that the pool of bound Ca^{2+} and Pi ions, previously thought to be a luminal cargo of the bilayered MVs

themselves, is rather associated to the non-vesicular particles (such as collagens and proteoglycans) present in crude MVs preparations. This reinterpretation also explains why the ability to induce fast mineralization could also be destroyed upon EDTA and citrate treatments, as we would not expect these highly charged molecules to cross the lipid bilayer to remove Ca^{2+} from the vesicle interior. Confirming our conclusions, Kirsch et al. reported that sucrose-fractionated low-dense MVs could recover the ability to induce fast mineral nucleation by adding native collagen to the medium[56]. Moreover, Wu et al. observed a marked reduction in the ability to trigger mineralization after treating MVs with hydrazine, that removed ~95% of the proteoglycans associated with MVs[58]. Therefore, our observations suggest that non-vesicular proteins dominated by fibrillar collagens and proteoglycans responds for the ability of crude MVs to trigger mineral nucleation, either for bringing a large amount of Ca^{2+} and Pi ions, thus increasing supersaturation or through their intrinsic nucleating activity[59]. To support our conclusions, we confirmed that the fraction collected at higher density in the iodixanol gradient induced the formation of crystalline mineral after 24 h when exposed to the same conditions in which low dense MVs did not. (Supplementary Figure S2.2).

The ability of crude MVs to trigger mineral nucleation has been historically assigned to the existence of a nucleational core within MVs that is converted to apatite when in contact to Ca^{2+} and Pi ions. This nucleation core was hypothesized to contain two main components as follow: a pool of Ca^{2+} and Pi ions bound to luminal proteins and a membrane-associated complex of Ca^{2+}, Pi, phosphatidylserine, and annexin that nucleates the formation of crystalline mineral[29]. Our results do not discard the possibility of intraluminal mineralization events during MV´s driven mineralization, however the association of mineral with the MV`s membrane confirm the importance of calcium-binding components to mediate mineral nucleation. The ability of Ca^{2+}-binding sites to mediate mineral nucleation is a well-known phenomenon in biomineralization[60]. From cryoTEM images, we observed only a limited amount of mineral associated with the membranes of vesicles. While it is true that complexes of phosphatidylserine and annexins with Ca^{2+} and Pi can effectively nucleate HAp *in vitro*[27,28,61], our results suggest that this capability might be of secondary importance when these components are present within the membrane of MVs, or occurring at a much slower rate.

The results also evidenced the primary functionality of MVs by making Pi available for mineralization through phosphatase activity. Upon exposure to ATP, both crude and low-dense MVs trigged mineral formation, as shown in the cryoTEM images

(Figure 2.9), that revealed the formation of mineral crystals around the vesicles. TNAP played a significant role in this process, since it can efficiently hydrolyse organophosphate substrates and increase the concentration of Pi, which leads to the precipitation of minerals and the formation of minerals in the extravesicular space. The observation of minerals in the extravesicular space is in accordance with experiments conducted by Hsu & Anderson, in which MVs were exposed to an ATP-containing mineralizing medium for 24 hours to reach maximal mineral deposition, sedimented, incubated with a calcium-chelating agent (EGTA) for 24 hours to remove MV-associated minerals, and further sedimented to reveal vesicles that seemed to lack minerals but can still trigger precipitation upon ATP readdition[17]. Moreover, besides TNAP, MVs harbour other different phosphatases that share a common functionality: producing Pi for mineralization by degrading organophosphate compounds[23]. The origin of organophosphates found in the extracellular matrix is yet unclear. Some possibilities are related to polyphosphates[62,63], the cell-mediate secretion of ATP[64], or the self-degradation of MVs' membrane phospholipids[65]. These different phosphatases are demonstrated *in vivo* to work in non-reductant way, since either individual or mutual genetic ablation of their functions always result in a certain level of deficient extracellular mineralization. These observations together emphasize the primary function of MVs, which is to provide enzymatic machinery able to locally regulate the concentration of Pi. Mineral precipitation occurs when an optimized environment that allows mineralization is achieved, which involves supersaturation and consumption of inhibitors guided by principles of thermodynamics. At this point, a secondary role of MVs related to accumulation of Ca^{2+} can be also highlighted: Ca^{2+}-binding sites of MVs act as motifs that interact with mineral ions and create boundaries through compartmentalization, changing energy barriers and creating smoother energy landscapes[66].

Finally, another important insight from our observations is about the relation between MVs and forming mineral during *in vitro* mineralization. From ultrastructural studies of tissue sections, in which crystals were observed in and out the membrane of vesicles, MV-driven mineralization is hypothesized to follow a biphasic phenomenon, where mineralization is first initiated within the lumen of vesicles and then after membrane rupture, the crystals are released to extracellular medium[67]. Therefore, attempts have been made to relate the sequence of steps observed during *in vitro* mineralization to the *in vivo* mechanisms by which MVs initiate mineralization. Extensive data has been collected on the mineralization of MVs in the presence of Ca^{2+} and Pi ions,

comprehensively reviewed by Wuthier[33]. By measuring the amount of mineral formed, it has been observed that MVs undergo a series of predictable stages. Initially, there is a lag period with minimal ion accumulation, followed by a period of rapid accumulation of Ca^{2+} and Pi. After this, there is an extended plateau period of slow ion accumulation, during which the Ca/P ratio gradually increases, approaching that of HAp after 24 hours. The first detectable mineral phase appears just after the period of rapid accumulation, which typically lasts 4 to 6 hours. This mineral phase is characterized by an acidic octacalcium phosphate (OCP)-like phase, with a Ca/P ratio close to 1.33, as determined by various spectroscopic methods[58,68,69]. The rationalization that the first detection of crystalline mineral after 4-6 hours reflects the biphasic process hypothesized to occur in MVs-driven mineralization has suggested a life span for these structures of short 4-6 h, after this membrane rupture should occur to grant the release the initially formed crystals. Herein, the cryoTEM images of crude MVs revealed that after 8 h, , which from our turbidimetric analysis represents the end of the so-called rapid acquisition phase, crystals were mostly restricted to the extravesicular space, and intact vesicles could be detected even after 24 h of reaction. The lag period is currently believed to be a rate-limiting step, which reflects the inability of ions to pass through the vesicle membrane and reach the lumen. Once they reach the lumen, "sink conditions" provided by the nucleational core drive the accumulation of Ca^{2+} and Pi, that is converted into the first detectable OCP-like crystals. After careful combination of turbidimetry and cryoTEM experiments, we have reached the conclusion that the rapid acquisition phase observed does not accurately represent the spatial process by which Ca^{2+} and Pi ions are taken up into the lumen of MVs to trigger mineralization. Rather, it appears to be a bulk event of nucleation occurring within the solution, triggered by the nucleating activity of non-vesicular components present in crude MVs. Therefore, this reinterpretation of bulk mineralization experiments suggests that MVs have a significantly longer lifespan than previously thought.

SCL is a metastable solution stabilized against precipitation in the absence of a nucleation-inducing agent. We calculated the supersaturation for calcium phosphate phases with the SCL composition. Supersaturation to ACP, OCP and HAp were found from these calculations (Supplementary Note 1). In fact, we observed the presence of 20 nm-sized calcium phosphate clusters, typical of metastable solutions. Therefore, the sequence of phase transformations from ACP, to OCP until the formation of HAp detected by spectroscopy during *in vitro* MVs mineralization reflects the sequence of

phase transitions observed during the precipitation of calcium phosphate from metastable solutions[39]. In line with this interpretation, same previously described factors can extend the lag period of MVs mineralization, such as addition of Mg^{2+} or Zn^{2+} ions[70–72], also known as inhibitors of HAp crystallization, stabilizing of precursor phases. Interestingly, the addition of ATP can effectively prolong the lag period during the formation and growth of HAp due to its pyrophosphate group, which strongly inhibits mineralization[52]. However, once the ATP is hydrolysed by TNAP , mineralization is enabled to proceed, revealing the primary role of MVs in controlling mineralization by providing a phosphatase machinery.

2.6 | Conclusions

The results presented in this chapter combined cryoTEM with bulk characterizations to track the sequence of events that controls MVs´ driven mineralization in a near-native state. From them, classical experiments and their interpretations were revisited, which enabled us to advance the understanding the mechanisms of MVs´ action. Our findings revealed that crude MVs isolated from chicken embryos growth plate are heterogeneous and consist not only of bilayered vesicles but also of non-vesicular material, dominated by soluble proteins and fibrillar collagens. The presence of this non-vesicular compounds hinder the precise interpretation of *in vitro* mineralization experiments.

It is important to note that non-vesicular components should not always be considered as contaminants. It has already been reported that the formation of a corona acquired from the extracellular milieu, composed by soluble proteins at the surface of extracellular vesicles can regulate and direct their function[73]. Proteoglycans, collagens, and non-collagenous proteins have been reported to be present in MVs preparations[74], and the coexistence of MVs with these components within the extracellular matrix, has been long recognized at the ultrastructural level[75]. Therefore, *in vivo* bone mineralization will require interaction among all these components. The results presented in this chapter suggest that the primary role of MVs is to provide an enzymatic machinery to locally control Pi concentration. However, future research should address the individual contribution and interaction between different components in the control of mineralization.

2.7 | References

1. Reznikov, N. *et al.* Biological stenciling of mineralization in the skeleton: Local enzymatic removal of inhibitors in the extracellular matrix. *Bone* **138**, 115447–115461 (2020).
2. Bonucci, E. Fine structure of early cartilage calcification. *J. Ultrastruct. Res.* **20**, 33–50 (1967).
3. Anderson, H. C. Electron microscopic studies of induced cartilage development and calcification. *J. Cell Biol.* **35**, 81–101 (1967).
4. Matsuzawa, T. & Anderson, H. C. Phosphatases of epiphyseal cartilage studied by electron microscopic cytochemical methods. *J. Histochem. Cytochem.* **19**, 801–808 (1971).
5. Landis, W. J. & Glimcher, M. J. Electron optical and analytical observations of rat growth plate cartilage prepared by ultracryomicrotomy: The failure to detect a mineral phase in matrix vesicles and the identification of heterodispersed particles as the initial solid phase of calcium p. *J. Ultrastruct. Res.* **78**, 227–268 (1982).
6. Hunziker, E. B., Herrmann, W., Cruz-Orive, L. M. & Arsenault, A. L. Image analysis of electron micrographs relating to mineralization in calcifying cartilage: Theoretical considerations. *J. Electron Microsc. Tech.* **11**, 9–15 (1989).
7. Bernard, G. W. & Pease, D. C. An electron microscopic study of initial intramembranous osteogenesis. *Am. J. Anat.* **125**, 271–290 (1969).
8. Sisca, R. F. & Provenza, D. V. Initial dentin formation in human deciduous teeth. *Calcif. Tissue Res.* **9**, 1–16 (1972).
9. Aikawa, E. & Blaser, M. C. 2020 Jeffrey M. Hoeg Award Lecture; Calcifying Extracellular Vesicles as Building Blocks of Microcalcifications in Cardiovascular Disorders. *Arteriosclerosis, Thrombosis, and Vascular Biology*. **41**, 117–127 (2021).
10. Ali, S. Y., Sajdera, S. W. & Anderson, H. C. Isolation and characterization of calcifying matrix vesicles from epiphyseal cartilage. *Proc. Natl. Acad. Sci. U. S. A.* **67**, 1513–1520 (1970).
11. Register, T. C., McLean, F. M., Low, M. G. & Wuthier, R. E. Roles of alkaline phosphatase and labile internal mineral in matrix vesicle-mediated calcification. Effect of selective release of membrane-bound alkaline phosphatase and

treatment with isosmotic pH 6 buffer. *J. Biol. Chem.* **261**, 9354–9360 (1986).

12. McLean, F. M., Keller, P. J., Genge, B. R., Walters, S. A. & Wuthier, R. E. Disposition of preformed mineral in matrix vesicles. Internal localization and association with alkaline phosphatase. *J. Biol. Chem.* **262**, 10481–10488 (1987).
13. Balcerzak, M. *et al.* A comparative analysis of strategies for isolation of matrix vesicles. *Anal. Biochem.* **361**, 176–182 (2007).
14. Ali, S. Y., Wisby, A., Evans, L. & Craig-Gray, J. The sequence of calcium and phosphorus accumulation by matrix vesicles. *Calcif. Tissue Res.* **22**, 490–493 (1976).
15. Robison, R. & Soames, K. M. The Possible Significance of Hexosephosphoric Esters in Ossification. *Biochem. J.* **18**, 740–754 (1924).
16. Orriss, I. R. Extracellular pyrophosphate: The body's "water softener". *Bone* **134**, 115243–115252 (2020).
17. Hsu, H. H. T. & Clarke Anderson, H. Evidence of the presence of a specific ATPase responsible for ATP- initiated calcification by matrix vesicles isolated from cartilage and bone. *J. Biol. Chem.* **271**, 26383–26388 (1996).
18. Hsu, H. H. T. In vitro calcium deposition by rachitic rat matrix vesicles: nucleoside triphosphate supported calcium deposition. *BBA - Gen. Subj.* **1116**, 227–233 (1992).
19. Hsu, H. H. T., Morris, D. C., Davis, L., Moylan, P. & Anderson, C. H. In vitro Ca deposition by rat matrix vesicles: Is the membrane association of alkaline phosphatase essential for matrix vesicle-mediated calcium deposition? *Int. J. Biochem.* **25**, 1737–1742 (1993).
20. Yadav, M. C. *et al.* Loss of skeletal mineralization by the simultaneous ablation of PHOSPHO1 and alkaline phosphatase function: A unified model of the mechanisms of initiation of skeletal calcification. *J. Bone Miner. Res.* **26**, 286–297 (2011).
21. Collins, M. T. *et al.* Skeletal and extraskeletal disorders of biomineralization. *Nat. Rev. Endocrinol.* **18**, 473–489 (2022).
22. Hessle, L. *et al.* Tissue-nonspecific alkaline phosphatase and plasma cell membrane glycoprotein-1 are central antagonistic regulators of bone mineralization. *Proc. Natl. Acad. Sci.* **99**, 9445–9449 (2002).
23. Millán, J. L. The role of phosphatases in the initiation of skeletal mineralization.

Calcif. Tissue Int. **93**, 299–306 (2013).

24. Narisawa, S., Yadav, M. C. & Millán, J. L. In vivo overexpression of tissue-nonspecific alkaline phosphatase increases skeletal mineralization and affects the phosphorylation status of osteopontin. *J. Bone Miner. Res.* **28**, 1587–1598 (2013).
25. Ciancaglini, P. *et al.* Kinetic analysis of substrate utilization by native and TNAP-, NPP1-, or PHOSPHO1-deficient matrix vesicles. *J. Bone Miner. Res.* **25**, 716–723 (2010).
26. Genge, B. R., Sauer, G. R., Wu, L. N. Y., McLean, F. M. & Wuthier, R. E. Correlation between loss of alkaline phosphatase activity and accumulation of calcium during matrix vesicle-mediated mineralization. *J. Biol. Chem.* **263**, 18513–18519 (1988).
27. Genge, B. R., Wu, L. N. Y. & Wuthier, R. E. In vitro modeling of matrix vesicle nucleation: Synergistic stimulation of mineral formation by annexin A5 and phosphatidylserine. *J. Biol. Chem.* **282**, 26035–26045 (2007).
28. Wu, L. N. Y., Genge, B. R. & Wuthier, R. E. Analysis and molecular modeling of the formation, structure, and activity of the phosphatidylserine-calcium-phosphate complex associated with biomineralization. *J. Biol. Chem.* **283**, 3827–3838 (2008).
29. Wu, L. N. Y. *et al.* Characterization of the nucleational core complex responsible for mineral induction by growth plate cartilage matrix vesicles. *J. Biol. Chem.* **268**, 25084–25094 (1993).
30. Wuthier, R. E. & Gore, S. T. Partition of inorganic ions and phospholipids in isolated cell, membrane and matrix vesicle fractions: Evidence for Ca-Pi-acidic phospholipid complexes. *Calcif. Tissue Res.* **24**, 163–171 (1977).
31. Register, T. C., McLean, F. M., Low, M. G. & Wuthier, R. E. Roles of alkaline phosphatase and labile internal mineral in matrix vesicle-mediated calcification. Effect of selective release of membrane-bound alkaline phosphatase and treatment with isosmotic pH 6 buffer. *J. Biol. Chem.* **261**, 9354–9360 (1986).
32. Genge, B. R., Wu, L. N. Y. & Wuthier, R. E. Differential fractionation of matrix vesicle proteins. Further characterization of the acidic phospholipid-dependent Ca2+-binding proteins. *J. Biol. Chem.* **265**, 4703–4710 (1990).
33. Wuthier, R. E. Matrix vesicles: structure, composition, formation and function in calcification. *Front. Biosci.* **16**, 2812–2902 (2011).

34. Wu, L. N. Y., Genge, B. R., Kang, M. W., Arsenault, A. L. & Wuthier, R. E. Changes in Phospholipid Extractability and Composition Accompany Mineralization of Chicken Growth Plate Cartilage Matrix Vesicles. *J. Biol. Chem.* **277**, 5126–5133 (2002).
35. Plaut, J. S. *et al.* Quantitative atomic force microscopy provides new insight into matrix vesicle mineralization. *Arch. Biochem. Biophys.* **667**, 14–21 (2019).
36. Patterson, J. P., Xu, Y., Moradi, M., Sommerdijk, N. A. J. M. & Friedrich, H. CryoTEM as an Advanced Analytical Tool for Materials Chemists. *Accounts of chemical research*. **50**, 1495–1501 (2017).
37. Nudelman, F. *et al.* The role of collagen in bone apatite formation in the presence of hydroxyapatite nucleation inhibitors. *Nat. Mater.* **9**, 1004–1009 (2010).
38. Xu, Y. *et al.* Intermolecular channels direct crystal orientation in mineralized collagen. *Nat. Commun.* **11**, 5068–5080 (2020).
39. Habraken, W. J. E. M. *et al.* Ion-association complexes unite classical and non-classical theories for the biomimetic nucleation of calcium phosphate. *Nat. Commun.* **4**, 1507–1519 (2013).
40. Murata, K. & Wolf, M. Cryo-electron microscopy for structural analysis of dynamic biological macromolecules. *Biochim. Biophys. Acta - Gen. Subj.* **1862**, 324–334 (2018).
41. Buchet, R., Pikula, S., Magne, D. & Mebarek, S. Isolation and Characteristics of Matrix Vesicles. in *Phosphatase Modulators* 115–124 (2013).
42. Hamburger, V. & Hamilton, H. L. A series of normal stages in the development of the chick embryo. *Dev. Dyn.* **195**, 231–272 (1992).
43. Jeppesen, D. K. *et al.* Reassessment of Exosome Composition. *Cell* **177**, 428–445 (2019).
44. Laemmli, U. K. Cleavage of Structural Proteins during the Assembly of the Head of Bacteriophage T4. *Nature* **227**, 680–685 (1970).
45. Balcerzak, M. *et al.* Proteome analysis of matrix vesicles isolated from femurs of chicken embryo. *Proteomics* **8**, 192–205 (2008).
46. Wu, L. N. Y., Genge, B. R., Lloyd, G. C. & Wuthier, R. E. Collagen-binding proteins in collagenase-released matrix vesicles from cartilage. Interaction between matrix vesicles proteins and different types of collagen. *J. Biol. Chem.* **266**, 1195–1203 (1991).
47. Wu, L. N. Y., Valhmu, W. B., Lloyd, G. C., Genge, B. R. & Wuthier, R. E.

Isolation of two glycosylated forms of membrane-bound alkaline phosphatase from avian growth plate cartilage matrix vesicle-enriched microsomes. *Bone Miner.* **7**, 113–125 (1989).

48. Webber, J. & Clayton, A. How pure are your vesicles? *J. Extracell. Vesicles* **2**, 19861–19867 (2013).
49. Wu, L. N. Y., Genge, B. R. & Wuthier, R. E. Association between proteoglycans and matrix vesicles in the extracellular matrix of growth plate cartilage. *J. Biol. Chem.* **266**, 1187–1194 (1991).
50. Broad, K. *et al.* Unraveling multilayered extracellular vesicles: Speculation on cause. *J. Extracell. vesicles* **12**, e12309–e12315 (2023).
51. Stetefeld, J., McKenna, S. A. & Patel, T. R. Dynamic light scattering: a practical guide and applications in biomedical sciences. *Biophys. Rev.* **8**, 409–427 (2016).
52. Li, L., Buchet, R. & Wu, Y. Dimethyl sulfoxide-induced hydroxyapatite formation: A biological model of matrix vesicle nucleation to screen inhibitors of mineralization. *Anal. Biochem.* **381**, 123–128 (2008).
53. Hsu, H. H. T. & Clarke Anderson, H. A role for ATPase in the mechanisms of ATP-dependent Ca and phosphate deposition by isolated rachitic matrix vesicles. *Int. J. Biochem. Cell Biol.* **27**, 1349–1356 (1995).
54. Hsu, H. H. T. & Anderson, H. C. A simple and defined method to study calcification by isolated matrix vesicles effect of ATP and vesicle phosphatase. *BBA - Gen. Subj.* **500**, 162–172 (1977).
55. Hasegawa, T. Ultrastructure and biological function of matrix vesicles in bone mineralization. *Histochem. Cell Biol.* **149**, 289–304 (2018).
56. Kirsch, T., Ishikawa, Y., Mwale, F. & Wuthier, R. E. Roles of the nucleational core complex and collagens (types II and X) in calcification of growth plate cartilage matrix vesicles. *J. Biol. Chem.* **269**, 20103–20109 (1994).
57. Register, T. C., Mclean, F. M., Lows, M. G. & Wuthier, R. E. Roles of Alkaline Phosphatase and Labile Internal Mineral in Matrix Vesicle-mediated Calcification. *J. Biol. Chem.* **261**, 9354–9360 (1986).
58. Wu, L. *et al.* Physicochemical Characterization of the Nucleational Core of Matrix Vesicles. *J. Biol. Chem.* **272**, 4404–4411 (1997).
59. Wojtas, M., Lausch, A. J. & Sone, E. D. Glycosaminoglycans accelerate biomimetic collagen mineralization in a tissue-based in vitro model. *Proc. Natl. Acad. Sci. U. S. A.* **117**, 12636–12642 (2020).

60. Dey, A. *et al*. The role of prenucleation clusters in surface-induced calcium phosphate crystallization. *Nat. Mater.* **9**, 1010–1014 (2010).

61. Boskey, A. L. & Posner, A. S. In vitro nucleation of hydroxyapatite by a bone calcium-phospholipid-phosphate complex. *Calcif. Tissue Res.* **22**, 197–201 (1976).

62. Omelon, S. *et al*. Control of vertebrate skeletal mineralization by polyphosphates. *PLoS One* **4**, e5634–e5650 (2009).

63. Omelon, S., Ariganello, M., Bonucci, E., Grynpas, M. & Nanci, A. A review of phosphate mineral nucleation in biology and geobiology. *Calcif. Tissue Int.* **93**, 382–396 (2013).

64. Szeri, F. *et al*. The Mineralization Regulator ANKH Mediates Cellular Efflux of ATP, Not Pyrophosphate. *J. Bone Miner. Res.* **37**, 1024–1031 (2022).

65. Dillon, S., Staines, K. A., Millán, J. L. & Farquharson, C. How To Build a Bone: PHOSPHO1, Biomineralization, and Beyond. *JBMR Plus* **3**, e10202–e10214 (2019).

66. Kahil, K., Weiner, S., Addadi, L. & Gal, A. Ion Pathways in Biomineralization: Perspectives on Uptake, Transport, and Deposition of Calcium, Carbonate, and Phosphate. *J. Am. Chem. Soc.* **143**, 21100–21112 (2021).

67. Anderson, H. C., Garimella, R. & Tague, S. E. The role of matrix vesicles in growth plate development and biomineralization. *Front. Biosci.* **10**, 822–837 (2005).

68. Sauer, G. R. & Wuthier, R. E. Fourier transform infrared characterization of mineral phases formed during induction of mineralization by collagenase-released matrix vesicles in vitro. *J. Biol. Chem.* **263**, 13718–13724 (1988).

69. Sauer, G., Zunic, W., Durig, J. & Wuthier, R. Fourier transform Raman spectroscopy of synthetic and biological calcium phosphates. *Calcif. Tissue Int.* **54**, 414–420 (1994).

70. Sauer, G. R., Wu, L. N. Y., Iijima, M. & Wuthier, R. E. The influence of trace elements on calcium phosphate formation by matrix vesicles. *J. Inorg. Biochem.* **65**, 57–65 (1997).

71. Wu, L. N. Y., Genge, B. R. & Wuthier, R. E. Differential effects of zinc and magnesium ions on mineralization activity of phosphatidylserine calcium phosphate complexes. *J. Inorg. Biochem.* **103**, 948–962 (2009).

72. Sauer, G. R., Adkisson, H. D., Genge, B. R. & Wuthier, R. E. Regulatory effect

of endogenous zinc and inhibitory action of toxic metal ions on calcium accumulation by matrix vesicles in vitro. *Bone Miner.* **7**, 233–244 (1989).

73. Ramos, A. P. *et al.* The functional role of soluble proteins acquired by extracellular vesicles. *J. Extracell. Biol.* **1**, e34–e55 (2022).
74. Nahar, N. N., Missana, L. R., Garimella, R., Tague, S. E. & Anderson, H. C. Matrix vesicles are carriers of bone morphogenetic proteins (BMPs), vascular endothelial growth factor (VEGF), and noncollagenous matrix proteins. *J. Bone Miner. Metab.* **26**, 514–519 (2008).
75. Bonucci, E. Bone mineralization. *Front. Biosci.* **17**, 33–50 (2012).
76. Verweij, F. J. *et al.* The power of imaging to understand extracellular vesicle biology in vivo. *Nat. Methods* **18**, 1013–1026 (2021).

Supplementary Figures

Figure S2.1. TEM of crude and low-dense MVs. Samples were fixed with 1% glutaraldehyde, dropped in a TEM grid and stained with uranyl acetate 1%. a) crude MVs were we can detect the presence of fibrillar proteins. b) Typical cup-shaped morphology of dried vesicles. c) Low-dense MVs, showing the removal of associated fibrillar proteins. Notice that due to staining is difficult to discern their content, i.e. if there is any electron-dense mineral associated with the vesicles.

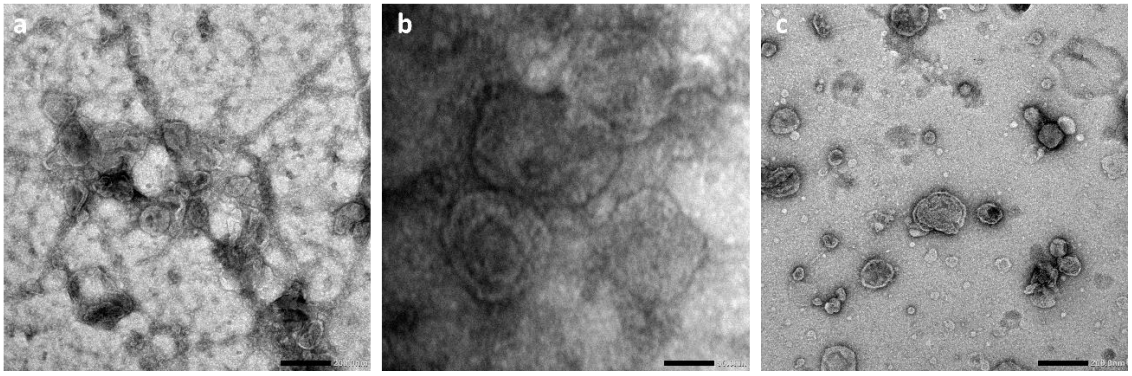

Figure S2.2. Mineralization triggered by non-vesicular particles. High-density fraction trigger mineral formation, observed after 24 h, when incubated at same conditions where low-dense MVs did not.

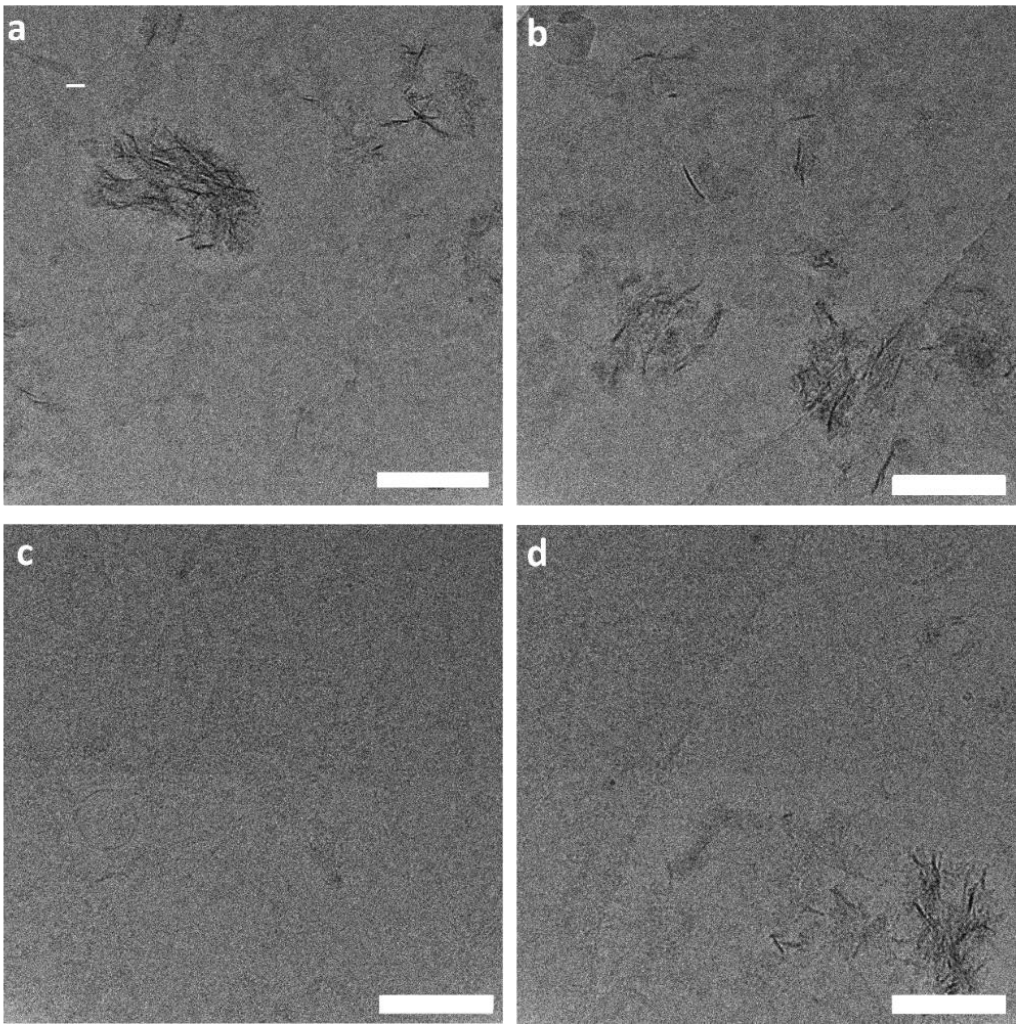

Supplementary Note

Supersaturation indices (σ) of ACP, OCP and HAp in the SCL solution was calculated by

$$\sigma = \log\frac{IP}{Ksp}$$

where IP is the ionic activity product, expressed using the species stoichiometry, n is the number of growth units in the material and Ksp is the solubility activity product. Chemical speciation was done using VMINTEQ 3.1. Davies' approximation of the Debye–Hückel equation was used for calculating the activity coefficients (parameter b = 0.3 is applied).

	SCL	
pH	7.5	
Temperature	37°C	
Ion	Added [ ] (mM)	
Ca^{2+}	2.0	
Cl^{-}	115.84	
CO_3^{2-}	1.83	
H^{+}	10.67	
K^{+}	12.7	
Mg^{2+}	0.57	
Na^{+}	106.40	
PO_4^{3-}	3.42	
SO_4^{2-}	0.57	
TES	10	
	logIP	σ
ACP $Ca_3(PO_4)_2$	-25.466	3.042
OCP $Ca_4H(PO_4)_3{:}3H_2O$	-44.192	4.257
HAp $Ca_5(PO_4)_3OH$	-32.214	12.395

3

A LANGMUIR MONOLAYER MODEL FOR MINERAL NUCLEATION

Mineralization is commonly found in close proximity to the MVs membranes. Although negatively charged phospholipids have been linked to the mineral nucleation driven by MVs, many aspects of this process are still unknown. The complexity of various proteins and lipids within MVs membranes makes it difficult to determine the influence of each component on calcium phosphate mineral nucleation and growth. This chapter presents a biomimetic model using Langmuir monolayers to examine the effect of phosphatidylserine, a negatively charged phospholipid, on the formation of calcium phosphate mineral on MVs surfaces. Infrared spectroscopy and transmission electron microscopy showed that mineralization only occurred when phosphatidylserine was present in the monolayers. Amorphous calcium phosphate mineral formed within four hours in phosphatidylserine-enriched Langmuir monolayers and was later converted to hydroxyapatite after 24 hours. We propose that formation of phosphatidylserine-rich nanodomains resulted in localized increases in supersaturation and triggered mineral nucleation at the lipidic interface. Finally, the use of monolayers containing lipids extracted from native MVs also showed mineral formation, similar to the artificial phosphatidylserine-enriched monolayers.

3.1| Introduction

The idea that phospholipids could control the nucleation of calcium phosphate during bone formation started from seminal studies of bone ultrastructure by histological and lipid solubilization of mineralizing epiphyseal cartilage[1,2]. Observing that most part of phospholipids were closely associated with the newly mineral phase formed in the primary ossification and that, upon increased mineralization, these lipids could only be extracted after tissue demineralization, specially the acid ones, such as phosphatidylserine (PS), it was proposed their influence in extracellular matrix mineralization[3]. In addition, these acidic phospholipids exist in higher concentrations at the sites of newly forming mineral than in areas of bone where mineralization is completed[1]. *In vitro* demonstration of complex formation between calcium (Ca^{2+}), phosphate (Pi) and acidic phospholipids support to the concept that phospholipids are involved in biological mineralization[4]. In the late 1960s, membranous structures were identified by electron microscopy within the extracellular matrix of mineralizing cartilage[5,6]. These structures are now recognized to be matrix vesicles (MVs). Isolation of MVs from tissues and the confirmation of their enrichment on acidic phospholipids led to the realization that these structures corresponds to the source of lipids associated with mineralization[7].

Partition of inorganic ions and phospholipids by extraction with organic and aqueous solvents revealed that about 4-12% of Ca^{2+} ions were complexed with phospholipids in MVs[8]. The complex Ca^{2+}-P_i-phosphatidylserine has been demonstrated to be an integral part of MVs, and proposed to play a role in the mechanisms by which MVs induce mineralization[9,10]. Indeed, Ca^{2+}-P_i-phosphatidylserine have been isolated from bone tissue[11], and demonstrate to induce mineral nucleation *in vitro* from metastable solutions[12,13]. In the literature, Ca^{2+}-P_i-phosphatidylserine complex is part of the so-called nucleation core of MVs, but many aspects of its nature and formation remain unclear. The nucleation core of MVs have been extensively studied *in vitro* by Wuthier's group [14–17]. These studies advanced to demonstrate that PS is the major entity responsible for the mineralization ability of the nucleation core. Their approach was to recreate the nucleation activity of MVs by adding PS in supersaturated solutions. From this, several features, such as the reduction of the nucleation efficiency of PS in presence of other phospholipids or some cations (e.g. Mg^{2+} and Zn^{2+}) were determined[17,18]. Moreover, the nucleation ability of PS can be triggered by addition of highly charged proteins (i.e.

annexin)[16]. However, these earlier studies were performed only in bulk solution, which do not determine the importance of the interfacial processes (i.e. at the lipid membrane).

To further delineate mechanisms of calcium phosphate nucleation and growth in PS-enriched interfaces, we explored calcium phosphate nucleation using Langmuir monolayers. Langmuir monolayers are formed by the spreading of an insoluble and amphiphilic molecule at an aqueous interface. Amphiphilic molecules are those that have well-defined polar and nonpolar regions in their structure. When these molecules are placed on an aqueous surface, they spontaneously spread across the liquid-air interface, adsorbing in an oriented manner so that their polar part comes into contact with water and their nonpolar part comes into contact with air, forming a monomolecular layer at the interface. Phospholipids are typical amphiphilic molecules. Therefore, the formation of monomolecular film of phospholipid molecules at the air-liquid interface is a biomimetic model of cell membranes, and has been classically used to understand the interactions between proteins, lipids and ions of biological relevance at a molecular level[19,20]. Langmuir monolayers are formed in a Langmuir through, by spreading a small amount of the amphiphilic molecule solution onto the surface of a subphase contained in a container internally coated with an inert material, like Teflon (Figure 3.1a).

The Langmuir Trough has one or two movable barriers that move, reducing the area occupied by molecules and organizing them at the interface. The adsorption of amphiphilic molecules at the liquid-air interface of the aqueous subphase with surface tension $\gamma 0$ causes a reduction in surface tension (γ). The difference between surface tension with and without the monolayer defines the surface pressure (π):

$$\pi = \gamma_0 - \gamma$$

Knowing how much surfactant was spread over a certain area, we can determine the available area per molecule. Thus, at constant temperature, as the mobile barrier compresses the monolayer, it is possible to determine the variation of π as a function of the area occupied per molecule, resulting in the surface pressure isotherm. The compression of the monolayer leads to different two-dimensional physical states that can be identified in the surface pressure isotherm. The different degrees of packing of the monolayer are named in analogy to the three-dimensional states of matter (Figure 3.1b). The first state of organization of a monolayer is the gas phase (G). At low surface pressures, the film consists of molecules sufficiently separated from each other such that lateral attractive forces are negligible. As the area occupied by each molecule is reduced, the next state of compactness is reached, the liquid phase. The liquid-expanded (LE)

phase is usually formed by molecules that have some kind of hindrance to compactness or relatively weak chain-chain interactions (branched or short chains, high temperatures), forming a highly elastic film where the chains of the molecules are disordered, like in a liquid. With the decrease in distance between molecules, the transition to the liquid-condensed (LC) phase occurs. The structure of this phase is controversial, but it is believed that the molecules can be organized such that their chains are somewhat disordered (like in a liquid) or that the molecules have their chains completely extended, but arranged angularly vertically. The solid phase (S) is characterized by a fairly linear region in the π - A isotherm, indicating low compressibility of the monolayer. Solid films are observed in systems where the molecules adhere strongly to each other through van der Waals interactions. Continuing the compression of the monolayer, a situation of maximum packing is reached and the molecules are unstructured from the surface, characterizing the collapse of the monolayer. Each amphiphilic molecule has a typical π - A isotherm, like a fingerprint, that directly reflects its structure. Therefore, study of π - A isotherms, and its characteristic features, is a easy way to track interactions between different components.

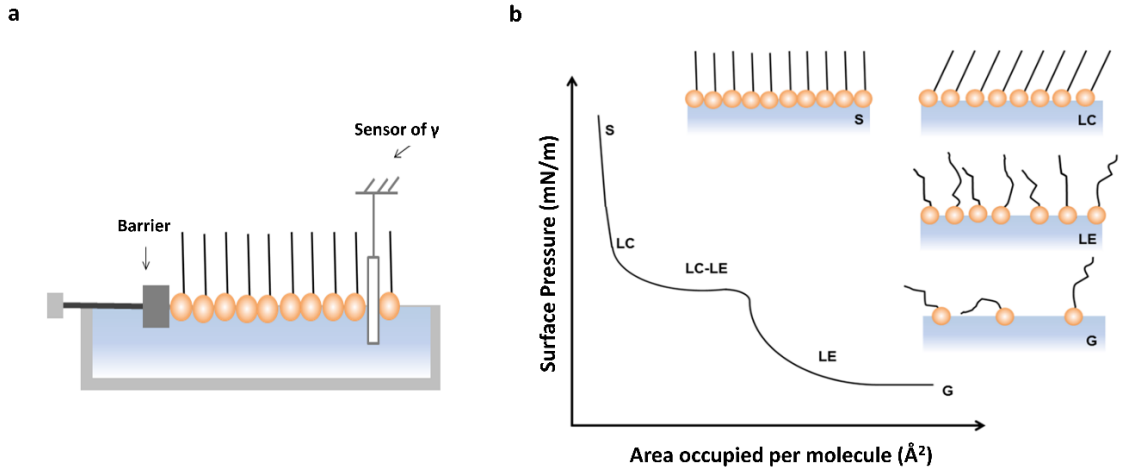

Figure 3.1. a) Scheme of a Langmuir through, where amphiphilic molecules are compacted through a movable barrier simultaneously to measurements of changes in the surface tension by a sensor. b) A typical π versus A isotherm for amphiphilic molecules spread at the liquid-air interface. As the area occupied by the surfactant molecule is reduced by moving the barrier in the trough, the monolayer reaches different states of compression: gas (G), liquid-expanded (LE), liquid-condensed (LC), and solid (S).

The advantages of Langmuir monolayers are the possibility of accessing thermodynamic parameters associated to the accurate control of the composition and the organization of the monolayer while allowing the coupling of several techniques for *in-*

situ characterization[19,21]. The combination of Langmuir monolayers with *in situ* imaging and spectroscopic techniques can provide a unprecedent understanding of events happening at membranes. Therefore, we used this technique to create a biomimetic model for the membrane MVs, to understand at molecular level, and with membrane-like organizations, how PS can affect the formation of calcium phosphate mineral.

3.2 | Objectives

General objective

Create a biomimetic model to understand the effect of PS in the nucleation of calcium phosphate mineral.

Specific aims

(i) Study the ability of DPPC, DPPS and DPPC-DPPS mixed Langmuir monolayers to induce calcium phosphate formation;

(ii) Create monolayers with lipids extracted from native MVs and study their mineralization ability in a Langmuir monolayer model;

3.3 | Methods

3.3.1 | Langmuir monolayers and surface pressure (π) vs area (A) isotherms

1,2-dipalmitoyl-sn-glycero-3-phosphatidylcholine (DPPC; purity > 99%, Avanti Lipids) and 1,2-dipalmitoyl-sn-glycero-3-phospho-L-serine (DPPS; > 99%; Avanti Lipids) or the lipid extract from MVs were used to build the Langmuir monolayers, using a Langmuir trough (Insight Brazil, 216 cm^2). Monolayers were obtained after spreading the lipids solubilized in chloroform:methanol (3:1 ratio) on a subphase containing either ultrapure water (surface tension of 72.3 mN m^{-1} and conductivity 1.1 μS cm^{-1}, at 25°C) or the solution of interest. After spreading the lipid solution, the monolayer was compressed at a rate of 0.42 mm^2 s^{-1} with a constant temperature of 25 ± 1°C and the π changes were acquired using a Wilhealmy plate, to construct the π-A isotherms.

The isothermal compressibility C_s^{-1} of the monolayers was calculated from the slope of the π-A isotherm in a given value of area occupied by molecule (A), according to the equation 1. The condensation state of the monolayer was identified from the values of C_s^{-1} at a given π according to [22]. Liquid-expanded (LE) state of the monolayer is characterized by C_s^{-1} values ranging from 12 to 50 mN/m, liquid-condensed states (LC) from 100 to 250 mN/m and solid state from values higher than 1000 mN/m.

$$C_s^{-1} = -A \left(\frac{\partial \pi}{\partial A}\right)_T \quad (1)$$

The Gibbs free energy of excess, ΔG_{exc}, for the DPPC:DPPS (8:2) mixture was calculated from the integration of the π - A isotherms of the mixed monolayer and the monolayers of the pure components, according to the equation 2,

$$\Delta G_{exc} = \int_o^{\pi} (A_{12} - (x_1 A_1 + x_2 A_2) d\pi \quad (2)$$

where A_{12} is the area occupied by the molecule in the mixture of components 1 and 2.

3.3.2 | *In situ* mineralization of Langmuir monolayers

Mineralization of the Langmuir monolayers was carried out with a modified SCL buffer (m-SCL) composed by 10.0 mM 2-[4-(2-hydroxyethyl)piperazin-1-yl]ethanesulfonic acid (HEPES), 5.13 mM Na_2HPO_4, 1.83 mM $NaHCO_3$, 12.7 mM KCl, 0.57 mM $MgCl_2$, 3.0 mM $CaCl_2$, 100 mM NaCl, 0.7 mM Na_2SO_4. The pH of solution was adjusted to 7.4 and promptly used for the experiments. All experiments were performed at 25°C and π kept constant at 30 mN/m simulating the lipid organization in cells[23]. During the experiment, aliquots were collected from the subphase below the movable barrier for subsequent potentiometric measurement of the concentration of free Ca^{2+} ($[Ca^{2+}]_{free}$) using an ion-selective electrode (Bante Instruments, Shanghai, China) using a Bante320 multiparameter meter.

Phase-modulated infrared absorption spectroscopy (PM-IRRAS) of mineralizing monolayers was performed *in situ* in the Langmuir trough, at π = 30 mN/m, in the 800-4000 cm^{-1} range, with a resolution of 8 cm^{-1} using a KSV PMI550 spectrophotometer (KSV Instruments) coupled to a polarizer modulator PEM100. The incidence angle was 81º. The spectra are presented as a function of the PM-IRRAS signal, obtained from the equation $S = \Delta R / R = (Rp - Rs) / (Rp + Rs)$, where Rp and Rs are the reflectance obtained from the incident beam polarized parallel (s) or perpendicular (p) to the plane of incidence. The PM-IRRAS signal is presented as $\Delta S = (S - S_0) / S_0$, where S is the response obtained for the subphase covered with the Langmuir monolayer and S_0 is the response obtained for the pure subphase. The changes in morphology of the monolayers due to mineralization as a function of time was investigated by TEM (JEM-2100-JEOL microscope) through the transfer of the monolayers to carbon-coated copper grids. After 240 min of mineralization, the material formed at the air-liquid interface was collected and immediately analyzed by Fourier-transform infrared spectroscopy (FTIR) coupled with an attenuated total reflectance (ATR) accessory (Shimadzu-IRPrestige-21).

The surface zeta-potential (ζ) of the samples was measured in a surface ζ-potential cell (ZEN 1020) hyphened to a Zetasizer Nano ZS (Malvern Instruments). Mobility of

the tracer particles (polystyrene nanospheres – Duke Scientific Corporation, 200 nm, $\zeta = -54.6 \pm 7.04$ mV in pure water) in the vicinity of the charged test surface mounted on a dip cell was measured by phase analysis light scattering and a simple model used to describe the electroosmotic flow near the fitted surface [30]. To this, Y-type LB film bilayers were transferred to silicon samples equal or smaller than 7 mm × 4 mm and with thickness of 1 mm, maintaining the surface pressure constant at 30 mN m^{-1}. After the transference, the samples were immersed in the m-SCL for different periods. The sample holder was carefully mounted in liquid medium to avoid LB film disruption. Measurements were repeated at least three times at 25°C.

3.3.3 | Extraction of the lipid fraction from MVs

MVs were isolated from embryonic chicken bones and characterized to confirm their functionality as described elsewhere[24]. The lipid fraction of the MVs was obtained from the protocol developed by Abdallah et al. [25]. Briefly, 100 µL of the MV suspension was mixed with 400 µL of methanol:chloroform (2:1 ratio), and shaken vigorously for 1 min, and then incubated at room temperature for 30 min. Chloroform and water were subsequently added to the supernatant. The phase separation was performed by centrifugation at 2,000 g for 10 min. The chloroform phase containing the lipid fraction of the MVs was then collected and used immediately for analysis.

3.3.4 | Solution Titration

The titration experiment was performed by titration of a 10 mM $CaCl_2$ stock at a rate of 125 µl/min to the 10 mM Na_2HPO_4 solution (initial volume of 30 mL). The solutions were prepared in Tris-buffered saline (50 mM Tris, 150 mM NaCl), monitoring the Ca^{2+}-concentration with an ISE Ca^{2+} electrode (Bante Instruments, China) and pH at a constant pH = 7.40. The ISE electrode was calibrated in Tris-buffered saline. This approach is the one used by[26]. O-phospho-L-serine (Sigma) was added in the phosphate solution at concentration of 1.0 mM.

3.4 | Results

3.4.1 | Langmuir monolayers mimicking MVs lipidic composition

Langmuir monolayers of selected lipid compositions allowed us to obtain thermodynamic parameters to investigate the effect of specific lipids on nucleation ability of MVs. Monolayers were built in a subphase containing the supersaturated solution m-SCL, at 25°C. Firstly, monolayers composed of DPPC and DPPS and the mixture (DPPC:DPPS 8:2, molar ratio) in a proportion similar to the one found in MVs was studied (Figure 3.2). The features of DPPC and DPPS isotherms, recorded at 25°C in subphase containing the m-SCL solution, were in accordance with previous reports [28,29]. DPPC isotherm (Figure, black line) exhibited an onset molecular area at 100 $Å^2$, corresponding to the beginning of the liquid-expanded (LE) phase, and a plateau at $\pi \sim$ 10 mN m^{-1} in the range of 65-80 $Å^2$, corresponding to LC-LE phase coexistence region. The increase of π after this plateau is assigned to the formation of pure LC phase. The phase transitions were also demonstrated by changes in the C_s^{-1} values of the monolayers (Figure 3.2-inset). Static surface elasticity values (C_s^{-1}) are a measurement of the tendency of the monolayers to resist to the compression at a given π, translating also into the packing state of the monolayer. Higher C_s^{-1} values indicates more compact monolayer. DPPS isotherm (Figure 3.2, blue line) exhibited an onset molecular area at 55 $Å^2$ and a better packing, revealed by the displacement to smaller mean molecular area, compared to pure DPPC monolayers. This was assigned to the smaller size of the serine group present on DPPS polar head compared to the choline group present at DPPC. Compact monolayers are a characteristic feature of phospholipids with small polar heads, e.g. DPPS, which facilitate strong van der Waals interactions between the nonpolar tails, in addition to the possibility of hydrogen bonds with the subphase[30]. The absence of phase-coexistence region is also a characteristic of DPPS isotherms. The mixed DPPC:DPPS (8:2) (Figure 3.2, red line) resembles the pure-DPPC isotherm with a slight expansion to higher molecular areas at condensed states. This might indicate repulsive interactions between the phospholipid molecules in the mixture.

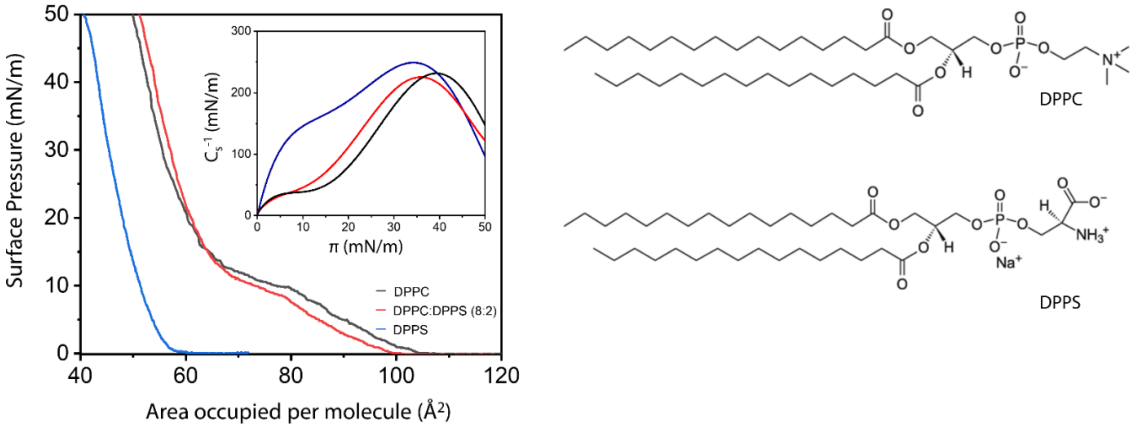

Figure 3.2 | π -A isotherms of DPPC (black line), DPPC:DPPS (8:2, molar ratio) (red line) and DPPS (blue line) monolayers in subphase containing m-SCL solution, at 25°C. Inset depicts the C_s^{-1} vs π curves for the monolayers. Right panel: chemical structures of DPPC and DPPS lipids.

To further infer about interactions between the different phospholipids in the monolayers, we calculate their thermodynamic properties. Monolayers formed with more than one insoluble component can be treated in analogy to the thermodynamics of mixtures. For an ideal two-component system, the average area per molecule (A_{12}^0) occupied at a given surface pressure is calculated with the additivity principle

$$(A_{12}^0) = A_1x_1 + A_2x_2$$

where A_1 and A_2 are the average molecular areas occupied by molecules (1) and (2) at pressure π, and x_1 and x_2 are the respective molar fractions. If the experimental A_{12} is larger or smaller than A_{12}^0, attractive and repulsive interactions are predominant, respectively. Likewise, the excess Gibbs energy (ΔG_{ex}) is calculated by comparing the experimental and theoretical values

$$\Delta G_{exc} = \int_o^{\pi} (A_{12} - (x_1A_1 + x_2A_2)d\pi$$

Indeed, calculation of the ΔG_{ex} for the DPPC:DPPS (8:2) mixture attested to the formation of a non-ideal mixture ($\Delta G_{ex} > 0$) and the predominance of non-favored interactions between the lipid molecules in the mixed monolayer over the pure ones (Figure 3.3b).

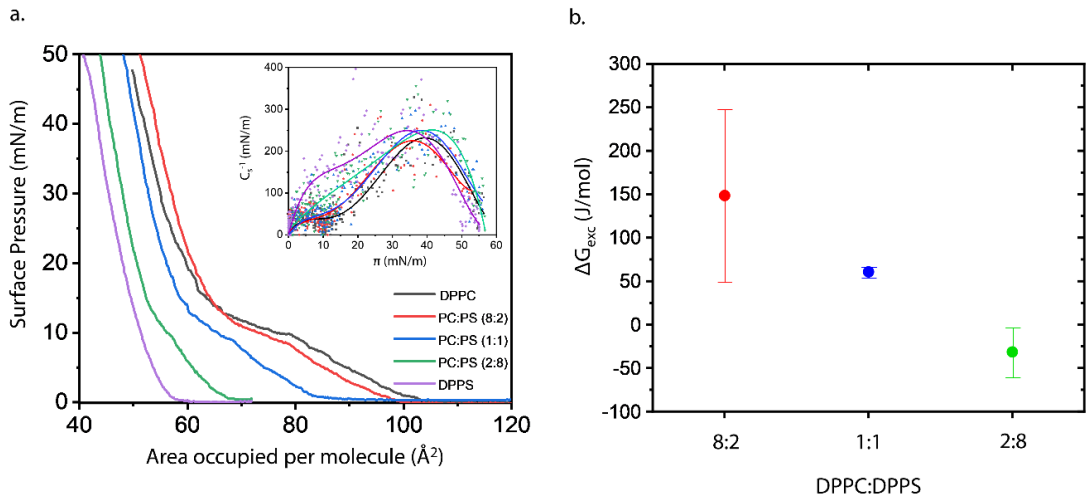

Figure 3.3 | Mixed DPPC:DPPS monolayers. (a) π-A isotherms for DPPC (black line), DPPC:DPPS (8:2) (red line), DPPC:DPPS (1:1) (blue line), DPPC:DPPS (2:8) (green line) and DPPS (purple line) monolayers in subphase containing m-SCL solution, at 25°C. Inset depicts the C_s^{-1} vs π curves for the monolayers. (b) Values of ΔG_{exc} for the mixed DPPC:DPPS monolayers with different molar ratios, at 30 mN/m.

3.4.2 | Mineralization induced on Langmuir monolayers composed by lipids of selected compositions

In situ mineralization experiments were performed with monolayers compressed at π = 30 mN/m. At this surface pressure, the pure DPPC, DPPC:DPPS (8:2), and pure DPPS monolayers displayed C_s^{-1} values higher than 200 mN/m, indicating that molecules are assembled in a LC state that resembles the lipid packing found in the liquid-ordered phases dispersed in a liquid-disordered matrix in biological membrane[31]. DPPS monolayers efficiently induces mineral formation within 240 min of reaction, as shown in Figure 3.4. To attest localized mineral formation at the air-liquid interface, changes in the chemical composition of the DPPS monolayer along the mineralization experiment was followed by PM-IRRAS (Figure 3.4a). This infrared spectroscopy technique is sensible to the presence and orientation of chemical groups at the air-liquid interface[32], and identify events occurring restricted to the interface. As shown in the PM-IRRAS spectrum of the DPPS monolayer (Figure 3.4a), longer is the reaction time, greater are the changes in the spectral region of 1150-950 cm^{-1}. At this spectral range, it is expected to observe absorptions from the ν_3 and ν_1 domains of the PO_4^{3-} group in the growing mineral phase [33]. However, other bands related to absorptions from chemical groups of the phospholipids can also be found in this range. The intensity of the band at 1020-1040 cm^{-1} ascribed to the absorption of the ν_3 of PO_4 groups in calcium phosphates (marked by the blue box in Figure 3.4a) increased after 180 minutes, indicating the formation of Ca-

phosphate species at the interface. This result corroborates previous investigations conducted experimentally[26] and by molecular dynamics[34] showing that Ca-phosphate species typically absorb in this infrared region. Formation of ACP at the DPPS monolayer after 240 min of mineralization was evidenced by FTIR spectrum of the material collected from the air-liquid interface (Figure 3.4b). A broad band centered at 1030 cm^{-1} (ν_3 PO_4) with a small shoulder at 950 cm^{-1} (ν_1) are spectral characteristics of ACP formation[33]. TEM images of the DPPS monolayer after 240 min of reaction shows particles with high contrast forming a homogenous film (Figure 3.4c). SAED confirmed the formation of amorphous structures (Figure 3.4c-insert).

Changes in the $[Ca^{2+}]_{free}$ in the subphase measured *in-situ* along mineralization in the presence of the DPPS monolayer gave insight into the multistep process occurring at the interface (Figure 3.4d). Within the first 60 min, no significant changes in the $[Ca^{2+}]_{free}$ was observed. However, from this time on, it was observed a decrease in the $[Ca^{2+}]_{free}$, indicating the consumption of Ca^{2+} from the subphase to form the ACP at the interface mediated by PS polar heads. Measurements of DPPS bilayer surface ζ-potential revealed a decrease of the negative surface charge along the mineralization (Figure 3.4e). Ca^{2+} interacts with DPPS polar heads[35] as confirmed by the decrease in the ζ-potential of the DPPS bilayer in presence of Ca^{2+}. The DPPS bilayers induced the stabilization of calcium-phosphate complexes that specifically interacts with the lipid headgroup in the calcium phosphate supersaturated solution. The coalescence of these complexes leads to the formation of ACP as indicated by a “more electroneutral” interface after 240 min.

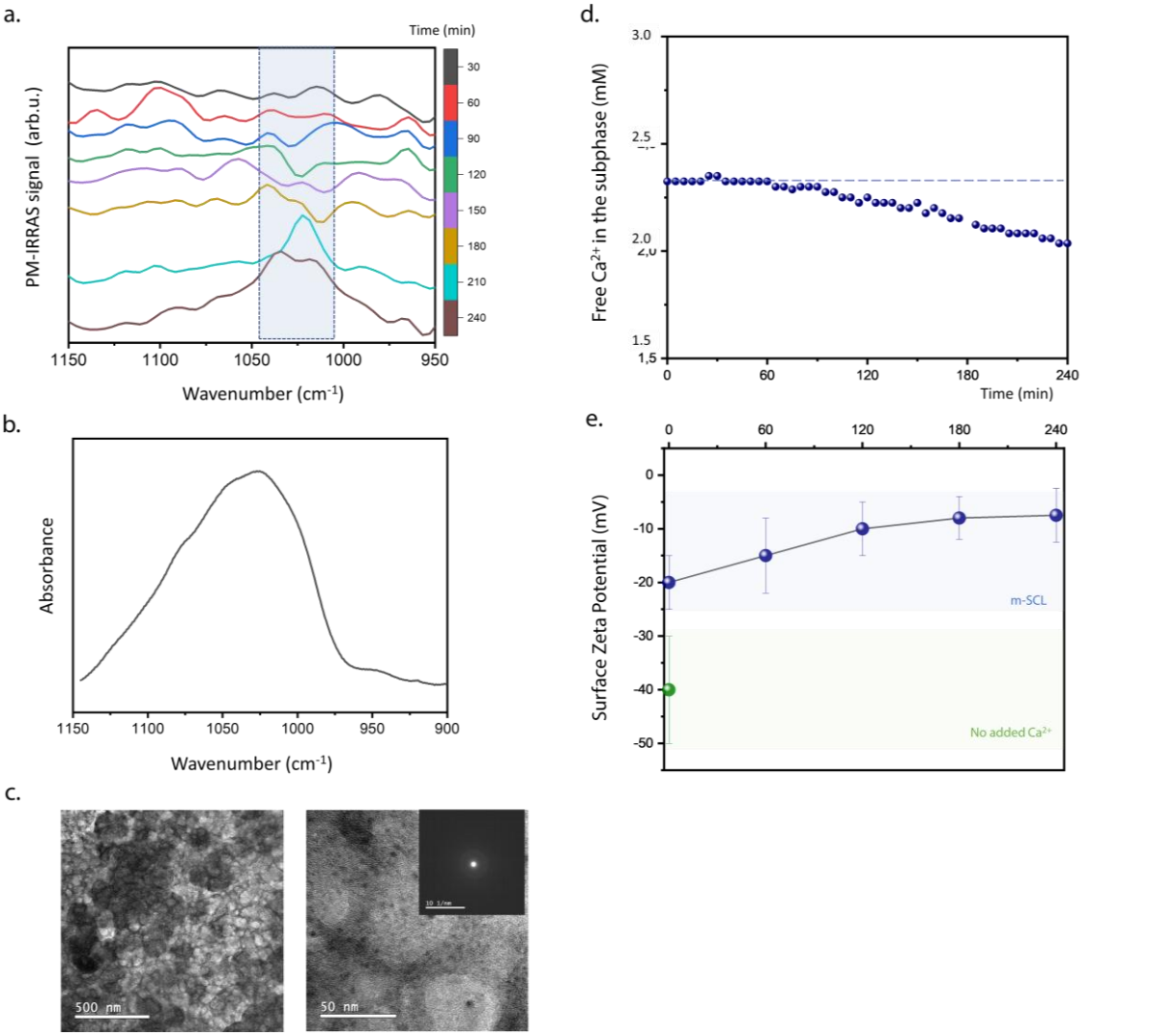

Figure 3.4 | DPPS monolayers control calcium phosphate nucleation at the air-liquid interface. (a) PM-IRRAS spectra in the 1150-950 cm^{-1} range for the DPPS monolayer in subphase composed of the m-SCL mineralizing buffer (pH 7.4), at 25°C and π = 30 mN/m. Spectra were obtained at different time intervals for a period of 240 min. Blue box in the spectra highlighted the region between 1045-1010 cm^{-1} assigned to the absorption bands of evolving inorganic phosphate group. (b) FTIR spectrum in the region of ν_3 PO_4^{3-} absorption obtained for the material collected from the monolayer of DPPS after 240 min of mineralization. (c) TEM images and SAED (inset) of DPPS monolayers transferred to Cu-grids after 240 min. (d) Potentiometric measurement of $[Ca^{2+}]_{free}$ in the subphase below the DPPS monolayer. (e) Ex-situ analysis of surface ζ-potential of DPPS monolayers in absence of Ca^{2+} ions (green dots) and after different mineralization time points (blue dots).

In order to access the ability of DPPS to stabilize ion complexes with the Ca^{2+} and phosphate ions to trigger the ACP nucleation, we performed a titration experiment to infer about chemical speciation in solution[26] (Figure). By using the approach developed by, a Ca^{2+} stock solution was slowly titrated to a phosphate solution in presence of phosphoserine, a water-soluble mimetic of the DPPS headgroup, as additive. In this

experiment, we evaluate changes in the $[Ca^{2+}]_{free}$ regarded to the addition of Ca^{2+} ($[Ca^{2+}]_{add}$) to the solution. Therefore, information about the equilibrium between bonded and free ions in solution was accessed. One import step during this crystallization experiment is the pre-nucleation stage, i.e. a linear range in the $[Ca^{2+}]_{free}$ *versus* $[Ca^{2+}]_{add}$ curve before any bulk precipitation is observed. This stage is marked by an equilibrium between soluble association complexes between Ca^{2+} and phosphate ions. In presence of phosphoserine, we observed a change in the slope of the prenucleation stage due to changes in how the solution is assimilating Ca^{2+}, which denote specific association between the ions and the charged PS group. This evidences the ability of PS to induce specific associations with Ca^{2+} and phosphate ions that leads to the ACP nucleation.

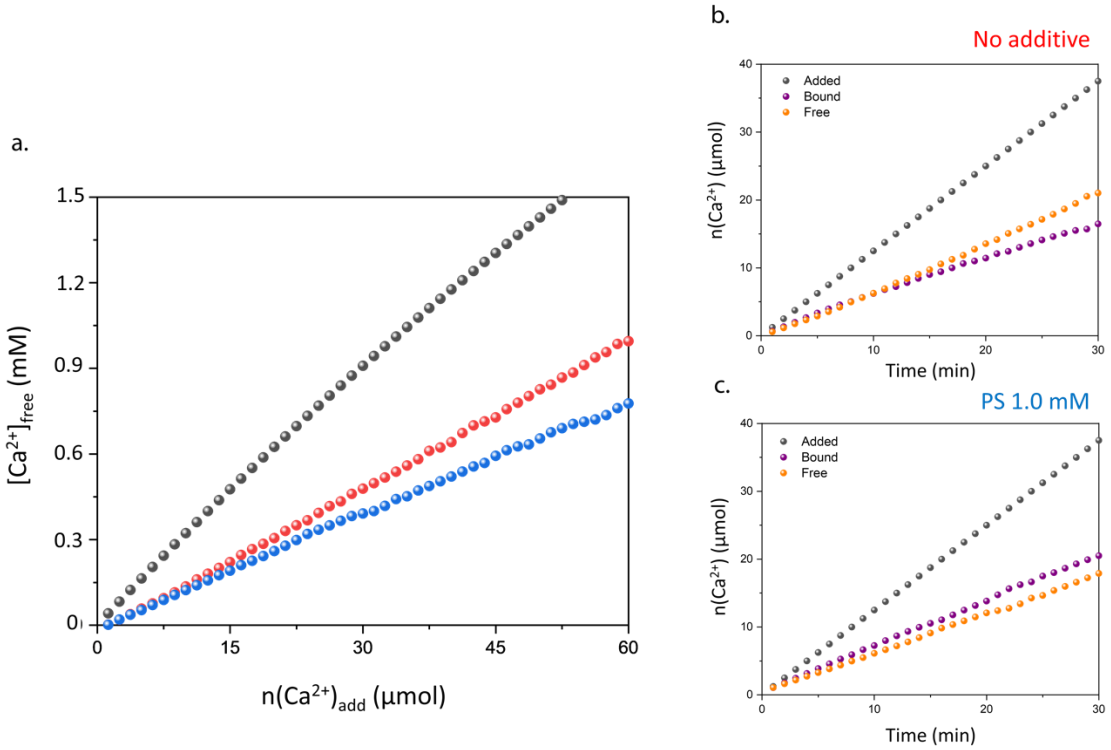

Figure 3.5 | PS changes nucleation pathway during calcium phosphate formation in solution. a) Titration data showing the measured free calcium $[Ca^{2+}]_{free}$ as a function of added calcium $[Ca^{2+}]_{add}$. The experiments were carried out by drop-wise addition of a 10 mM Ca^{2+} stock solution at constant rate to a 10 mM phosphate stock solution, while simultaneously adding appropriate amounts of NaOH to keep the pH constant at 7.4. This experiment is sensible to changes in the chemical composition of the solution[26,36]. In the additive-free solution (grey), initially we can observe a linear increase of $[Ca^{2+}]_{free}$, characteristic of a prenucleation stage, then a sudden drop in the $[Ca^{2+}]_{free}$ related to a bulk phase transition and precipitation of ACP, precursor of apatite, was observed. In the presence of 1 mM PS as additive (red) the prenucleation stage was evidenced by an abrupt change of slope and the presence of a plateau. Moreover, a change in the slope at the linear range of the prenucleation stage in presence of PS indicates changes in how the solution is assimilating Ca^{2+}, which indicates specific association between the ions and the charged PS group. Panels b and c shown the especiation in free calcium, bound calcium and added (free + bound).

In native MVs, PS molecules are dispersed in a lipid membrane, therefore the next step was to evaluate the effect on mineralization by DPPS molecules diluted in a DPPC monolayer, mimicking a native-like lipid composition. Unlike in DPPS monolayer, the structures formed on DPPC:DPPS (8:2, molar ratio) monolayer are heterogeneously distributed along the surface (Figure 3.6). Spherical structures of ~ 5 nm with amorphous SAED pattern are observed forming the micrometric aggregates. After 12 h, this amorphous phase crystallizes (as shown by the presence of diffraction rings in the SAED patterns), forming platelets homogeneously distributed along the monolayer. This morphology is characteristic of biomimetic apatite[26,37]. After 24 h, these structures grow leading to the monolayer rupture and formation of crystalline agglomerates with micrometric dimensions.

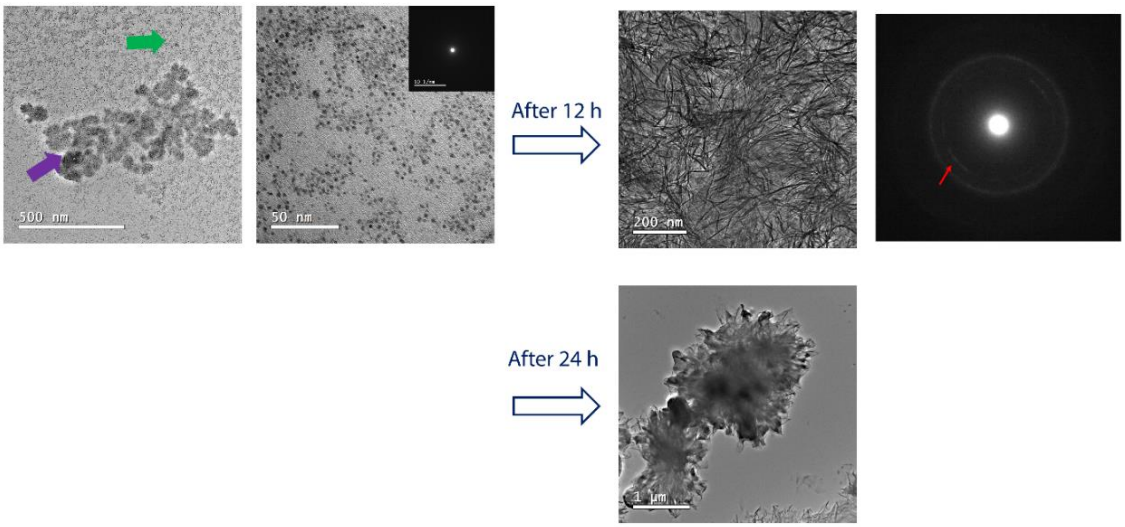

Figure 3.6 | Morphology of DPPS-enriched monolayers after mineralization. TEM images and their respective SAED electron diffraction patterns for the monolayers of DPPC:DPPS (8:2) molar ratio, transferred after 240 min of mineralization at 25°C. For the mixed DPPC:DPPS monolayer, the presence of nanometric complexes (~ 5 nm) indicated by the green arrow aggregates into larger structures (purple arrow). It is observed that these initially amorphous complexes crystallize after 12 h (red arrow in the SAED pattern). The formation of micrometric aggregates and a complete rupture of the transferred monolayer is observed after 24 h.

DPPC monolayers did not induce mineral formation within 240 min. This was evidenced by no significant changes in the PM-IRRAS spectra of the monolayer along 240 min of reaction (Figure 3.7). Monolayers composed of pure DPPC did not promote formation of mineralized structures after 240 min, as shown by TEM images (Figure 3.8).

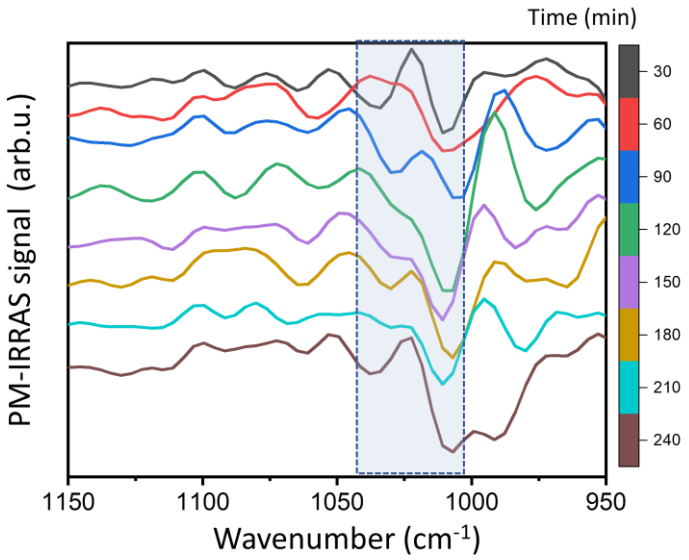

Figure 3.7 | PM-IRRAS spectra in the region between 1150-950 cm^{-1} for the DPPC monolayer in subphase composed of the m-SCL mineralizing buffer (pH 7.4), at 25°C and π = 30 mN/m. Spectra were obtained at different time intervals for a period of 240 min.

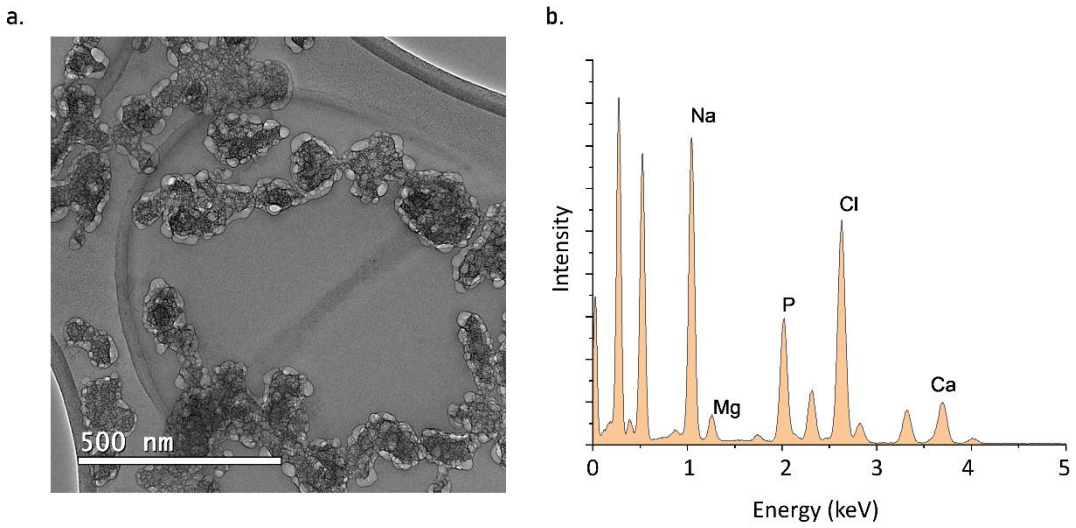

Figure 3.8 | Morphology of DPPC monolayer. (a) TEM image of the DPPC monolayer transferred after 240 min under the m-SCL subphase. It was not observed any structure similar to the ones found in the DPPS monolayers. The matrix was fast damaged by the electron beam. (b) EDS spectrum revealed the presence of Na, Mg and Cl from the buffer. The presence of Ca, Mg, and P, probably comes from the buffer and the phosphate from the phospholipid.

3.4.3 | Mineralization induced on Langmuir monolayer composed by the lipid extract of MVs

To further explore mineral formation in a native-like lipid environment, the ability to induce mineral formation on monolayers formed by the lipid fraction extracted from MVs was evaluated. The lipid fraction extracted from the MVs forms an expanded monolayer that reaches the LC state (C_s^{-1} > 100 mN/m) at π close to 30 mN/m (Figure 3.9), which is the surface pressure where the mineralization was evaluated. High expanded monolayers are expected for monolayers composed by biological extracts due to presence of non-identical lipids with different levels of unsaturation.

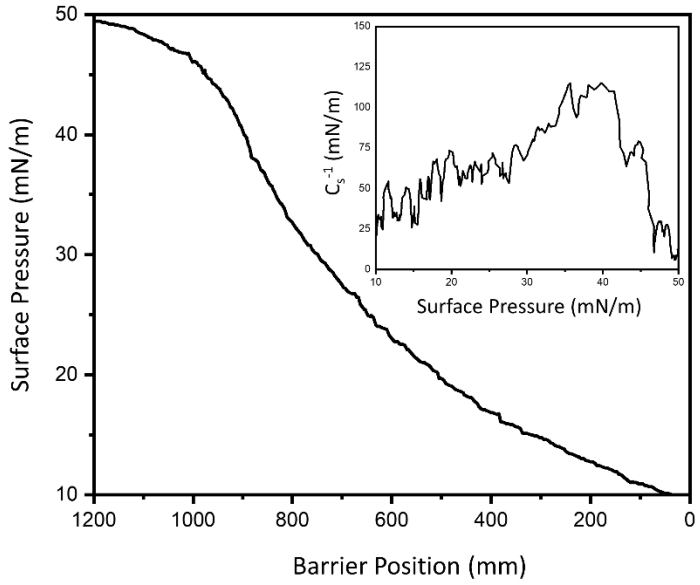

Figure 3.9 | Langmuir monolayer behavior for the lipid extract of MVs. Changes in the surface pressure as a function of movable barrier position in the Langmuir trough. Since the molar concentration of the lipid extract is not known, it cannot be constructed the classical π-A isotherm for the Langmuir monolayer. Therefore, the packing behavior of the monolayer is depicted as π in function of the barrier position, that it is proportional to area available per molecule at the interface. Monolayer is formed in subphase containing the m-SCL solution, at 25°C. The insert shows the variation of the compressional modulus (C_s^{-1}) as a function of surface pressure.

PM-IRRAS of MV-lipid extracts changed with the incubation time in the 1100-950 cm^{-1} region, characteristic of calcium phosphate absorption bands (Figure 3.10a). This suggests the formation of calcium phosphate complexes that enabled the nucleation of ACP at the interface. TEM images of the monolayers transferred after 240 min (Figure 3.10a) revealed the presence of nanometric particles that aggregated into bigger structures (red arrow). It is worth to notice the similarity between the mineral structures observed

on the monolayer of the MV-lipid extract and the ones observed on the mixed DPPC:DPPS monolayer. The nucleation points emerged on the monolayer leading to the aggregation of nanometric structures into larger ones. It is now perceivable that the lipids in MVs had the ability to induce mineral formation. This ability can be mimetized by a simple monolayer composed by a DPPS-enriched monolayer, recreating *in vitro* the ability of the membrane of MVs to induce mineral formation.

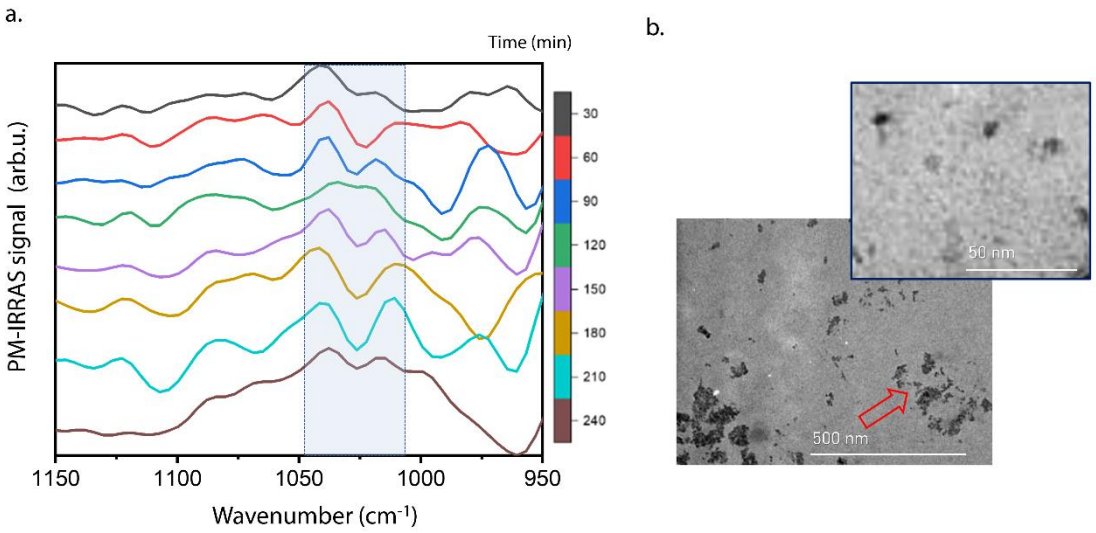

Figure 3.10 | Mineralization mediated by Langmuir monolayers composed of lipids extracted from MVs. (a) PM-IRRAS spectra in the region between 1150-950 cm^{-1} for the monolayer formed by the lipid extract of MVs, in subphase composed of the m-SCL mineralizing buffer (pH 7.4), at 25°C and π = 30 mN/m. Spectra were obtained at different time intervals for a period of 240 min. Blue boxes in the spectra highlight the region between 1045-1010 cm^{-1} assigned to the absorption bands of evolving inorganic phosphate group. (b) TEM images for the monolayer formed by the lipid extract of MVs transferred after 4 hours of mineralization at 25°C.

3.5 | Discussion

Here, we developed a biomimetic model using Langmuir monolayers to reproduce Calcium phosphate nucleation was fastly induced on DPPS-enriched monolayers. Since no mineralization was observed in pure DPPC monolayers, it is notable that PS-enrichment is the driven force to trigger mineral nucleation, recreating *in vitro*, in conditions of membrane-like structure, the nucleation ability of the MVs.

Accumulation of phosphate and Ca^{2+} under charged monolayers has been promptly observed to occur in supersaturated solutions[40]. However, the simple addition and accumulation of the ionic species at the interface is not enough to promote mineral phase formation, being necessary to decrease an energetic barrier to the nucleation of the first nuclei[41–43]. To fulfill this task, the role of the organic matrix in the nucleation of calcium phosphates comes into play. Highly charged species act to stabilize calcium phosphate complexes[41], as extensively studied for non-collagenous proteins and their charged polymers analogues (e.g. polyaspartic acid). Zhao[44] recently showed that osteocalcin bears highly charged amino acid residues in a specific arrangement that helps the stabilization of calcium phosphate complexes, energetically favoring their growth towards the formation of ACP. Herein, we show that PS is able to stabilize pre-nucleation complexes prior to ACP formation, mainly due to specific and favorable association between charged groups in DPPS polar head and precursor ions from the solution. The ability to form energetic favorable complexes between PS and surrounding Ca^{2+} and phosphate ions has been also proposed by other authors[15,45,46].

The role of PS-enrichment on the membrane of MVs to nucleate calcium phosphate can also be analyzed from a thermodynamic point-of-view. The nucleation of the monolayer composed by the DPPC:DPPS mixture, observed in Figure 3.4, started by discreet dots distributed along the interface, that aggregated into bigger assemblies. The ΔG_{exc} value found for mixed DPPC:DPPS monolayer 8:2 (molar ratio) was +130 J/mol in the conditions in this study, at π=30 mN/m. Positive values for ΔG_{exc} can be understood as the driving force that directs the formation of lipid domains[47] and has been described in the literature for PC:PS mixtures[48,49]. Thus, clustering of PS molecules in the MVs is the origin of the nucleation core. PS-enriched nanometric domains within the MVs membrane create local sites where ACP nucleation is favored. *In vivo*, this mechanism of PS-rich nanodomains formation may also have the participation of proteins. Faiβ et al[50] demonstrated that the presence of annexin, a family of calcium-binding proteins,

promotes intensification in the formation of PS-rich nanodomains in lipid bilayers composed of PC/PS. Indeed, isolation of nucleation core of MVs revealed the presence of annexins strongly bound to the PS-calcium phosphate complexes extracted from native MVs[10]. Therefore, it cannot be excluded that mineral nucleation in MVs could also have the participation of other molecules different than PS.

3.6 | Conclusions

DPPS-enriched Langmuir monolayers were suitable models to mimic the inner leaflet of MVs to initiate mineralization. The mineralization induced on DPPS-enriched monolayers was reproduced in a similarly manner on the monolayers composed by lipid-extract of MVs. Therefore, Langmuir monolayers were revealed as promising approach to determine lipid-lipid and lipid-protein interactions occurring during the mineralization induced by MVs. Association with other advanced characterization methods not used herein (e.g., cryo-TEM morphological analysis and *in-situ* fluorescence and X-ray scattering/diffraction techniques) opens a window to future studies using Langmuir monolayers to delineate molecular mechanisms of bone biomineralization. Finally, our findings suggest the possibility of PS playing a major role during ossification, making provision for future studies to explore their role not only in physiological mineralization process, but also in pathological conditions, such as dystrophic vascular calcification where the presence of PS-exposing extracellular vesicles have been extensively described.

3.7 | References

1. Irving, J. T. & Wuthier, R. E. Histochemistry and Biochemistry of Calcification With Special Reference to the Role of Lipids. *Clin. Orthop. Relat. Res.* **56**, 237–260 (1968).
2. Wuthier, R. E. A zonal analysis of inorganic and organic constituents of the epiphysis during endochondral calcification. *Calcif. Tissue Res.* **4**, 20–38 (1969).
3. Wuthier, R. E. Zonal analysis of phospholipids in the epiphyseal cartilage and bone of normal and rachitic chickens and pigs. *Calcif. Tissue Res.* **8**, 36–53 (1971).
4. Cotmore, J. M., Nichols, G. & Wuthier, R. E. Phospholipid-calcium phosphate complex: Enhanced calcium migration in the presence of phosphate. *Science.* **172**, 1339–1341 (1971).
5. Bonucci, E. Fine structure and histochemistry of 'calcifying globules' in epiphyseal cartilage. *Zeitschrift für Zellforsch. und Mikroskopische Anat.* **103**, 192–217 (1970).
6. Anderson, H. C. Vesicles associated with calcification in the matrix of epiphyseal

cartilage. *J. Cell Biol.* **41**, 59–72 (1969).

7. Wuthier, R. E. Lipid composition of isolated epiphyseal cartilage cells, membranes and matrix vesicles. *Biochim. Biophys. Acta - Lipids Lipid Metab.* **409**, 128–143 (1975).
8. Wuthier, R. E. & Gore, S. T. Partition of inorganic ions and phospholipids in isolated cell, membrane and matrix vesicle fractions: Evidence for Ca-Pi-acidic phospholipid complexes. *Calcif. Tissue Res.* **24**, 163–171 (1977).
9. Wu, L. N. Y. *et al.* Characterization of the nucleational core complex responsible for mineral induction by growth plate cartilage matrix vesicles. *J. Biol. Chem.* **268**, 25084–25094 (1993).
10. Wu, L. *et al.* Physicochemical Characterization of the Nucleational Core of Matrix Vesicles. *J. Biol. Chem.* **272**, 4404–4411 (1997).
11. Boskey, A. L. & Posner, A. S. Extraction of a calcium-phospholipid-phosphate complex from bone. *Calcif. Tissue Res.* **19**, 273–283 (1975).
12. Boskey, A. L. & Posner, A. S. The role of synthetic and bone extracted Ca-phospholipid-PO4 complexes in hydroxyapatite formation. *Calcif. Tissue Res.* **23**, 251–258 (1977).
13. Boskey, A. L. & Posner, A. S. In vitro nucleation of hydroxyapatite by a bone calcium-phospholipid-phosphate complex. *Calcif. Tissue Res.* **22**, 197–201 (1976).
14. Wu, L. N. Y., Genge, B. R., Sauer, G. R. & Wuthier, R. E. Characterization and Reconstitution of the Nucleational Complex Responsible for Mineral Formation by Growth Plate Cartilage Matrix Vesicles. *Connect. Tissue Res.* **35**, 309–315 (1996).
15. Wu, L. N. Y., Genge, B. R. & Wuthier, R. E. Analysis and molecular modeling of the formation, structure, and activity of the phosphatidylserine-calcium-phosphate complex associated with biomineralization. *J. Biol. Chem.* **283**, 3827–3838 (2008).
16. Genge, B. R., Wu, L. N. Y. & Wuthier, R. E. In vitro modeling of matrix vesicle nucleation: Synergistic stimulation of mineral formation by annexin A5 and phosphatidylserine. *J. Biol. Chem.* **282**, 26035–26045 (2007).
17. Wu, L. N. Y., Genge, B. R. & Wuthier, R. E. Differential effects of zinc and magnesium ions on mineralization activity of phosphatidylserine calcium phosphate complexes. *J. Inorg. Biochem.* **103**, 948–962 (2009).

18. Genge, B. R., Wu, L. N. Y. & Wuthier, R. E. Kinetic analysis of mineral formation during in vitro modeling of matrix vesicle mineralization: Effect of annexin A5, phosphatidylserine, and type II collagen. *Anal. Biochem.* **367**, 159–166 (2007).
19. Caseli, L., Nobre, T. M., Ramos, A. P., Monteiro, D. S. & Zaniquelli, M. E. D. The Role of Langmuir Monolayers To Understand Biological Events. in *Recent Progress in Colloid and Surface Chemistry with Biological Applications*, 65–88 (2015).
20. Oliveira, O. N., Caseli, L. & Ariga, K. The Past and the Future of Langmuir and Langmuir–Blodgett Films. *Chem. Rev.* **122**, 15232–15241 (2022).
21. Derradi, R. *et al.* Cholesterol Regulates the Incorporation and Catalytic Activity of Tissue-Nonspecific Alkaline Phosphatase in DPPC Monolayers. *Langmuir* **35**, 6459–6513 (2019).
22. Davies, J. T. & Rideal, E. K. *Interfacial Phenomena*. (1963).
23. Blume, A. A comparative study of the phase transitions of phospholipid bilayers and monolayers. *Biochim. Biophys. Acta - Biomembr.* **557**, 32–44 (1979).
24. Cruz, M. A. E. *et al.* Phosphatidylserine controls calcium phosphate nucleation and growth on lipid monolayers: A physicochemical understanding of matrix vesicle-driven biomineralization. *J. Struct. Biol.* **212**, 107607–107617 (2020).
25. Abdallah, D. *et al.* Fatty acid composition in matrix vesicles and in microvilli from femurs of chicken embryos revealed selective recruitment of fatty acids. *Biochem. Biophys. Res. Commun.* **446**, 1161–1164 (2014).
26. Habraken, W. J. E. M. *et al.* Ion-association complexes unite classical and non-classical theories for the biomimetic nucleation of calcium phosphate. *Nat. Commun.* **4**, 1507–1519 (2013).
27. Rodrigues, R. T. *et al.* Carbon Nanotubes and Algal Polysaccharides To Enhance the Enzymatic Properties of Urease in Lipid Langmuir–Blodgett Films. *Langmuir* **34**, 3082–3093 (2018).
28. Chen, X., Huang, Z., Hua, W., Castada, H. & Allen, H. C. Reorganization and Caging of DPPC, DPPE, DPPG, and DPPS Monolayers Caused by Dimethylsulfoxide Observed Using Brewster Angle Microscopy. *Langmuir* **26**, 18902–18908 (2010).
29. Ma, G. & Allen, H. C. DPPC Langmuir Monolayer at the Air−Water Interface: Probing the Tail and Head Groups by Vibrational Sum Frequency Generation

Spectroscopy. *Langmuir* **22**, 5341–5349 (2006).

30. Hauser, H., Pascher, I., Pearson, R. H. & Sundell, S. Preferred conformation and molecular packing of phosphatidylethanolamine and phosphatidylcholine. *Biochim. Biophys. Acta - Rev. Biomembr.* **650**, 21–51 (1981).
31. Vollhardt, D. & Fainerman, V. B. Progress in characterization of Langmuir monolayers by consideration of compressibility. *Adv. Colloid Interface Sci.* **127**, 83–97 (2006).
32. Volpati, D. *et al.* Vibrational spectroscopy for probing molecular-level interactions in organic films mimicking biointerfaces. *Adv. Colloid Interface Sci.* **207**, 199–215 (2014).
33. Rey, C. *et al.* Characterization of Calcium Phosphates Using Vibrational Spectroscopies. in *Advances in Calcium Phosphate Biomaterials* 229–266 (2014).
34. Lin, T. J. & Chiu, C. C. Structures and infrared spectra of calcium phosphate clusters by: Ab initio methods with implicit solvation models. *Phys. Chem. Chem. Phys.* **20**, 345–356 (2017).
35. Melcrová, A. *et al.* The complex nature of calcium cation interactions with phospholipid bilayers. *Sci. Rep.* **6**, 38035–38047 (2016).
36. Ibsen, C. J. S., Gebauer, D. & Birkedal, H. Osteopontin Stabilizes Metastable States Prior to Nucleation during Apatite Formation. *Chem. Mater.* **28**, 8550–8555 (2016).
37. Hentrich, D., Brezesinski, G., Kübel, C., Bruns, M. & Taubert, A. Cholesteryl Hemisuccinate Monolayers Efficiently Control Calcium Phosphate Nucleation and Growth. *Cryst. Growth Des.* **17**, 5764–5774 (2017).
38. Ruiz, G. C. M. *et al.* Biomimetic collagen/phospholipid coatings improve formation of hydroxyapatite nanoparticles on titanium. *Mater. Sci. Eng. C* **77**, 102–110 (2017).
39. Zhang, L.-J. *et al.* Mineralization mechanism of calcium phosphates under three kinds of Langmuir monolayers. *Langmuir* **20**, 2243–2249 (2004).
40. Uysal, A., Stripe, B., Lin, B., Meron, M. & Dutta, P. Assembly of amorphous clusters under floating monolayers: A comparison of in situ and ex situ techniques. *Langmuir* **29**, 14361–14368 (2013).
41. Yang, X. *et al.* Physical origin underlying the prenucleation-cluster-mediated nonclassical nucleation pathways for calcium phosphate. *Phys. Chem. Chem.*

Phys. **21**, 14530–14540 (2019).

42. Mancardi, G., Hernandez Tamargo, C. E., Di Tommaso, D. & de Leeuw, N. H. Detection of Posner's clusters during calcium phosphate nucleation: a molecular dynamics study. *J. Mater. Chem. B* **5**, 7274–7284 (2017).
43. Garcia, N. A. *et al.* Simulation of Calcium Phosphate Prenucleation Clusters in Aqueous Solution: Association beyond Ion Pairing. *Cryst. Growth Des.* **19**, 6422–6430 (2019).
44. Zhao, W., Wang, Z., Xu, Z. & Sahai, N. Osteocalcin facilitates calcium phosphate ion complex growth as revealed by free energy calculation. *Phys. Chem. Chem. Phys.* **20**, 13047–13056 (2018).
45. Taylor, M. G., Simkiss, K., Simmons, J., Wu, L. N. Y. & Wuthier, R. E. Structural studies of a phosphatidyl serine-amorphous calcium phosphate complex. *Cell. Mol. Life Sci.* **54**, 196–202 (1998).
46. Kesseli, F. P., Lauer, C. S., Baker, I., Mirica, K. A. & Van Citters, D. W. Identification of a calcium phosphoserine coordination network in an adhesive organo-apatitic bone cement system. *Acta Biomater.* **105**, 280–289 (2020).
47. Almeida, P. F. F. Thermodynamics of lipid interactions in complex bilayers. *Biochim. Biophys. Acta - Biomembr.* **1788**, 72–85 (2009).
48. Boettcher, J. M. *et al.* Atomic View of Calcium-Induced Clustering of Phosphatidylserine in Mixed Lipid Bilayers. *Biochemistry* **50**, 2264–2273 (2011).
49. Ross, M., Steinem, C., Galla, H.-J. & Janshoff, A. Visualization of Chemical and Physical Properties of Calcium-Induced Domains in DPPC/DPPS Langmuir−Blodgett Layers. *Langmuir* **17**, 2437–2445 (2001).
50. Faiß, S., Kastl, K., Janshoff, A. & Steinem, C. Formation of irreversibly bound annexin A1 protein domains on POPC/POPS solid supported membranes. *Biochim. Biophys. Acta - Biomembr.* **1778**, 1601–1610 (2008).

4

AUTOPHAGY IMPAIRMENT AND THE RELEASE OF MVs

The role of matrix vesicles (MVs) in bone mineralization has been deeply investigated. However, the cellular and molecular processes underlying the biogenesis of these vesicles are not well understood. It has been demonstrated that mature mineralizing cells release MVs as mineralization-competent structures. The differentiation of osteoblasts towards a mineralizing phenotype is complex and autophagy (an intracellular process by which cells break down and recycle their own components) has been demonstrated to tightly control osteoblast mineralization. Since MVs are thought to control ECM mineralization, it is possible that the pathways of autophagy and MV biogenesis are interconnected, but this subject has never been explored. In this chapter, we aim to investigate the hypothesis that autophagy and the biogenesis of MVs are connected by characterizing vesicles isolated from osteoblasts with impaired mineralization due to treatment with chloroquine (CQ). Our findings suggest that the amount of MVs present within the extracellular matrix of osteoblasts treatment and not treated with chloroquine is similar. However, they bear a different molecular cargo and reduced expression of mineralization-related proteins. These results suggest that the release of mineralization-competent vesicles is tightly controlled at the cellular level. Our research opens a new avenue for investigating the molecular players involved in MVs' biogenesis and provides insights into the complex relation between autophagy and bone mineralization.

4.1 | Introduction

Autophagy is a mechanism conserved in eukaryotes, from yeast to humans, and is involved in maintaining cellular homeostasis by degrading organelles, proteins, lipids, and nucleic acids and recycling their constituent building blocks when cells face nutritional deficits [1]. The term autophagy (from the Greek αὐτόφαγος, *"self-eating"*), was coined by Christian de Duve more than half a century ago to denote the degradation of self-constituents by the lysosome, an organelle containing hydrolytic enzymes that are capable of breaking down and digesting various types of biological macromolecules[2]. Since then, autophagy has been implicated in many physiological/pathological processes, much beyond the simple role of supplying energy when needed. Dysregulation of autophagy has been associated with many diseases, including neurodegenerative diseases, infections, inflammation, metabolic dysfunction, cancer, and aging[3].

The full completion of autophagy involves a series of highly conserved autophagy-related proteins (ATGs) essential for cargo selection and delivery to the lysosomes[4], usually described as involving a set of ~16–20 core conserved genes. Triggers can induce bulk autophagy that nonspecifically engulfs any cytoplasmic material or can evoke selective autophagy where specific cargos are targeted for degradation (Figure 4.1). Depending on the cargo, selective autophagy receives specific names, such as mitophagy (for mitochondria) and peroxiphagy (for peroxisomes). The completion of the autophagy pathway comprises four major steps: initiation/nucleation, elongation, degradation and termination. The mechanistic detail of this process is out of our scope in this chapter, and we will just give a brief view on the process. The starring role in the process is the formation of the autophagosome, a double-membraned vesicle with the ability to engulf large parts of the cytoplasm (including entire organelles) and dictates the high catabolic potential of autophagy[5]. In response to different conditions of stress, autophagosome formation for cargo engulfment is initiated by the recruitment of ATGs to a specific subcellular location, where a cup-shaped isolation membrane (called phagophore) is formed[6]. The main already characterized pathway that triggers autophagy is cell starving by deprivation of amino acids, resulting in the inhibition of the master cell growth regulator serine/threonine kinase mTOR and the nonspecifically engulfment of any cytoplasmic material to be used as energy supply[7]. However, cellular conditions can also induce selective autophagy by labelling specific cargos with "eat-me" signals (mainly ubiquitin chains) that are recognized by molecular receptors that link the cargo

to the forming-autophagosome membrane via their light chain 3 (LC3)-interacting region. As an example, upon loss of mitochondria membrane potential, the phosphatase and tensin homologue (PTEN)-induced putative kinase 1 (PINK1)–Parkin pathway regulates the ubiquitin-dependent clearance of dysfunctional mitochondria through mitophagy[8]. In mitophagy, Parkin ubiquitinylates various proteins in the outer membrane of mitochondria that are recognized by the adapter p62/sequestosome 1 (p62/ SQSTM1) that contains a LC3-interaction region[9].

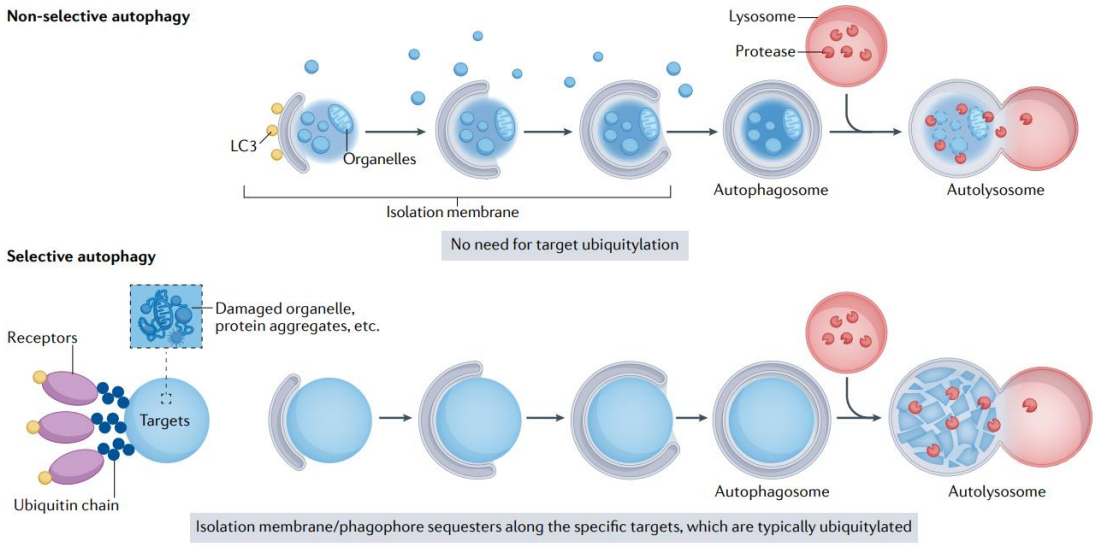

Figure 4.1 | Comparison of non-selective autophagy and selective autophagy. Autophagy breaks down cellular components through a double-membrane structure called autophagosome in both non-selective and selective ways. Non-selective autophagy generates an isolation membrane in response to various stimuli and engulfs cytoplasmic contents and organelles randomly. On the other hand, autophagosomes specifically targeting certain cellular components are formed in selective autophagy. The recognition of these targets varies, but ubiquitylation of cargo plays a crucial role in both the process. Receptor clusters then link isolation membranes with targets via binding to lipidated LC3 proteins. Autophagosomes formed during selective autophagy are usually bigger to accommodate large cargo, such as entire organelles. Adapted with permission from Vargas et al.[10]

After the phagophore formation, the autophagosome membrane is elongated by incorporation of phospholipids from various sources including the endoplasmic reticulum, recycling endosomes, and mitochondria, until it completely closes engulfing the cargo per complete[5]. Following the sealing of the phagophore, the autophagosome membrane matures by the gradual clearance of ATGs from their nascent outer membrane and prepare for the next step in the completion of the autophagy pathway. This involves the recruitment of the machineries responsible for lysosomal delivery (microtubule-based kinesin motors) and to mediate the fusion of the autophagosome with the lysosome, that encompass different proteins from the SNAREs (soluble NSF attachment receptor)

family[4]. Fusion of autophagosome with lysosome creates the autolysosome, the final organelle in the autophagy pathway. In the autolysosomes, degradation of autophagy substrates proceeds as the lysosomal lumen is acidified (owing to the activity of an ATP-dependent proton pump commonly known as V-type ATPase)[11], upon disassembly of the inner autophagosome membrane supported by the ATG conjugation systems[12]. In the autolysosomes, several hydrolytic enzymes break macromolecules to its constituents and release then to the cytosol, completing the autophagy pathway.

Bones undergo a continuous remodeling cycle to maintain their structural homeostasis and functionality[13–16]. Given the recycling role of autophagy, it is not surprising that its action is closely regulated in this tissue. Multiple ATGs proteins have been described to contribute to mediating the survival and functioning of bone cells, enabling them to survive to hypoxia or nutrition-deficient environments[17]. Recent evidences suggest a strong correlation between autophagy and the progression of osteoporosis, a pathological condition related to the disbalance between bone formation and resorption, leading to fragile bones[18,19]. Moreover, i*n vitro* studies revealed that an appropriate autophagy level is a prerequisite for the maintenance of homeostasis and survival of osteoblasts [19,20]. Either pharmacological and gene-knockdown downregulation of autophagy results to increased oxidative stress in osteoblasts, whereas upregulation of autophagy in these cells is correlated with reduced oxidative stress and decreased apoptosis[21,22]. Furthermore, autophagy plays an important role in the signaling pathways associated to osteoblast differentiation and mineralization, including the insulin-like growth factor-I (IGF-I) and bone morphogenetic protein (BMP)[23–25]. Interestingly, autophagy has been shown to play a crucial role in osteoblast mineralization. In particular, pharmacological inhibition of autophagy or knockdown of specific autophagy-related genes (ATGs) has been shown to impair the ability of osteoblasts to mineralize[21,26–28]. As an example, osteocytes (the terminal cells in the osteoblastic lineage) lacking EphrinB2, a check-point gene along the osteoblast-osteocyte differentiation pathway, displayed more autophagosomes and elevated autophagy *in vivo* and *in vitro*, that resulted in elevated secondary mineralization and brittle bone[29].

Although various studies have investigated the role of autophagy in osteoblast mineralization, the exact mechanisms underlying this regulation are still not fully understood and remain largely hypothetical. The most speculated pathway is by the exploitation of autophagy machinery in a non-canonical way, by the way cells handle intracellular mineral. The seminal observation of calcium phosphate formation inside

mitochondria led to the creation of a paradigm that the mineralization of extracellular matrix might be intracellularly initiated[30]. Although the mechanisms still not completely understood, large amounts of Ca^{2+} and PO_4^{3-} are handled in order to form the mineral precursor phase required to mineralize the massive mass of collagen fibrils found in mature bone[31]. Therefore, it is hypothesized that mineralizing cells might initially concentrate ions intracellularly before their release to the extracellular matrix. Corroborating this hypothesis, insoluble calcium phosphate aggregates have been observed in different intracellular compartments, such as mitochondria[32,33], vacuoles[34] and lysosomes[27]. In a seminal study, Nollet and colleagues[28] observed that intracellular mineral in osteoblasts are localized in autophagosomes, the main organelle along the autophagic pathway. By using knockdown of autophagy-essential genes and osteoblast-specific autophagy-deficient mice, the authors demonstrated that autophagy deficiency reduces mineralization capacity[28]. Recently, another study proposed that mitophagy provides the mechanism for transfer of mineral precursors from Ca^{2+}-loaded mitochondria to the extracellular matrix by means of transportation in autophagosomes[35]. Pei et al. demonstrated in their study that mitophagy is upregulated during osteogenic differentiation, leading to the accumulation of dysfunctional mitochondria overloaded with amorphous calcium phosphate (ACP), which are then targeted for removal through mitophagy[35]. Upon fusion with lysosomes, the mitochondrial ACP precursors coalesce to form larger intravesicular granules, prior to their release into the extracellular matrix. However, what triggers the intracellular accumulation of ions and how the accumulated precursor phase is translocated to the extracellular matrix are poorly defined and remain hypothetical.

Additionally, autophagy may also be non-canonically exploited by mineralizing cells through its intersection with the release of mineralizing extracellular vesicles[36]. Despite strong evidence that MVs are released as ectosomes from the plasma membrane, the conditions that facilitate and trigger their biogenesis are poorly understood. Current hypotheses posit that an increase in intracellular Ca^{2+} concentration leads to changes in the localization of membrane phospholipids and proteins (annexins), thus initiating vesiculation[37], mediated by depolymerization of the actin cytoskeleton[38]. Assigning a distinct biogenesis pathway to a given extracellular vesicle class is extraordinarily difficult, since there are still no universal markers of a distinct biogenesis pathway, and certainty can be given only if the vesicle is caught in the act of being released; for example, by live imaging techniques[39]. However, an interesting observation is that during

the events that leads to the cartilage mineralization in the growth plate, the release of MVs is observed concomitantly to an increase in intracellular Ca^{2+} concentration, that as previously discussed, might be related to autophagy. Moreover, the intracellular pathways that lead to the selection of MVs' cargo remain scarcely defined. Growing evidence suggest ATGs in multiple pathways mediate cellular secretion, which have been unitedly called "secretory autophagy"[40]. For example, a recent study uncovered that the autophagy machinery can be used to specifying the proteins and RNAs that are loaded into EVs for secretion outside the cell[41]. Moreover, autophagy impairment has been demonstrated to affect the cargo of released EVs[42–45]. These expanding roles for autophagy pathway components in secretion, poignantly suggest that cellular catabolism and secretion are functionally coordinated within cells[46]. Since autophagy is tightly regulated during osteoblast mineralization, it is tempting to speculate that it can also affects the release of mineralizing MVs, a topic that has never been explored. Autophagy could play a role in either tuning the cell state by which MVs' biogenesis is triggered or having a yet-to-be-uncovered specific role in selecting and loading cargo prior to MVs release. Further research is necessary to fully understand the relation between autophagy and MV release and uncover the potential therapeutic applications of targeting this pathway in bone mineralization. Herein, we hypothesized that autophagy might play a role in biogenesis and function of MVs. To get insight into hypothesis, we characterized MVs isolated from osteoblasts cultivated in osteogenic medium in the presence of chloroquine (CQ), a classical inhibitor of autophagy[47], and compared the results with MVs isolated from osteoblasts cultivated in absence of CQ.

4.2 | Objectives

General Objective

To determine if impairment of autophagy affect the content and functionality of MVs isolated from osteoblast cultures.

Specific aims

(i) To validate the hypothesis that impairment of autophagy upon CQ treatment reduce the mineralization of osteoblasts *in vitro*;

(ii) To compare the content and functionality of MVs from control (cells cultivated in absence of CQ) and CQ-treated osteoblasts;

4.3 | Methods

4.3.1 | Chick calvaria osteoblasts *in vitro* culture

Osteoblast cells were isolated from chicken calvaria accordingly to Gerstenfeld et al.[48]. Briefly, calvaria bones were freshly dissected from 17-days-old chicken embryo and cells were isolated by three sequential digestions in an enzyme mixture containing 0.05% trypsin (Gibco BRL) and 0.1% type II collagenase (Sigma C6885, from *Clostridium histolyticum*), at 37°C. The third fraction was collected, resuspended in α-MEM supplemented with 10 wt.% FCS, 1 vol.% penicillin/streptomycin and 0.3 $\mu g.mL^{-1}$ fungizone, until 80% confluence was reached. Then, cells were trypsinized and plated at density of 1 x 10^4 cells/cm^2 and cultured for 3 days until reach confluence. All experiments were carried out at passage 2. After confluence, the basal culture medium was replaced by osteogenic medium (α-MEM supplemented with 10% FCS, 50 $\mu g.mL^{-1}$ of ascorbic acid, and 5 mM of β-glycerophosphate). The addition of osteogenic medium was considered day 0, and medium was changed every 72 h. Chloroquine diphosphate (CQ- MP Biomedicals) at convenient concentrations depicted in the results section was added to the medium when needed. All procedures involved in the euthanasia of animals were approved by the institutional ethics committee (FFCLRP protocol 19.1.842.59.13).

4.3.2 | Cell viability and apoptosis assay

To assure that differences in mineralization observed for the osteoblasts would not be assigned to any cytotoxicity of CQ, we determined the maximum concentration of CQ added to the medium with no reduction in cells viability. For this, 3-(4,5-dimethylthiazol-2-yl)-2,5-diphenyltetrazolium bromide (MTT) assay was employed to determine the cytotoxicity of CQ to the osteoblasts[49]. 4000 cells/well in 96-well plates (N=6) were first cultivated in basal medium for 48 h, then the medium was replaced by osteogenic medium containing different concentrations of CQ. After 6 and 72 h, MTT was added at final concentration of 0.8 mg/mL and incubated at 37°C for 3 hours. Formazan produced by the cells was dissolved in acidified isopropanol (0.15% HCl) and absorbance was measured at 560 and 690 nm, using a microplate reader (SpectraMax® 190, Molecular Devices). Changes in absorbance (A_{560} - A_{690}) were expressed was % compared to the control cells (cells cultivated in absence of CQ).

Cell apoptosis was evaluated using a Annexin V-FITC Apoptosis Detection Kit (Sigma-Aldrich, code APOAF), following fabricant protocol[50]. Briefly, after culturing for 72 h with the optimized concentration of CQ (10 μM), cells were washed twice with cold PBS, centrifuged and resuspended in binding buffer containing Annexin V-FITC and Propidium Iodide (PI), incubated for 10 min in the dark and then analysed by flow cytometry (FACSCanto II, BD Biosciences). Viable cells were FITC Annexin V and PI-negative; cells that were in early apoptosis were Annexin V-positive and PI-negative; and cells that were in late apoptosis or necrosis were Annexin V- and PI-positive. Experiments were performed in triplicate.

4.3.3 | Isolation of matrix vesicles (MVs)

For MVs isolation, osteoblasts were cultivated in a density of 10^4 cells/cm^2 in a 75 cm^2., following the same procedure previously described for cultivation in the plates. After 14 days, the cell culture medium was removed, the cell monolayer washed two times with cold phosphate buffer saline and then digested with collagenase, according to the protocol described by Buchet et al.[51] The digestion was proceeded for 3 h, at 37°C, SCL buffer supplemented with 1 mM $CaCl_2$ and 100 U/mL type II collagenase (Sigma C6885, from *Clostridium histolyticum*).. After digestion, the suspension was filtered through a nylon membrane (100 μm mash size). The supernatant was centrifuged at 600 g to collect all released cell material. The MVs were purified by consecutive centrifugations at 20,000 g

for 30 min and 80,000 g for 1 h, both at 4°C using a fixed angle rotor P50AT2 (Hitachi). The final pellet was homogenized in 200 µL of synthetic cartilage lymph (SCL). SCL is composed of 1.42 mM NaH_2PO_4, 1.83 mM $NaHCO_3$, 12.7 mM KCl, 0.57 mM $MgCl_2$, 5.55 mM D-glucose, 63.5 mM saccharose, 16.5 mM Tris (2-Amino-2-hydroxymethyl-propane-1,3-diol), 100 mM NaCl, 0.7 mM Na_2SO_4 in water at pH 7.5.

4.3.4 | Nanoparticle tracking analysis

The concentration of MVs dispersed in PBS was determined by nanoparticle tracking analysis (NTA) using a NanoSight LM20 (NanoSight) (λ = 635 nm) at 25°C (FCFRP-USP).

4.3.5 | Atomic force microscopy and transmission electron microscopy of MVs

MVs were fixed by adding 1 vol.% of glutaraldehyde to the dispersions containing the vesicles to avoid deformation and disruption. Then, the sample was dropped onto freshly cleaved mica, dried at room temperature, and imaged by an AFM (model SPM-9600 Scanning Probe Microscope, Shimadzu Corporation, Japan, DQ-FFCLRP/USP) operating in tapping mode, as previously described by Bolean et al.[52]. Scanning was performed in air at 25°C by using silicon probes with a resonance frequency ranging from 324 to 369 kHz (Nanosensors™, Neuchâtel, Switzerland). The scan rate was set to 0.2–0.3 Hz to avoid tip-induced vesicle deformations and/or damages. The cantilevers had a spring constant of a 38 ± 8 N/m and a resonance frequency of 336 ± 67 kHz. Images were analyzed by using WSxM 4.0 Beta 9.1 software[53].

For TEM analysis, MVs were also fixed with 1 vol% dropped on a TEM grid, stained with 1% uranil acetate and imaged in a JEOL JEM 100CXII microscope.

4.3.5 | Alkaline phosphatase (TNAP) assay and in vitro mineralization of MVs

The activity of TNAP present in the vesicles was determined by the hydrolysis of *p*-nitrophenyl phosphate (p-NPP, Sigma-Aldrich) in a reaction medium containing 10 mM p-NPP and 1 mM $MgCl_2$ in AMPOL buffer (2-amino-2-methyl-1-propanol), pH 10.3, at 37°C. The reaction was monitored by changes in the absorbance at 405 nm related to the formation of the yellowish product p-nitrophenolate $(p\text{-}NP)^-$ and the specific activity was expressed as µmol pNP^-/min/mg of protein. The total protein content was determined by Hartree methodology[54]. The mineralization of MVs was evaluated in SCL supplemented

with 2 mM Ca^{2+} and 3.42 mM NaH_2PO_4, at 37°C. The concentration of MVs in the medium was standardized at 50 µg of protein/mL. Mineralization was followed by changes in turbidimetry at 340 nm, measured every minute without stirring, in a 200 µL reaction volume using a 96-well plate, at 37°C, with the aid of a Molecular Devices M3 microplate reader. After 24 h, the samples were centrifuged and placed on a germanium crystal of an attenuated total reflectance (ATR) accessory to assess the chemical groups in the formed minerals by means of FTIR spectroscopy (Shimadzu-IRPrestige-21, DQ-FFCLRP/USP).

4.3.5 | Gene Expression by RT-PCR

The total RNA was extracted using the SV Total RNA Isolation System kit (Promega, Fitchburg, WI, USA) and reverse transcription reaction was carried out to synthesize the complementary DNA (cDNA) using the High-Capacity cDNA Reverse Transcription Kit (Thermo Fisher Scientific, Waltham, MA, USA). For RT-PCR, the SYBR Green system, and primers (Table 1) were used in the QuantStudio™ 7 Flex System device (Applied Biosystems, Waltham, MA, USA). The reactions were done (n = 4) and the data analysed using the cycle threshold value (Ct). The expression of the housekeeping gene GAPDH was evaluated, and the 2-ddCt method was used to compare the gene expression of the experimental groups.

Table 1. Primer sequences for RT-PCR

Gene	Forward sequence	Reverse sequence
ALPL	ATATGGTGTATGAGCTGGAC	TTTCTGCAGCATCCTTATG
SQSTM1	GCACTATAAGGATGAAGACG	TTTCTCTTTGATGTACACGC
COL1A1	GAACCCCAAGGAGAAGAAG	CAGGAAGGTCAGTTGGATG
RUNX2	GTCAAAGTAAAGCTCTTCCC	CTGAATGGGAAGCTTACTG
GAPDH	CATCATACTTGGCTGGTTTC	ATCACGTGGATTCTCAGTC
SPP1	GTAATGAGTCTGCTGAAGTG	TGGTCTTCGATTTTGATGG
PHOSPHO1	GCTGCATGTACTCATTGTAG	AAGCTTTAAACACGATGCC
LAMP1	CCAATCGTAGAGTCCTGTAG	TTGCAAAGAAGTACAGCAG
MAP1LC3B	CGTTCACAAGGCTTACTTC	CGAACGGAACTAAACAGAG

4.3.6 | SEM and TEM analysis of cells

For SEM and TEM analysis, cells were cultivated for 14 days on 24-well Nunc™ Thermanox™ coverslips. Cells were then fixed with glutaraldehyde and postfixed with 1% osmium tetroxide. For SEM analysis, postfixed cells were dehydrated with a CO_2 gradient, coated with gold by using cathodic pulverization (Bal-Tec, SCD-050 Sputter Coater) and imaged in a Shimadzu SS-550 Superscan microscope. For TEM, postfixed cells were dehydrated in a series of ethanol solutions, transferred to propylene oxide, and embedded in epoxy resin. Ninety nanometer-thick sections were obtained with a ultramicrotome and stained with uranyl acetate and Reynold's lead citrate, and examined using a JEOL JEM 100CXII microscope, FMRP/USP.

4.3.7 | Proteomic analysis

50 µg of total protein of isolated MVs were lysed in RIPA buffer and then the buffer exchanged to 100 mM ammonium bicarbonate, pH 8, with the aid of a 10K MWCO Amicon filter. Protein was reduced with 50 mM dithiothreitol (DTT) at 60°C for 30 min followed by alkylation with 100 mM iodoacetamide (IAM). Then, sequencing-grade trypsin (Promega) was added at a ratio of 1:50 (w:w) and digestion allowed to proceed overnight at 37°C. For proteomic analysis, 10 µl of sample was loaded on the microUPLC-ESI-qTOF-MS system; microUPLC (microACQUITY ultra pressure liquid chromatography and XEVO G2 Xs QToF mass spectrometer equipped with lockspray ion source, LaCTAD/UNICAMP). Prior to the injection, the columns were equilibrated with 93% mobile phase A (water with 0.1% formic acid) and 7% mobile phase B (acetonitrile containing 0.1% formic acid). The column temperature was set to 40°C.

First, peptides were trapped on a ACQUITY UPLC Symmetry C18 Trap column (Waters, Corp., Milford, USA) 5 µm particle size, 300 µm i.d. 25 mm length, at 15 µl/min flow rate for 4 min. Peptides were separated from the trap column by gradient elution to an analytical column ACQUITY UPLC M-Class HSS T3 column, 1.8 µm particle size, 300 µm i.d. 150 mm length (Waters, Corp., Milford, USA), at 5 µL/min flow rate with a gradient 7% to 40% acetonitrile over 155 min, followed by a 6 min rinse of 85%. The column was re-equilibrated at initial conditions for 24 min. Data independent acquisition mode (MSE) was carried out by operating the instrument at positive ion V mode, applying the MS and MS/MS functions over 0.5 s intervals with 6 V low energy and 15–45 V high energy collision to collect the peptide mass to charge ratio (m/z) and the product ion

information to deduce the amino acid sequence. Capillary voltage and source temperature was set to 3.0 kV and 80°C, respectively. To correct for the mass drift, the internal mass calibrant Leucine enkephalin (556.2771 Da) was infused at every 30 s through the lockspray ion source at 3 µl/min flow rate. Peptide signal data were collected between 100–2000 m/z values.

Identification of the proteins present in the samples was performed with a Proteome ID 9031 (*Gallus gallus*) from UniProt (Swiss-Prot/TrEMBL) specific database. After an assessment query, the software automatically sets the peptide and fragment mass tolerances. The lock mass correction was performed using the monoisotopic value 556.2771 Da of the mono charge precursor mass of Leucine-Enkephalin and operating the instrument at a resolution of at least 30,000 FWHM. Peptide and protein identifications were performed by setting the minimal number of fragment ion matches per peptide to 3 and that per protein to 5. The minimal peptide match per protein was initially set to 1, but final identification was only accepted with a minimum of 3 peptides per proteins. No more than one missed cleavage was allowed. The tolerated modifications were cysteine carbamidomethylation and oxidation of methionine. The protein false positive rate was set to 3%. Protein identification was made with Progenesis QI for proteomics (Nonlinear Dynamics). For quantification, the use of the internal standard Phosphorilase B (rabbit - UniProt P00489) was used at 200 fmol.

4.5 | Results

4.5.1 | Validation of CQ treatment upon cell viability and apoptosis

We initiated our investigation by titrating the concentration of CQ to guarantee no cytotoxicity of the compound to the cells. To validate the effect of CQ treatment on cell viability, we performed a series of assays. First, we evaluated the cytotoxicity of CQ by treating osteoblasts with increasing concentrations of the drug during 6 h, 72 h and 7 days hours and assessing cell viability using a colorimetric assay (MTT). The MTT assay works by converting MTT, a yellow tetrazolium salt, into purple formazan crystals by mitochondrial dehydrogenases of viable cells[49]. As shown in Figure 4.2a, we observed a dose-dependent decrease in the optical density by increasing concentrations, indicating a reduction in cell viability at CQ concentration higher that 10 µM. Consequently, we decided to use 10 µM as working concentration, which also matches the range used by other studies for long-term treatment aiming aft autophagy impairment[55]. To further ensure that the use of 10 µM CQ did not induce cell apoptosis, we performed Annexin V/propidium iodide staining followed by flow cytometry analysis. Annexin V binds to phosphatidylserine that becomes exposed on the outer leaflet of the plasma membrane during the early stages of apoptosis. Propidium iodide is a DNA intercalating agent that stains the DNA of cells with compromised membrane integrity, such as late apoptotic or necrotic cells. As shown in the Figure 4.2b, we observed negligible staining for Annexin V-positive cells in both control and CQ-treated cells, indicating that treatment with 10 µM CQ did not induce significant levels of early apoptosis. Similarly, we observed no significant staining for propidium iodide in either control or CQ-treated cells, suggesting that CQ treatment did not cause membrane rupture or necrosis (Figure 4.2b).

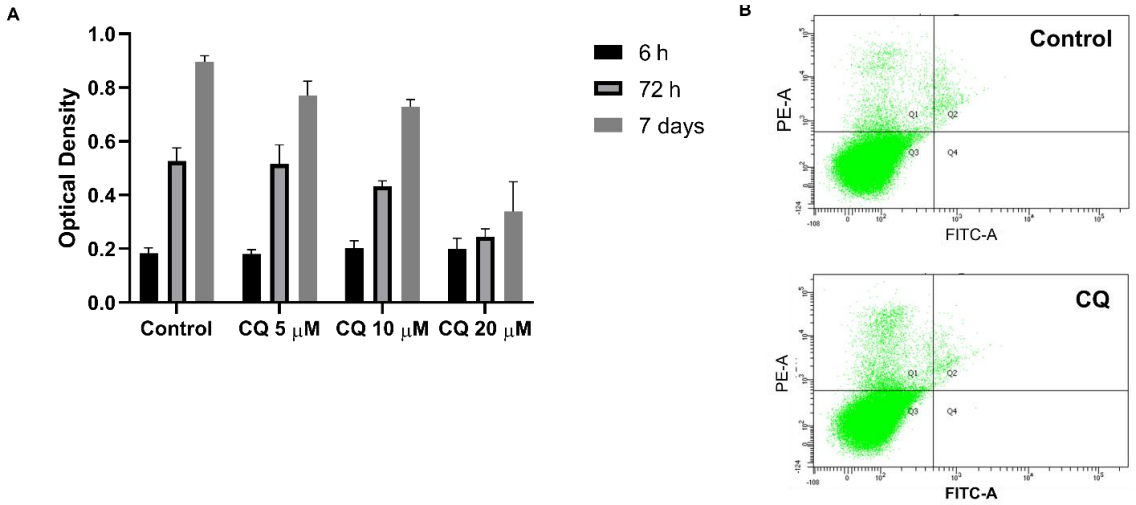

Figure 4.2 | Effect of the treatment with chloroquine (CQ) on osteoblasts viability. A) Optical density measured at 560 nm and a function of CQ concentration, measured by MTT assay. **B)** The potential of CQ treatment at 10 μM to induce apoptosis/necrosis was evaluated using flow cytometry. Representative 2D dot plots showing the staining for annexin V (early apoptotic, channel FITC-A) and propidium iodide (necrotic, PE-A).

To assess the effect of CQ on osteoblasts autophagy, we examined the expression of autophagy-related genes using quantitative reverse-transcription polymerase chain reaction (qRT-PCR). In autophagy, the cellular components to be degraded are sequestered within a double-membraned vesicle called autophagosome. The autophagosome fuses with a lysosome, forming an autolysosome, where the components are degraded by lysosomal hydrolases. This process involves several autophagy-related (ATG) genes, including LC3B, p62, and LAMP1 [56–58], that we choose to evaluate using qRT-PCR as autophagy markers. The analysis of expression of these three proteins targets different steps of the autophagy pathway. LC3B, encoded by the gene *MAP1LC3B* is a protein required for autophagosome formation and is commonly used to monitor autophagy levels. p62, also known as sequestosome-1 (SQSTM1), is a selective autophagy receptor that targets ubiquitinated cargo to autophagosomes for degradation. It binds to LC3B and is degraded upon autophagy completion. Finally, LAMP1, or lysosomal-associated membrane protein 1, is a transmembrane protein that is present at the lysosomal membrane. It is involved in lysosomal biogenesis and is used as a marker for lysosomes and late endosomes.[56–58]

As depicted in the Figure 4.3a, the exposure of osteoblasts to osteogenic medium in absence of CQ upregulated the expression of mRNA related to LC3B, p62, and LAMP1, consistent with previous reports indicating that autophagy is activated during osteoblast mineralization[28,35]. It is widely reported that induction of autophagy is

accompanied by changes in mRNA level of several autophagy-related genes[47], which corroborate the results. Next, we investigated the effects of exposing osteoblasts to CQ in mineralizing medium (Figure 4.3b). We observed a significant decrease in mRNA levels of p62 (SQSTM1) and LAMP1 at day 7 in CQ-treated cells, which suggests a compensatory transcriptional response to the inhibition of autophagy. Previous studies have also reported reduced LAMP1 levels in osteoblasts treated with other lysosomotropic compounds, such as bafilomycin A1[27,35]. The expression levels of LC3B (MAP1LC3B)-related m RNA did not show any significant changes upon treatment with CQ. However, it is important to note that assessing the autophagic state at the mRNA level can be challenging in situations where the autophagic pathway is impaired, as the changes in gene expression levels may not reflect the actual autophagic activity in the cells. Therefore, it is important to use complementary techniques, such as TEM to image the state of organelles, to validate the findings obtained by qRT-PCR.

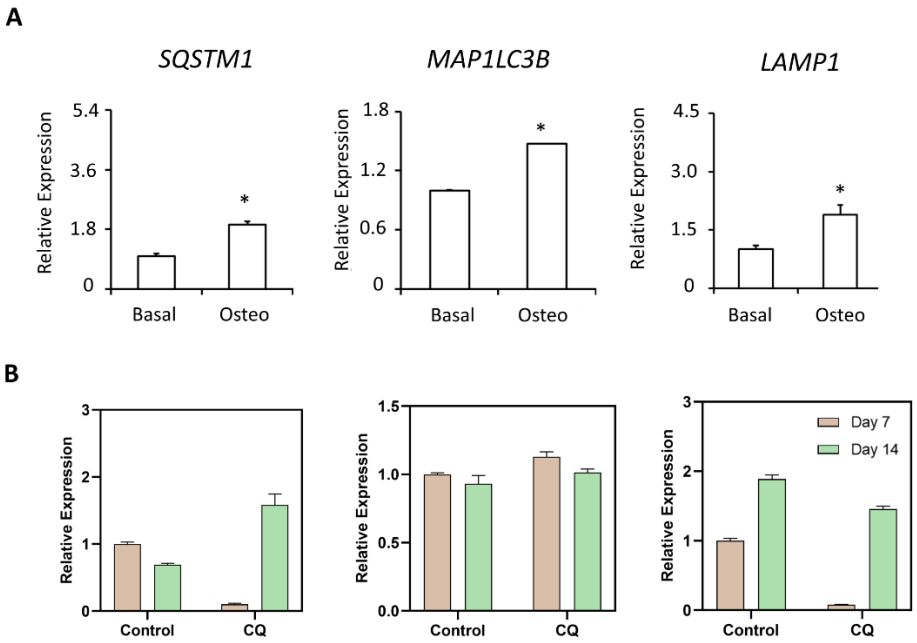

Figure 4.3 | Effect of treatment with CQ in mineralizing medium on the expression of autopghagy-related genes. A) qPCR of autophagy-related genes in osteoblasts cultivated in basal medium and osteogenic (osteo) medium for 7 days. Osteogenic medium is made by supplementation with 5 mM βGP and ascorbic acid. (*) $p < 0.05$. **B)** qPCR of autophagy-related genes in osteoblasts cultivated in osteogenic medium (Control) or treated with CQ (10 μM) after 7 and 14 days. Expression level relative to the housekeeping gene *GAPDH*.

Treatment with CQ is known to inhibit autophagy primarily by impairing the fusion of autophagosomes with lysosomes, which in the long term ultimately leads to disorganization of the endo-lysosomal system[59]. This phenomenon is due to incomplete

degradation of autophagic cargos, which accumulate within cells. The effectiveness of CQ treatment in impairing autophagic degradation was confirmed by TEM images (Figure 4.4). While cells cultivated in osteogenic medium in absence of CQ presented only a few autophagic vacuoles (arrows in Figure 4.4a), CQ-treated cells showed a significant presence of autophagic vacuoles (Figure 4.4b) and late endosomes with intraluminal vesicles (arrow, Figure 4.4c). Interestingly, autophagy impairment has been described to trigger the release of accumulated cargos through endosomal-originated extracellular vesicles[44,55]. Finally, it can be also noticed in the Figure 4.4d the presence of different organelles filled with an electron dense material in CQ-treated osteoblasts, a characteristic of typical for degradative autophagic organelles[47].The accumulation of autophagic structures within the cell, including autophagic vacuoles and late endosomes with intraluminal vesicles, indicated incomplete degradation due to impaired autophagy[44]. Therefore, the ultrastructural evaluation using TEM was useful to confirm the success of autophagy impairment upon treatment with CQ used in our study.

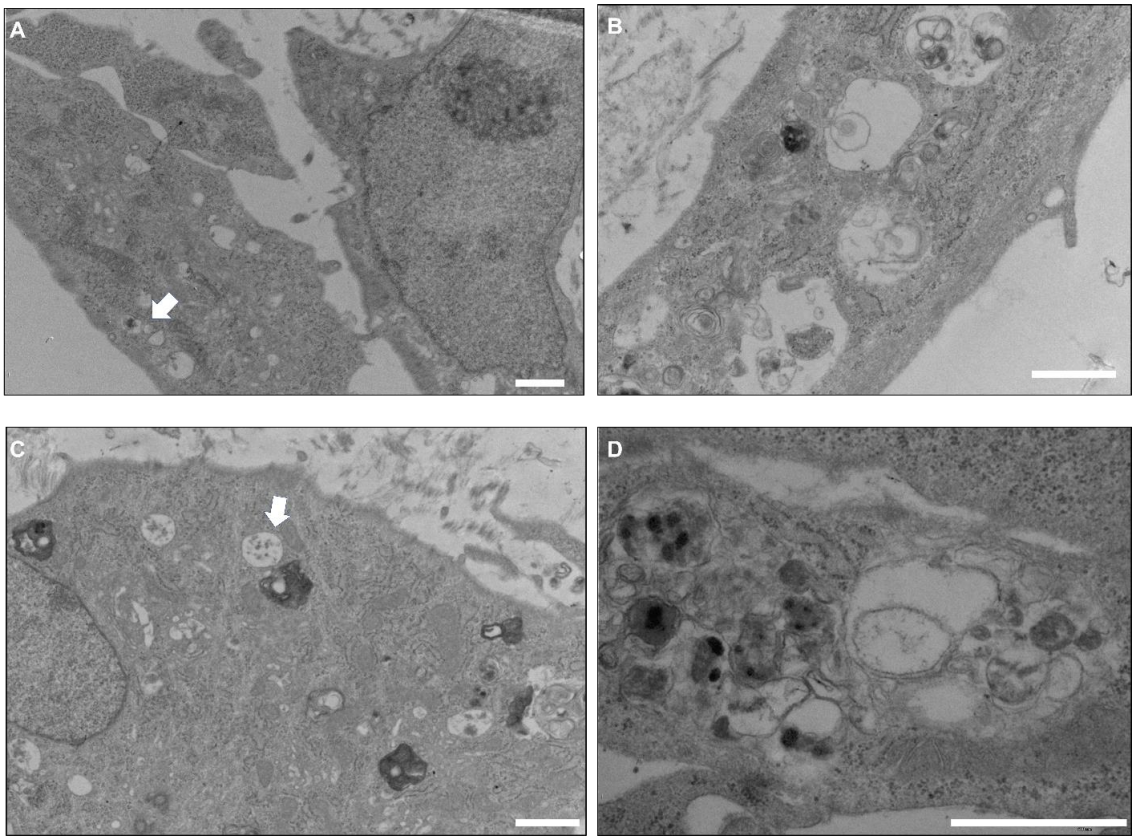

Figure 4.4 | Autophagy impairment confirmation at ultrastructural level. Representative TEM images of osteoblasts cultured for 14 days in osteogenic medium (control) (A) or treated with CQ (10 μM) (B-D). Scale bars, 1 μm.

4.5.2 | Autophagy impairment affects osteoblast mineralization

We then sought to investigate the impact of autophagy impairment on the ability of osteoblasts to mineralize. We started analyzing the morphology of cells and the extracellular matrix secreted by them using scanning electron microscopy (SEM) (Figure 4.5). After culture in osteogenic medium in absence of CQ for 14 days, osteoblasts secreted a great amount of collagen matrix and displayed a typical polygonal morphology bearing abundant membrane protrusions (Figure 4.5a-b). We found that the deposition of extracellular matrix by osteoblasts was not affected after treatment with CQ, as evidenced by SEM images (Figure 4.5c-d). Additionally, we observed nanoparticles associated to fibrils in the collagen matrix, which we attempt to identify as extracellular vesicles (Figure 4.5d, white arrows).

To assess osteoblast mineralization ability, we used alizarin red staining, which stains calcium phosphate mineral. Optical microscopy images of the cell layer revealed that the alizarin staining spread over the osteoid depositions in the control group (Figure 4.5e). In contrast, the CQ-treated group presented small centers of staining that failed to spread through the monolayer, suggesting delayed mineralization of the extracellular matrix (Figure 4.5e). This finding was confirmed by dissolving the bound alizarin and measuring its concentration colorimetrically, which revealed decreased mineralization in the presence of CQ (Figure 4.5f). These results corroborate previous studies using lysosomotropic compounds, which impair autophagy, that resulted in decreased osteoblast mineralization[27,35,60].

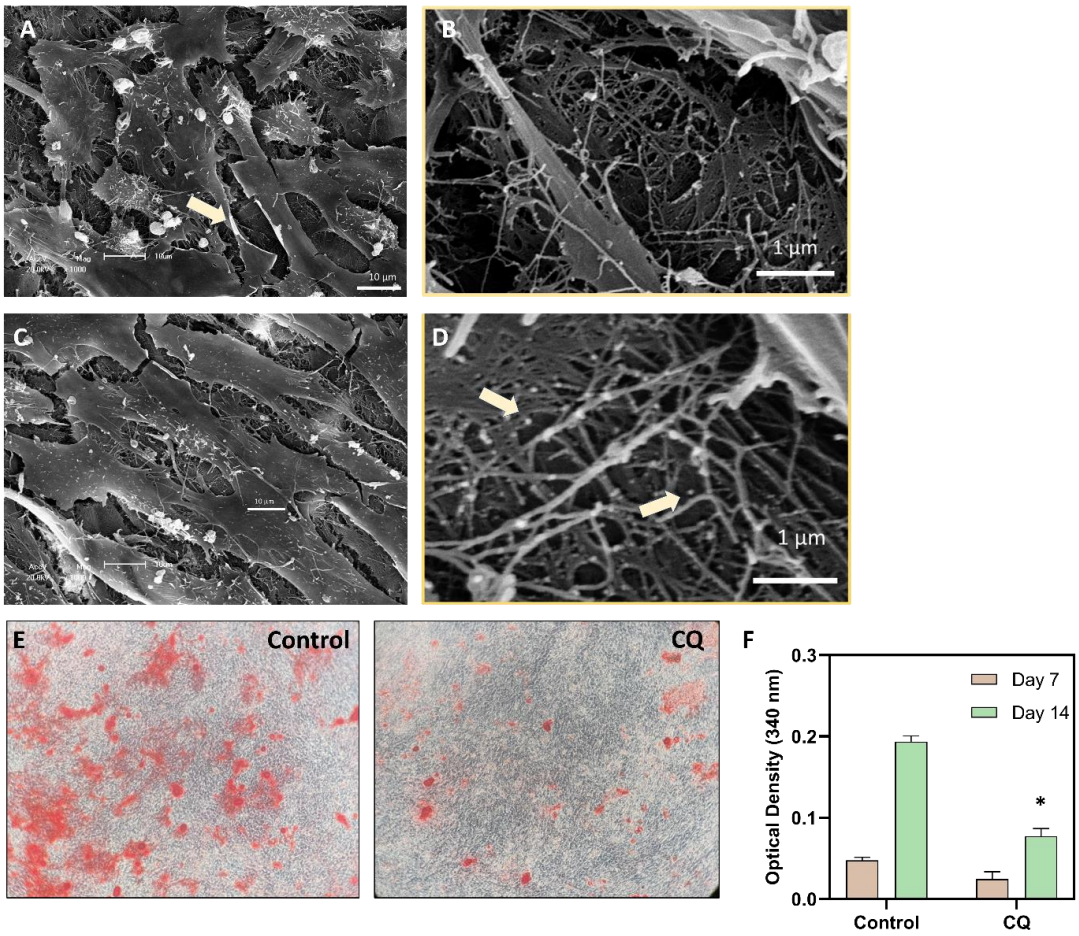

Figure 4.5 | Representative SEM images of osteoblasts cultured in osteogenic medium in absence (control) **(A-B)** and in the presence of CQ (10 µM) **(C-D)** for 14 days. White arrows indicate the interaction between extracellular vesicles and fibrillar collagen matrix. Despite of the treatment condition, a dense collagen matrix was formed by the cells and several nanometric particles can be identified within the extracellular matrix. **E)** Optical images of culture monolayers stained with Alizarin Red S after 14 days of culture revealed the formation of mineralized nodules (red) in a less extent upon CQ treatment. **F)** Quantification of mineralized nodules stained with Alizarin Red by changes in optical density at 340 nm after solubilization. Results represent the mean ± SD for triplicate determination for one experiment.

Then, we proceed to characterize how osteogenesis-related markers were affected upon treatment with CQ. For this, we first measured the activity of TNAP isolated from cells (Figure 4.6a). TNAP is a marker of osteoblast differentiation and its increased activity in the cell indicates differentiation towards mature mineralizing phenotype. We observed a decrease in the TNAP activity for cells treated with CQ, both at 7 and 14 days (Figure 4.6a), suggesting that CQ-treated osteoblasts are less mature than the control ones. RT-qPCR measurement of expression levels of *ALPL* gene, that encodes for TNAP was decreased upon CQ treatment (Figure 4.6b), which confirmed the observation at protein level by measurement of enzyme activity (Figure 4.6a). We then evaluated the expression level of other major osteogenesis-related genes: *RUNX2*, *COL1A1*, *SPP1* and

PHOSPHO1. RT-qPCR data for *RUNX2* (runt-related gene 2), which encodes the master transcription factor for osteoblast differentiation[61], was only slightly changed at day 7 for CQ-treated cells and unaltered at day 14 (Figure 4.6c). The relatively unaffected expression of Runx2 may indicate that the osteoblasts isolated from the calvaria were already committed to their fate, or that autophagy impairment by CQ treatment did not significantly affect the expression of this transcription factor. However, the expression of other osteogenesis-related genes, *COL1A1*, *SPP1* and *PHOSPHO1* was down regulated upon CQ treatment. Actually, *COL1A1* expression was unchanged at day 7, and decreased only at day 14 (Figure 4.6d). This result is in accordance with the fact that the collagen expression, an early marker of the proliferative stage of osteoblasts, was not altered upon CQ-treatment, also confirmed by SEM images (Figure 4.6a-d). We also observed a decrease in the expression of SPP1 upon CQ treatment. *SPP1* encodes for osteopontin, a non-collagenous protein that plays a critical role in the mineralization of the extracellular matrix and is expressed by mature osteoblasts [62–65]. While control cells showed a 3-fold increase in the mRNA related to SPP1, attesting their differentiation towards a mature mineralizing osteoblast, CQ-treated cells showed a remarkable decrease (Figure 4.6e). This was also observed for PHOSPHO1 (Figure 4.6f), that encodes for a phosphatase involved in the generation of inorganic phosphate ions from phosphoetanolamine and phosphocholine substrates, and which expression is key for bone mineralization[66]. Therefore, the gene expression data confirm that impairment of autophagy affected the osteogenesis of osteoblasts, supporting previous observations in the literature[35].

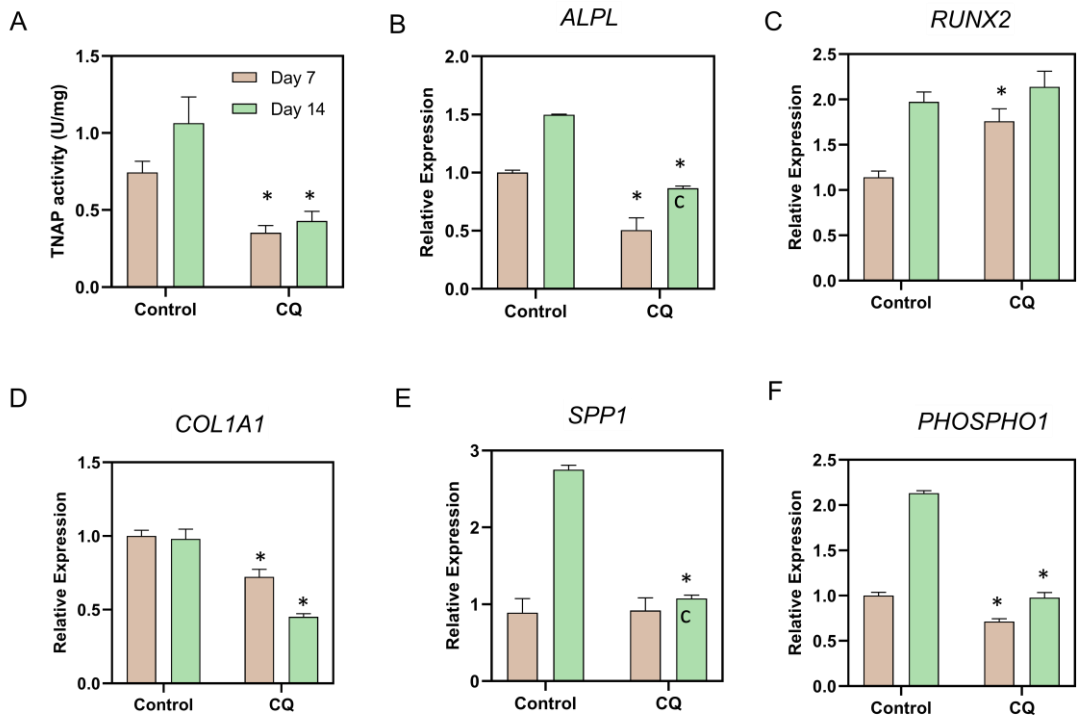

Figure 4.6 | CQ treatment affect the expression of osteogenesis-related genes. A) TNAP activity measured for osteoblasts after 7 and 14 days of culture in osteogenic medium in absence (control) and in the presence of 10 μM CQ. Results represent the mean ± SD for triplicate determination. **(B-F)** Expression of the osteogenesis-related genes for osteoblasts after 7 and 14 days in osteogenic medium (control) or in presence of CQ (10 μM). Gene expression is relative to the housekeeping gene *GAPDH* and data are presented as mean ± standard deviation (n=3), and asterisks (*) indicate statistically significant differences ($p \leq 0.05$).

Finally, ultrastructural analysis of thin sections of the cell monolayers by TEM revealed the presence of cells at a high metabolic state for osteoblasts cultured for 14 days in the osteogenic medium, as evidenced by the presence of a mitochondrial network and abundant endoplasmic reticulum and the formation of an extracellular matrix where collagen fibrils could be easily discerned (Figure 4.7a). At the periphery of the cells, it was discernible the presence of some outward budding vesicles (Figure 4.7b). Intimately associated to the collagen fibrils, we also identified some 100-nm diameter vesicular structures with mineral crystals associated to their surface (Figure 4.7c). Within the extracellular matrix, we also identified the presence of vesicular structures, as shown in representative images in Figure 4.7d-e. As shown, in Figure 4.7f, osteoblasts treated with CQ for 14 days also produced a dense collagenous extracellular matrix. The presence the collagen fibrils can be discerned by their typical banding pattern [67–70]. Interestingly, we identified the presence of vesicular structures embedded within the extracellular matrix (Figure 4.7g). These observations highlight that both control and CQ-treated cells released vesicles able to bind to extracellular components.

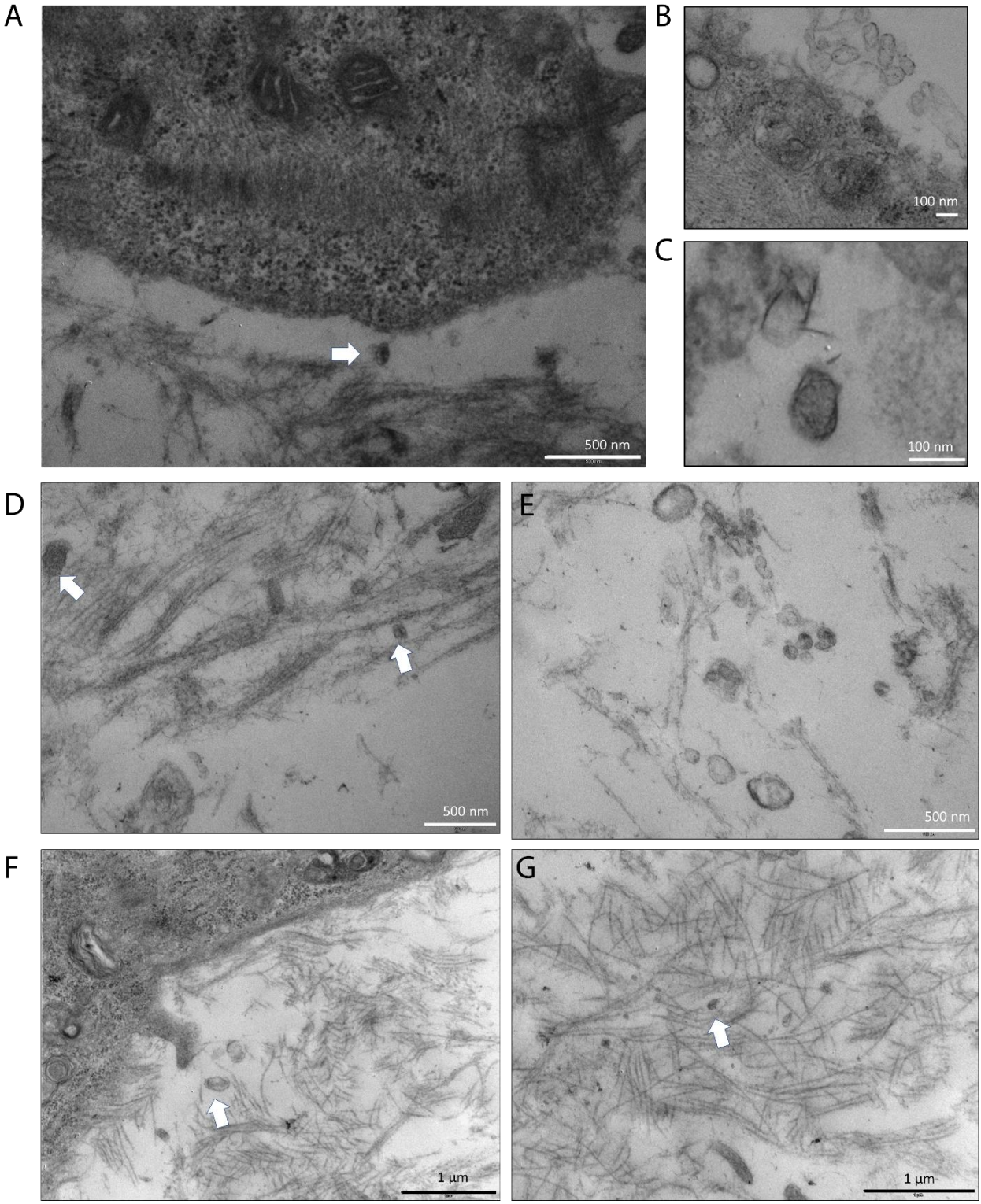

Figure 4.7 | TEM images of osteoblasts and their ECM. Control osteoblasts were cultured in osteogenic medium for 14 days in absence **(A-E)** and in the presence of 10 µM CQ **(F-G)**.

4.5.3 | Impairment of autophagy affect the biophysical and functional properties of MVs

Although the effect of autophagy impairment on osteoblasts mineralization has been described, its association with the release of matrix vesicles (MVs) has not been explored. Based on this, we investigated the effect of treatment with CQ on the release and function of these vesicles. For this, we started our investigation by quantifying the number of MVs isolated from osteoblasts cultures in osteogenic medium for 14 days in the presence of 10 µM CQ. As observed on Figure 4.8a, nanoparticle tracking analysis (NTA) revealed no significant differences in the global number of MVs isolated from control and CQ-treated cells. Additionally, TEM images of fixed and stained MVs confirmed the presence of cup-shaped vesicles with size and morphology consistent with small EVs (Figure 4.8b). To further access the biophysical properties of MVs, we examined vesicles dropped onto mica and imaged by means of atomic force microscopy (AFM), followed by qualitative evaluations of their composition by AFM phase analysis. The left panels of Figure 4.8c show AFM height images of MVs, which confirmed the spherical shape of the isolated vesicles in both the control and CQ-treated groups. Interestingly, the evaluation of phase images for the MVs revealed differences between the groups. Specifically, MVs isolated from CQ-treated osteoblasts exhibited phase angles that were almost homogeneously distributed across the vesicle's cross-section, unlike those isolated from control osteoblasts. Changes in biophysical properties detected by AFM phase analysis of MVs have been extensively studied. Mineralization-competent MVs, for instance, exhibit spots with high variation in phase angles, which arises from the presence of highly viscoelastic content. Although the nature of this content remains unclear, it is a common feature of mineralization-competent MVs[71–73]. Thus, our observations suggest that MVs isolated from control and CQ-treated osteoblasts may have different contents that could affect their ability to control the mineralization of extracellular matrix.

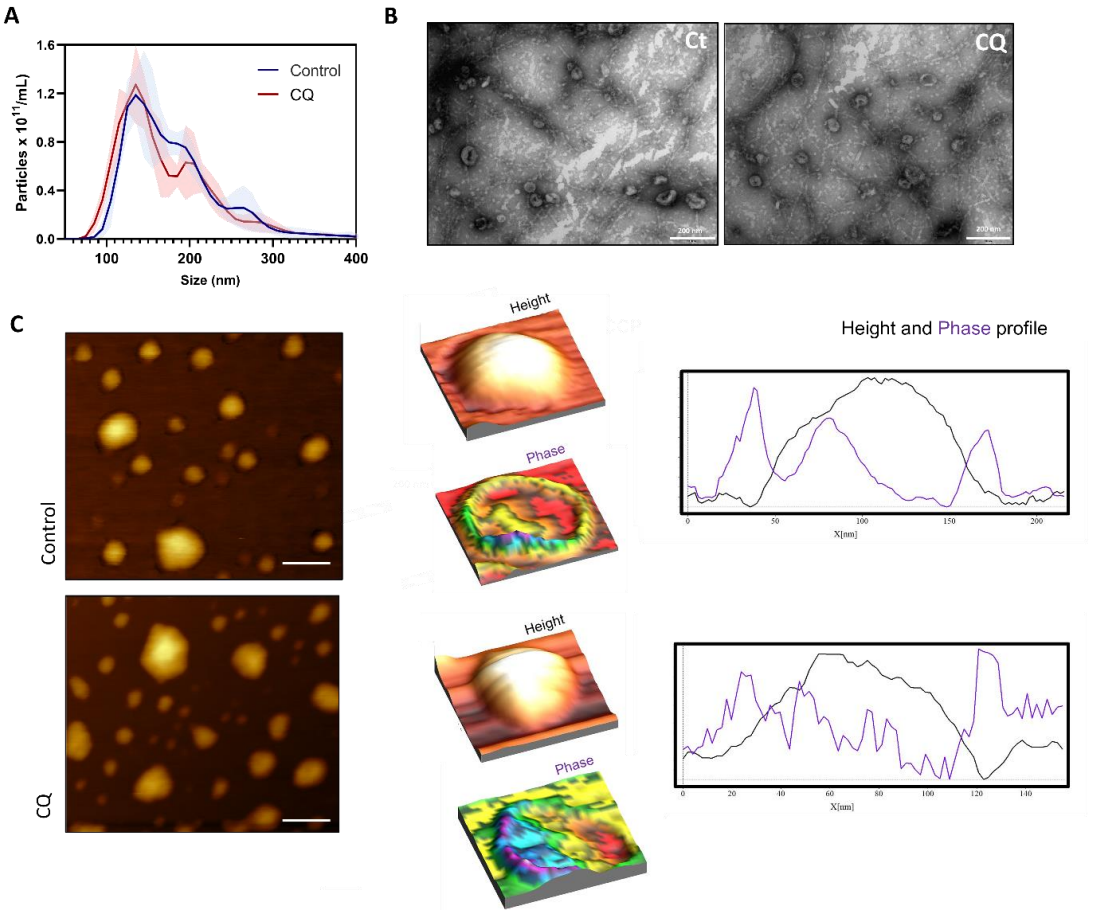

Figure 4.8 | Effect of autophagy impairment in the amount, size, and morphology of MVs released by osteoblasts. A) Size and concentration distribution of isolated MVs measured by NTA (N=3). For MVs isolation, osteoblasts were cultured in osteogenic medium (Control) or treated with CQ (10 µM) for 14 days. **B)** Representative TEM images of MVs isolated from control and CQ-treated samples. **C)** Representative AFM images (height and phase representations) of MVs isolated from control and CQ-treated groups. Scale bar on left panel, 100 nm. Right panel shows the height (black) and phase (purple) cross-sectional profile of a respective MVs imaged by AFM.

We also evaluated the functionality of MVs by measuring two major markers of their function: intrinsic alkaline phosphatase (TNAP) activity and ability to mediate mineralization. As shown in the Figure 4.9a, MVs isolated from CQ-treated cells show decreased TNAP activity compared to the control. The remarkable reduction in the TNAP activity of MVs isolated from CQ-treated osteoblasts demonstrate their lower propensity to control extracellular mineralization, since TNAP enrichment on MVs has a major function in the extracellular control of Pi/PPi ratio required for mineral propagation[74]. To further verify MVs functionality, their ability to mediate mineralization was assessed (Figure 4.9b). Incubation of MVs isolated from control cells led to an increase in the turbidity of the solution within 2 h, that is associated to the formation of mineral triggered

by the presence of the vesicles. However, for CQ-treated MVs the propagation of mineralization was delayed. Lower mineralization ability was confirmed by infrared absorption spectroscopy (FTIR), that allows the identification of chemical groups present in the samples. After 24 h of incubation, FTIR spectrum of MVs revealed differences related to the composition of mineral (Figure 4.9c). The splitting of the band related to the P-O stretching (1200-950 cm^{-1}) affords for the precipitation of less matured and less crystalline minerals, in the presence of MVs isolated from cells treated with CQl [75].

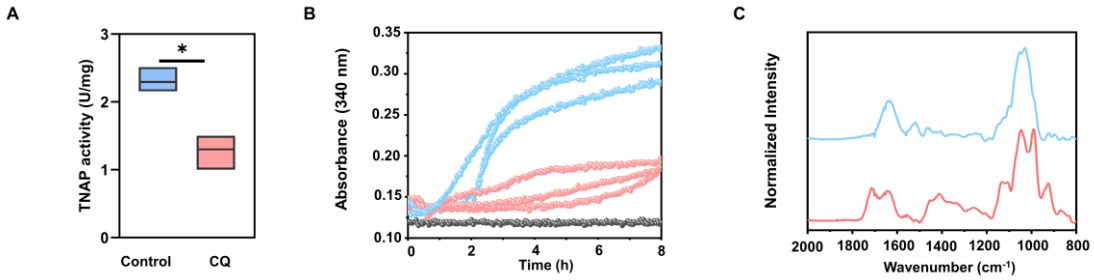

Figure 4.9 | Effect of CQ-treatment on the mineralization ability of osteoblast cultures. A) TNAP activity measured for MVs isolated from control and CQ-treated cells after 14 days (*p < 0.05). **B)** Mineralization curve for MVs isolated from control (blue) and CQ-treated (red) osteoblasts. **C)** FTIR spectrum of mineral collected after 24 h of incubation of MVs in the mineralization medium. Blue for MVs isolated from control osteoblasts and red for MVs isolated from CQ-treated osteoblasts.

4.5.4 | Comparative proteomics reveals difference in the proteome of MVs

To investigate the effect of CQ treatment on the content of MVs at a proteome level, we employed label-free comparative proteomics to identify and quantify proteins present in MVs. We identified and quantified 153 proteins that were differentially expressed among control and CQ-treated groups by using proteomic analysis. Hierarchical clustering analysis using all differentially abundant proteins revealed a clear separation of the identified proteins into the two groups, suggesting that most variance in the data was related to different treatments of the cells (Figure 4.10a). Principal component analysis (PCA) also evidences different protein profiles, able to be discriminated CQ treated and non-treat samples (Figure 4.10b). Several proteins identified were already described in previous proteomic studies of MVs [76–78], such as proteins present ate the extracellular matrix (collagen VI), cytoskeletal components and their regulatory proteins (actin gamma 1, actin alpha 2, myristoylated alanine rich protein kinase C substrate, myosin), and signaling proteins (SMAD-bind domain-containing protein, transforming growth factor beta induced, Ig-like domain-containing protein).

Actin dynamics are essential for MVs biogenesis[38], and SMAD-bind domain-containing protein was enriched in CQ-treated MVs. The BMP-SMAD signaling pathway is pivotal during osteogenic differentiation and has already been demonstrated to be affected by autophagy[35]. Most interestingly, we identified alterations in the abundance of the core proteins in mineralization-competent MVs, including the enzyme TNAP and the annexins (Figure 4.10c). CQ-treated MVs exhibited a lower normalized abundance of TNAP, in agreement with the enzymatic activity measured for this protein. Annexins are the most abundant class of protein found in MVs[79].We identified and quantified the abundance of four members of the annexin family (AnxA1, AnxA2, AnxA5, AnxA6). Interestingly, the abundance of annexins was significantly decreased for the CQ-treated MVs. AnxA1 has been described as a putative marker of extracellular vesicles derived from plasma membrane[80,81], and AnxA5 and AnxA6 have been described to actively contribute to the mineralization ability of MVs due to their intrinsic Ca^{2+}-binding properties[37]. Therefore, the lower abundance of annexins in MVs isolated from CQ-treated cells might indicate a reduced ability of the vesicles produced under impaired autophagy to mineralize.

We also identified that proteins involved in vesicular trafficking were present in different amount comparing the control and CQ-treated samples, including transmembrane p24 trafficking protein 10, trafficking kinesin protein 1, secretion-associated Ras-related GTPase 1A, receptor for activated C kinase 1, myotubularin related protein 9 like pseudogene, lectin, kinase suppressor of ras 1, Rho guanine nucleotide exchange factor 26, and G protein subunit alpha transducin 2. The differences in the expression of proteins involved in vesicular trafficking may provide evidence that autophagy might be involved in the apical targeting of lipids and proteins from the trans-Golgi network and the endosomal compartments to MV membrane. Autophagy has been shown to be associated with the trafficking of proteins to the plasma membrane[40].

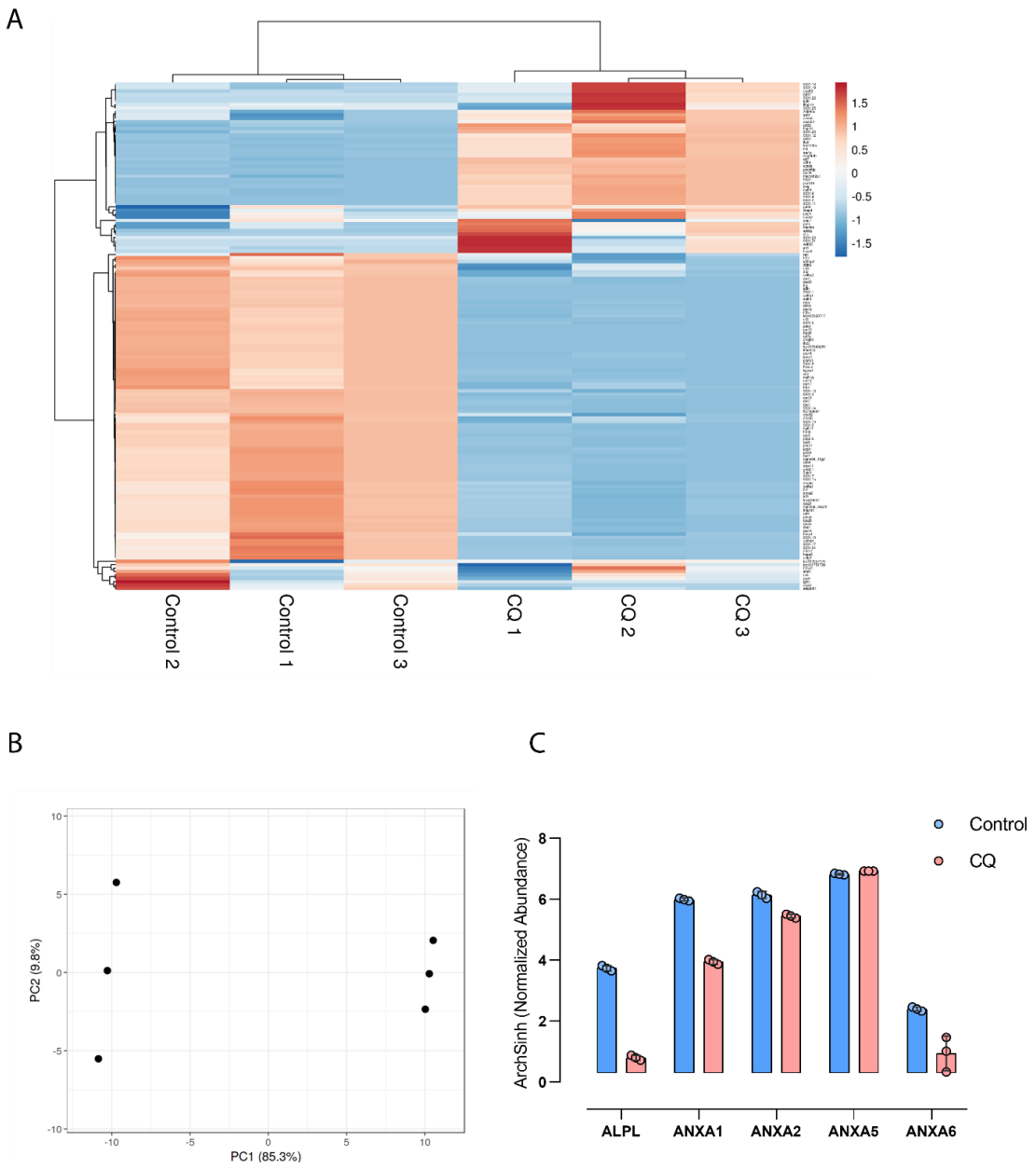

Figure 4.10 | Proteomic analysis of MVs isolated from osteoblasts cultivated in osteogenic medium in the presence and absence of 10 µM CQ. A) Heatmap of hierarchical clustering grouping differentially regulated proteins from MVs isolated from control cells, and cells treated with CQ. Rows were centered; unit variance scaling was applied to rows. Both rows and columns were clustered using correlation distance and average linkage. **B)** Principal component analysis (PCA) of proteins abundance measured for MVs isolated from control and CQ-treated cells. X and Y axis show principal component 1 and principal component 2 that explain 85.3% and 9.8% of the total variance, respectively. For Heatmap and PCA analysis, we applied the default parameters from ClustVis software[82]. **C)** Normalized abundance of major proteins of mineralization-competent MVs quantified for MVs isolated from control and CQ-treated cells.

4.6 | Discussion

Although it is well-established that impaired autophagy reduces the ability of osteoblasts to mineralize their ECM, the precise mechanisms involved in this process

remain unclear. The hypothesis explored in this chapter is that impaired autophagy might change the mineralization ability of MVs, an explored topic in the literature. Our study sheds light on this issue by demonstrating that autophagy impairment affects both the content and function of MVs, thereby suggesting a promising avenue for further investigation.

The treatment of osteoblasts with CQ resulted in a reduction of both their ability to mineralize, as evidenced by down-regulation of mineralization-related genes and the production of mineralized nodules by the cells as suggested by alizarin red staining. Since MVs mediate the mineralization of the extracellular matrix, it would be reasonable to hypothesize a significant reduction in the amount of MVs secreted upon CQ-treatment if autophagy was related to the biogenesis of these vesicles. However, examination of the extracellular matrix produced by osteoblasts by TEM revealed the presence of MVs bound to collagen fibrils in both control and CQ-treated cells. NTA analysis showed no change in the number of vesicles following treatment, thus corroborating the TEM analysis. However, MVs isolated from CQ-treated cells exhibited different content and functionality. Notably, we observed a decrease in TNAP activity in isolated MVs after CQ-treatment. Proteomic analysis confirmed the decrease in TNAP levels in MVs isolated after CQ-treatment, along with a reduction in the expression of annexins, Ca^{2+}-binding proteins that dominates the proteome of mineralization-competent MVs.

Although EVs resident within the extracellular matrix have been traditionally thought to be a unique feature MVs in bone, recent studies have shown that they are also present in other non-mineralizing tissues. This assigns other function to the vesicles as matrix degradation and cross-linking of matrix proteins[83,84]. Interestingly, MVs were demonstrated to be already present in the extracellular matrix of cartilage even before mineralization, but increased TNAP activity of the vesicles is found as they approach the calcification front[85]. This observation suggests that along the events that lead to the mineralization of cartilage, MVs acquire a mineralization-competent phenotype. Further confirmation of this finding was obtained *in vitro*, as demonstrated by ultrastructural analysis, which revealed that both non-mineralizing control chondrocytes and chondrocytes treated with osteogenic factors produced and released microvesicles). However, the MVs released by mineralizing chondrocytes exhibited significantly stronger tissue-nonspecific alkaline phosphatase (TNAP) activity and expressed annexins, unlike the control vesicles[86]. Interesting, it has been demonstrated that along the

differentiation of chondrocytes towards a mineralizing phenotype, these cells demonstrate increase autophagy[87,88].

Unfortunately, identifying unique markers for mineralization-competent MVs remains a challenge, making it difficult to distinguish different vesicle's populations. This suggests that MVs may comprise a mixture of vesicles with different functionalities and subcellular origins. However, as soon as cells acquire a mineralizing phenotype, their vesicle content is finely tuned to express mineralization-related proteins. Our initial results suggest that autophagy impairment reduces the release of MVs containing mineralization-related molecules, indicating that autophagy plays a direct role in controlling the production of mineralization-competent MVs. However, the exact mechanism by which autophagy mediates this process remains unclear and warrants further investigation. The methods employed in our study do not allow to draw mechanistic conclusions, since we descried the content and function of a pool of MVs at a certain timepoint. To gain a better understanding of how autophagy affects the biogenesis of mineralization-competent MVs, it will be necessary to conduct further studies using molecular tools. For instance, knocking down key proteins involved in both autophagy and MVs biogenesis pathways could help elucidate the specific mechanisms involved. By carrying this out, researchers could determine whether autophagy has a direct constitutive effect on MV biogenesis or if it acts in an inducible way by altering the cell state upon the trigging the release of mineralization-competent MVs. Such experiments will be crucial to fully comprehend the role of autophagy in the production of mineralization-competent MVs, which in turn are essential for proper mineralization of the extracellular matrix.

An interesting point that adds another level of complexity to the discussion is the observation that in vascular smooth muscle cells (VSMCs), the major cells in the arterial wall, autophagy impairment has an opposite effect, exacerbating the mineralization and the release of mineralization-competent MVs[89,90]. During vascular calcification, a pathological condition that results in the hardening of arteries, vascular cells subjected to conditions of stress, such as the one imposed by high levels of circulating mineral ions, shift to a mineralizing phenotype and trigger the mineralization of their extracellular matrix, in a process that resembles the events observed in physiological bone mineralization, including the release of mineralizing MVs[91]. Dai et al. described the potential role for autophagy in vascular calcification by showing that VSMCs treated with high phosphate levels in vitro upregulate autophagic markers such as LC3 and exhibit

autophagosomes within their cytoplasm[89]. However, in contrast to what is commonly observed in osteoblasts, inhibition of autophagy in the presence of phosphate exacerbated VSMC calcification augmented the release of mineralization-competent vesicles. It is now accepted that induction of autophagy is actually an adaptive response in the context of pathological calcification[92]. These observations highlight the complexity between MVs and autophagy, and further detailed studies are necessary to fully comprehend this mechanism. Nevertheless, our study brings forth two important concepts: firstly, the secretion of mineralization-competent MVs is crucial for proper mineralization of the extracellular matrix during bone formation, and secondly, the regulation of autophagy is intertwined with the pathways that control this process.

4.7 | Conclusions

Overall, our study sheds new light on the mechanisms by which impaired autophagy reduces the ability of osteoblasts to mineralize, by showing that it affects the function of mineralization-competent MVs. This indicate that the release of mineralization-competent MVs is context specific and required for proper mineralization of the ECM. Although these findings are promising and suggest a new avenue for research on matrix vesicle's biogenesis, further detailed and meticulous studies on molecular biology are necessary to fully comprehend the underlying mechanisms.

4.8 | References

1. Rehman, N. U. *et al.* Conserved and Diversified Mechanism of Autophagy between Plants and Animals upon Various Stresses. *Antioxidants* **10**, 1736–1759 (2021).

2. de Duve, C. & Wattiaux, R. Functions of Lysosomes. *Annual Review of Physiology* **28**, 435–492 (1966).

3. Aman, Y. *et al.* Autophagy in healthy aging and disease. *Nature Aging* **1**, 634–650 (2021).

4. Dikic, I. & Elazar, Z. Mechanism and medical implications of mammalian autophagy. *Nature Reviews Molecular Cell Biology* **19**, 349–364 (2018).

5. Nakatogawa, H. Mechanisms governing autophagosome biogenesis. *Nature Reviews Molecular Cell Biology* **21**, 439–458 (2020).

6. Amaya, C., Fader, C. M. & Colombo, M. I. Autophagy and proteins involved in vesicular trafficking. *FEBS Letters* **589**, 3343–3353 (2015).

7. Kim, Y. C. & Guan, K. L. MTOR: A pharmacologic target for autophagy regulation. *Journal of Clinical Investigation* **125**, 25–32 (2015).

8. Narendra, D., Tanaka, A., Suen, D. & Youle, R. J. Parkin is recruited selectively to impaired mitochondria and promotes their autophagy. *Journal of Cell Biology* **183**, 795–803 (2008).

9. Narendra, D. P., Kane, L. A., Hauser, D. N., Fearnley, I. M. & Youle, R. J. p62/SQSTM1 is required for Parkin-induced mitochondrial clustering but not mitophagy; VDAC1 is dispensable for both. *Autophagy* **6**, 1090–1106 (2010).

10. Vargas, J. N. S., Hamasaki, M., Kawabata, T., Youle, R. J. & Yoshimori, T. The mechanisms and roles of selective autophagy in mammals. *Nature Reviews Molecular Cell Biology* **24**, 167–185 (2023).

11. Yim, W. W. Y. & Mizushima, N. Lysosome biology in autophagy. *Cell Discovery* **6**, 6–18 (2020).

12. Feng, Y., He, D., Yao, Z. & Klionsky, D. J. The machinery of macroautophagy. *Cell Research* **24**, 24–41 (2014).

13. Suchacki, K. J. *et al*. Skeletal energy homeostasis: a paradigm of endocrine discovery. *Journal of Endocrinology* **234**, R67–R79 (2017).

14. Al-Bari, A. A. & Al Mamun, A. Current advances in regulation of bone homeostasis. *FASEB Bioadv* **2**, 668–679 (2020).

15. Staines, K. A., MacRae, V. E. & Farquharson, C. The importance of the SIBLING family of proteins on skeletal mineralisation and bone remodelling. *Journal of Endocrinology* **214**, 241–255 (2012).

16. Prideaux, M., Findlay, D. M. & Atkins, G. J. Osteocytes: The master cells in bone remodelling. *Curr Opin Pharmacol* **28**, 24–30 (2016).

17. Wang, S. *et al*. The role of autophagy and mitophagy in bone metabolic disorders. *International Journal of Biological Sciences* **16**, 2675–2691 (2020).

18. Zhang, L. *et al*. Pathway-based genome-wide association analysis identified the importance of regulation-of-autophagy pathway for ultradistal radius BMD. *Journal of Bone and Mineral Research* **25**, 1572–1580 (2010).

19. Yin, X. *et al*. Autophagy in bone homeostasis and the onset of osteoporosis. *Bone Res* **7**, 28–44 (2019).

20. Zhu, C. *et al*. Autophagy in Bone Remodeling: A Regulator of Oxidative Stress. *Front Endocrinol (Lausanne)* **13**, 1376–1386 (2022).

21. Li, H. *et al*. Defective autophagy in osteoblasts induces endoplasmic reticulum stress and causes remarkable bone loss. *Autophagy* **14**, 1726–1741 (2018).

22. Li, D. Y. *et al*. Autophagy attenuates the oxidative stress-induced apoptosis of Mc3T3-E1 osteoblasts. *European Review for Medical and Pharmacological Sciences* **21**, 5548–5556 (2021).

23. Xi, G., Rosen, C. J. & Clemmons, D. R. IGF-I and IGFBP-2 stimulate AMPK activation and autophagy, which are required for osteoblast differentiation. *Endocrinology* **157**, 268–281 (2016).

24. Yang, J., Ueharu, H. & Mishina, Y. Energy metabolism: A newly emerging target of BMP signaling in bone homeostasis. *Bone* **138**, 115467–115484 (2020).

25. Chen, J. & Long, F. MTOR signaling in skeletal development and disease. *Bone Research* **6**, 1–6 (2018).

26. Liu, F. *et al*. Suppression of autophagy by FIP200 deletion leads to osteopenia in mice through the inhibition of osteoblast terminal differentiation. *Journal of Bone and Mineral Research* **28**, 2414–2430 (2013).

27. Iwayama, T. *et al*. Osteoblastic lysosome plays a central role in mineralization. *Science Advances* **10**, 1–10 (2019).

28. Nollet, M. *et al*. Autophagy in osteoblasts is involved in mineralization and bone homeostasis. *Autophagy* **10**, 1965–1977 (2014).

29. Vrahnas, C. *et al*. Increased autophagy in EphrinB2-deficient osteocytes is associated with elevated secondary mineralization and brittle bone. *Nature Communications* **10**, 3436–3452 (2019).

30. Lehninger, A. L. Mitochondria and calcium ion transport. *The Biochemical journal* **119**, 129–138 (1970).

31. Kahil, K., Weiner, S., Addadi, L. & Gal, A. Ion Pathways in Biomineralization: Perspectives on Uptake, Transport, and Deposition of Calcium, Carbonate, and Phosphate. *Journal of the American Chemical Society* **143**, 21100–21112 (2021).

32. Boonrungsiman, S. *et al*. The role of intracellular calcium phosphate in osteoblast-mediated bone apatite formation. *Proceedings of the National Academy of Sciences* **109**, 14170–14175 (2012).

33. Tang, C. *et al*. Biomineral Precursor Formation Is Initiated by Transporting Calcium and Phosphorus Clusters from the Endoplasmic Reticulum to Mitochondria. *Advanced Science* **7**, 1902536–1902545 (2020).

34. Rohde, M. & Mayer, H. Exocytotic process as a novel model for mineralization by osteoblasts in vitro and in vivo determined by electron microscopic analysis. *Calcified Tissue International* **80**, 323–336 (2007).

35. Pei, D. dan *et al*. Contribution of Mitophagy to Cell-Mediated Mineralization: Revisiting a 50-Year-Old Conundrum. *Advanced Science* **5**, 1800873–1800885 (2018).

36. Shapiro, I. M., Landis, W. J. & Risbud, M. V. Matrix vesicles: Are they anchored exosomes? *Bone* **79**, 29–36 (2015).

37. Wuthier, R. E. Matrix vesicles: structure, composition, formation and function in calcification. *Frontiers in Bioscience* **16**, 2812–2902 (2011).

38. Hale, J. E. & Wuthier, R. E. The mechanism of matrix vesicle formation. Studies on the composition of chondrocyte microvilli and on the effects of microfilament-perturbing agents on cellular vesiculation. *Journal of Biological Chemistry* **262**, 1916–1925 (1987).

39. Van Niel, G., D'Angelo, G. & Raposo, G. Shedding light on the cell biology of extracellular vesicles. *Nature Reviews Molecular Cell Biology* **19**, 213–228 (2018).

40. Ponpuak, M. *et al*. Secretory autophagy. *Current Opinion in Cell Biology* **35**, 106–116 (2015).

41. Leidal, A. M. *et al*. The LC3-conjugation machinery specifies the loading of RNA-binding proteins into extracellular vesicles. *Nature Cell Biology* **22**, 187–199 (2020).

42. Miranda, A. M. *et al*. Neuronal lysosomal dysfunction releases exosomes harboring APP C-terminal fragments and unique lipid signatures. *Nature Communications* **9**, 291–307 (2018).

43. Hessvik, N. P. *et al*. PIKfyve inhibition increases exosome release and induces secretory autophagy. *Cellular and Molecular Life Sciences* **73**, 4717–4737 (2016).

44. Solvik, T. A. *et al*. Secretory autophagy maintains proteostasis upon lysosome inhibition. *Journal of Cell Biology* **221**, e202110151–e202110175 (2022).

45. Xu, J. *et al*. Chloroquine treatment induces secretion of autophagy-related proteins and inclusion of Atg8-family proteins in distinct extracellular vesicle populations. *Autophagy* **18**, 2547–2560 (2022).

46. Leidal, A. M. & Debnath, J. Emerging roles for the autophagy machinery in extracellular vesicle biogenesis and secretion. *FASEB BioAdvances* **3**, 377–386 (2021).

47. Klionsky, D. J. *et al.* Guidelines for the use and interpretation of assays for monitoring autophagy. *Autophagy* **17**,1–382 (2021).

48. Gerstenfeld, L. C., Chipman, S. D., Glowacki, J. & Lian, J. B. Expression of differentiated function by mineralizing cultures of chicken osteoblasts. *Developmental Biology* **122**, 49–60 (1987).

49. Mosmann, T. Rapid colorimetric assay for cellular growth and survival: application to proliferation and cytotoxicity assays. *Journal of immunological methods* **65**, 55–63 (1983).

50. Sigma-Aldrich. Annexin V-FITC Apoptosis Detection Kit (Cat. No. APOAFA). *Product Information*.

51. Buchet, R., Pikula, S., Magne, D. & Mebarek, S. Isolation and Characteristics of Matrix Vesicles. *Phosphatase Modulators* **1**, 115–124 (2013).

52. Bolean, M. *et al.* Topographic analysis by atomic force microscopy of proteoliposomes matrix vesicle mimetics harboring TNAP and AnxA5. *Biochimica et Biophysica Acta (BBA) - Biomembranes* **1859**, 1911–1920 (2017).

53. Horcas, I. *et al.* WSXM: A software for scanning probe microscopy and a tool for nanotechnology. *Review of Scientific Instruments* **78**, 013705–013714 (2007).

54. Hartree, E. F. Determination of protein: a modification of the Lowry method that gives a linear photometric response. *Analytical biochemistry* **48**, 422–427 (1972).

55. Xu, J. *et al.* Chloroquine treatment induces secretion of autophagy-related proteins and inclusion of Atg8-family proteins in distinct extracellular vesicle populations. *Autophagy* **18**, 2547–2560 (2022).

56. Peña-Ramos, O. *et al.* Autophagosomes fuse to phagosomes and facilitate the degradation of apoptotic cells in Caenorhabditis elegans. *Elife* **11**, e72466–e72503 (2022).

57. Lőrincz, P. & Juhász, G. Autophagosome-Lysosome Fusion. *J Mol Biol* **432**, 2462–2482 (2020).

58. Yim, W. W.-Y. & Mizushima, N. Lysosome biology in autophagy. *Cell Discov* **6**, 6–18 (2020).

59. Mauthe, M. *et al.* Chloroquine inhibits autophagic flux by decreasing autophagosome-lysosome fusion. *Autophagy* **14**, 1435–1455 (2018).

60. Both, T. *et al.* Hydroxychloroquine decreases human MSC-derived osteoblast differentiation and mineralization in vitro. *Journal of Cellular and Molecular Medicine* **22**, 873–882 (2017).

61. Komori, T. Requisite roles of Runx2 and Cbfb in skeletal development. *Journal of Bone and Mineral Metabolism* **21**, 193–197 (2003).

62. França, C. M. *et al.* The influence of osteopontin-guided collagen intrafibrillar mineralization on pericyte differentiation and vascularization of engineered bone scaffolds. *J Biomed Mater Res B Appl Biomater* **107**, 1522–1532 (2019).

63. Icer, M. A. & Gezmen-Karadag, M. The multiple functions and mechanisms of osteopontin. *Clin Biochem* **59**, 17–24 (2018).

64. Addison, W. N., Azari, F., Sørensen, E. S., Kaartinen, M. T. & McKee, M. D. Pyrophosphate Inhibits Mineralization of Osteoblast Cultures by Binding to Mineral, Up-regulating Osteopontin, and Inhibiting Alkaline Phosphatase Activity. *Journal of Biological Chemistry* **282**, 15872–15883 (2007).

65. Foster, B. L. *et al.* Osteopontin regulates dentin and alveolar bone development and mineralization. *Bone* **107**, 196–207 (2018).

66. Dillon, S., Staines, K. A., Millán, J. L. & Farquharson, C. How To Build a Bone: PHOSPHO1, Biomineralization, and Beyond. *JBMR Plus* **3**, e10202–e10214 (2019).

67. de Wildt, B. W. M. *et al.* From bone regeneration to three-dimensional in vitro models: tissue engineering of organized bone extracellular matrix. *Curr Opin Biomed Eng* **10**, 107–115 (2019).

68. Nudelman, F., Lausch, A. J., Sommerdijk, N. A. J. M. & Sone, E. D. In vitro models of collagen biomineralization. *J Struct Biol* **183**, 258–269 (2013).

69. Nudelman, F. *et al.* The role of collagen in bone apatite formation in the presence of hydroxyapatite nucleation inhibitors. *Nat Mater* **9**, 1004–1009 (2010).

70. Habraken, W. J. E. M. *et al.* Ion-association complexes unite classical and non-classical theories for the biomimetic nucleation of calcium phosphate. *Nat Commun* **4**, 1507–1519 (2013).

71. Yadav, M. C. *et al.* Skeletal Mineralization Deficits and Impaired Biogenesis and Function of Chondrocyte-Derived Matrix Vesicles in Phospho1-/- and Phospho1/Pit1 Double-Knockout Mice. *Journal of Bone and Mineral Research* **31**, 1275–1286 (2016).

72. Chaudhary, S. C. *et al.* Phosphate induces formation of matrix vesicles during odontoblast-initiated mineralization in vitro. *Matrix Biology* **52–54**, 284–300 (2016).

73. Plaut, J. S. *et al*. Quantitative atomic force microscopy provides new insight into matrix vesicle mineralization. *Archives of Biochemistry and Biophysics* **667**, 14–21 (2019).

74. Millán, J. L. The role of phosphatases in the initiation of skeletal mineralization. *Calcified Tissue International* **93**, 299–306 (2013).

75. Sauer, G. R. & Wuthier, R. E. Fourier transform infrared characterization of mineral phases formed during induction of mineralization by collagenase-released matrix vesicles in vitro. *Journal of Biological Chemistry* **263**, 13718–13724 (1988).

76. Balcerzak, M. *et al*. Proteome analysis of matrix vesicles isolated from femurs of chicken embryo. *Proteomics* **8**, 192–205 (2008).

77. Thouverey, C. *et al*. Proteomic characterization of biogenesis and functions of matrix vesicles released from mineralizing human osteoblast-like cells. *Journal of Proteomics* **74**, 1123–1134 (2011).

78. Xiao, Z., Blonder, J., Zhou, M. & Veenstra, T. D. Proteomic analysis of extracellular matrix and vesicles. *Journal of Proteomics* **72**, 34–45 (2009).

79. Genge, B. R., Wu, L. N. Y. & Wuthier, R. E. Identification of phospholipid-dependent calcium-binding proteins as constituents of matrix vesicles. *Journal of Biological Chemistry* **264**, 10917–10921 (1989).

80. Jeppesen, D. K. *et al*. Reassessment of Exosome Composition. *Cell* **177**, 428-445 (2019).

81. Rogers, M. A. *et al*. Annexin A1-dependent tethering promotes extracellular vesicle aggregation revealed with single-extracellular vesicle analysis. *Science Advances* **6**, eabb1244–eabb1259 (2020).

82. Metsalu, T. & Vilo, J. ClustVis: A web tool for visualizing clustering of multivariate data using Principal Component Analysis and heatmap. *Nucleic Acids Research* **43**, W566–W570 (2015).

83. Lewin, S., Hunt, S. & Lambert, D. W. Extracellular vesicles and the extracellular matrix: A new paradigm or old news? *Biochemical Society Transactions* **48**, 2335–2345 (2020).

84. Rilla, K. *et al*. Extracellular vesicles are integral and functional components of the extracellular matrix. *Matrix Biology* **75–76**, 201–219 (2019).

85. Matsuzawa, T. & Anderson, H. C. Phosphatases of epiphyseal cartilage studied by electron microscopic cytochemical methods. *Journal of Histochemistry & Cytochemistry* **19**, 801–808 (1971).

86. Kirsch, T., Nah, H. D., Shapiro, I. M. & Pacifici, M. Regulated production of mineralization-competent matrix vesicles in hypertrophic chondrocytes. *Journal of Cell Biology* **137**, 1149–1160 (1997).

87. Srinivas, V., Bohensky, J. & Shapiro, I. M. Autophagy: A new phase in the maturation of growth plate chondrocytes is regulated by HIF, mTOR and AMP kinase. *Cells Tissues Organs* **189**, 88–92 (2008).

88. Shapiro, I. M., Layfield, R., Lotz, M., Settembre, C. & Whitehouse, C. Boning up on autophagy :The role of autophagy in skeletal biology. *Autophagy* **10**, 7–19 (2014).

89. Dai, X. Y. *et al.* Phosphate-induced autophagy counteracts vascular calcification by reducing matrix vesicle release. *Kidney International* **83**, 1042–1051 (2013).

90. Cai, Y., Wang, X. L., Flores, A. M., Lin, T. & Guzman, R. J. Inhibition of endo-lysosomal function exacerbates vascular calcification. *Scientific Reports* **8**, 1–11 (2018).

91. Durham, A. L., Speer, M. Y., Scatena, M., Giachelli, C. M. & Shanahan, C. M. Role of smooth muscle cells in vascular calcification: Implications in atherosclerosis and arterial stiffness. *Cardiovascular Research* **114**, 590–600 (2018).

92. Phadwal, K., Feng, D., Zhu, D. & MacRae, V. E. Autophagy as a novel therapeutic target in vascular calcification. *Pharmacology and Therapeutics* **206**, 107430–107439 (2020).

5

FINAL DISCUSSION

The hard extracellular matrix of bone is an impressive material made up of organized collagen fibrils and carbonated hydroxyapatite crystals. Despite not fully understanding how it forms, the presence of MVs in areas where mineralization begins suggests they play a critical role in the process. However, there is still debate surrounding how MVs function. Understanding these mechanisms will have a significant impact on biomineralization research and potentially lead to better biomaterials for bone replacement or treatments for diseases involving dysregulated mineralization, such as inherited hypophosphatasia, osteoarthritis, and vascular calcification. The observations presented in this thesis confirm the importance of MVs in initiating mineralization and provide new insights into the underlying mechanisms.

In Chapter 2, we utilized cryoTEM to observe mineralization induced by isolated MVs. The ability to combine bulk observation of functionality with imaging at a single-vesicle level brought significant resolution to the factors that drive MVs mineralization. Our results successfully reproduced classical concepts in the literature at the bulk level of turbidimetric measurements, such as the fractionation of isolated MVs into low and high dense contents by density-gradient ultracentrifugation yielding a low-dense TNAP-rich fraction that is unable to trigger direct nucleation from soluble Ca^{2+} and Pi ions. However, our unprecedented capability to visualize single vesicles in a close-to-native state challenges previous interpretations. We discovered that, contrary to the belief that fractionation would cause the loosening of luminal content responsible for mineral nucleation, fractionation actually removes non-vesicular contents (mostly ECM components) that are present in MV preparations co-sedimented during the isolation procedure. This showcases that achieving single-vesicle resolution will be imperative to comprehensively discover the underlying mechanisms involved in MV mineralization in future research.

In the literature, it is common to find descriptions of MVs as having a dual function: to provide enzymatic machinery for local control of Pi availability as well as to enable the transport of preformed mineral cargo to the ECM. However, in our cryoTEM observations, we could not identify evidence of preformed mineral associated with the lumen of bilayered vesicles, especially after density-fractionation where a fraction of vesicles with high alkaline phosphatase activity was enriched. This conclusion does not imply that cells cannot release mineral-filled vesicles, but rather suggests that mineral-filled vesicles may represent a different subtype within the spectrum of vesicles that can be secreted to the ECM, as we will discuss further. Consistent with this conclusion, we

also infer that mineral-filled vesicles, due to their higher density, would be rapidly pelleted at much lower ultracentrifugation forces than the 80,000 g commonly used to enrich small-sized MVs.

A promising approach that can be used to disentangle the participation of different components within MVs during mineralization is by creating biomimetic membrane models, where the composition is minimized and targeted to answer a specific question. This was demonstrated in Chapter 3, where we used Langmuir monolayers to show that the formation of phosphatidylserine-rich nanodomains, resulting in increased local supersaturation to trigger mineral nucleation, recreates the ability of membrane components of MVs to control mineralization. In fact, our group is already using Langmuir monolayers to explore the mode of action of MVs at the enzymatic level, such as the effect of lipid composition on the activity of alkaline phosphatase[1]. As Langmuir monolayers are highly versatile and allow for the combination of a multitude of *in-situ* compositional and structural techniques, this biomimetic model can be further exploited, for example, to understand the interrelation between different MVs components as well as their interaction with extravesicular components. Moreover, as developed for the first time in this thesis, we can also recreate monolayers with lipids extracted from native MVs, extending the possibilities for future research.

Chapter 4 emphasized the crucial role of MVs in ECM mineralization and prompted further investigation into the molecular pathways that give rise to them. When osteoblasts were treated with chloroquine to impair autophagy, MVs were found to be dysfunctional, with significantly reduced alkaline phosphatase activity. Although the involvement of autophagy in cell mineralization is not fully understood, some researchers have suggested that the autophagic machinery can be utilized to transport intracellular mineral precursors to the ECM[2,3], but the origin of these intracellular mineral precursors and the form in which they are released remain poorly defined. The most immediate hypothesis would be that autophagy affect the loading of mineral precursors into MVs to be delivered to the ECM. However, our observations in Chapter 2 suggest that alkaline phosphatase-enriched vesicles do not coexist with preformed mineral. The biogenesis of MVs are still poorly understood, but various reports suggest that they are released by cells in a context-specific manner. For instance, osteoblasts exposed to osteogenic stimuli (e.g., an added phosphate source) trigger the release of mineralization-competent MVs[4]. Given our findings of a significant effect of autophagy impairment on the secretion of mineralization-related proteins within MVs, a comprehensive molecular-level

investigation is required to determine whether autophagy is impacting the release of mineralization-competent MVs either by blocking a specific biogenesis pathway or by altering the cell context in which their release is triggered. Such research could result in the identification of a molecular pathway/marker for the release of mineralization-competent MVs, which could open up new avenues for treating mineralization-related disorders.

The topic of MV heterogeneity deserves further exploration at this point. Although MVs have traditionally been defined as a "class of extracellular vesicles originated from the plasma membrane of mineralizing cells with a unique ability to bind to collagen fibrils," it is now widely recognized that vesicles are an integral component of the ECM, not only in mineralizing tissues but also in a variety of other tissues, and they are implicated in a variety of functions within the ECM[5–7]. Moreover, several markers of vesicles originated from the endosomal pathway, not the plasma membrane, challenge the idea that MVs represent a single population of vesicles from the same origin[8]. As Chapter 2 made clear, when characterizing a pellet of MVs obtained after differential centrifugation, we are actually examining a pool of different vesicular and non-vesicular particles. This heterogeneity is now widely accepted in the field of extracellular vesicles and extends beyond the presence of non-vesicular particles to encompass different subtypes of vesicles based on biogenesis pathway and functionality[9,10]. For MVs, several reports have described functions other than mineralization, such as the transport of informational cargos such as bone morphogenetic proteins[11] and microRNAs[12]. These observations collectively challenge current assumptions about MVs and highlight the need for future research to address the heterogeneity of vesicles present within the ECM, taking into account the function and biogenesis origin of different subtypes. It will be crucial to determine whether MVs, as a mineralization-competent entity, represent a distinct subtype with a specific cargo and biogenesis pathway.

As the challenge of dealing with heterogeneity is not unique to MVs but shared with the extracellular vesicle community in general, an evolving toolbox is continuously being developed to study these structures with higher purity and specificity. To advance MVs research, it will be crucial to develop methods that can efficiently separate bilayered vesicles and non-vesicular particles while preserving functionality and inherent heterogeneity. These methods might include advanced fractionation techniques[13,14] or affinity purification with antibodies that recognize specific surface markers[15]. Moreover, the application of single-vesicle characterization technologies to phenotype vesicles for

different subtypes[16] will be required to identify specific molecular markers of mineralization-related MVs. As "seeing is believing," the application of advanced imaging techniques will have an unprecedented impact in investigating the underlying processes in MV mineralization[17]. We demonstrated this by employing cryoTEM, which provided important insights by preserving the components in a near-native hydrated state. However, we could only obtain snapshots of the underlying processes and are still lacking information about the underlying heterogeneity in vesicle subtypes that might be present. Therefore, a combination of subtype-specific isolation strategies with cryoTEM imaging could be a next step. Moreover, dynamic information could also be obtained by employing other advanced microscopy techniques, such as liquid-phase electron microscopy, where mineralization events can be tracked in real-time, in a liquid medium, and under physiological-like conditions[18]. Imaging approaches should also evolve towards obtention of 3D resolution, the only way that the positioning between MVs and forming mineral can be precisely determined.

Finally, this thesis highlights the predominant role of phosphatase enzymes in the function of MVs. Chapter 2 revealed that phosphatase-dependent production of Pi is the primary pathway by which MVs trigger mineralization *in vitro*. Additionally, Chapter 4 demonstrated at the cellular level that MVs with reduced alkaline phosphatase activity are related to defective ECM mineralization. One of the most debated aspects of MV participation in bone mineralization is where the mineralization triggered by them fits in the achievement of a mature mineralized matrix. However, the literature neglects the observation that MVs are abundantly present in the mineralization front, which correlates perfectly with the crossfibrillar mineral tessellation pattern described in section 1.5. It is tempting to speculate that a major role of MVs is to transport and target a enzymatic cargo to be evenly dispersed in the preformed collagenous matrix. The phosphatase machinery of MVs then works in concert to locally produce Pi, leading to localized increases in supersaturation, which nucleates the first mineral nuclei, and crystal growth propagates through the continuous supply of Pi from the enzymatic degradation of organophosphate sources yielding the typical crossfibrillar pathern of collagen mineralization, guided by mineral-organic interactions within different ECM components (e.g., proteoglycans and NCPs). By controlling Pi availability enzymatically, biology can control chemistry, creating smoother energy landscapes by introducing inhibitors and catalysts along the crystallization pathway.

References

1. Derradi, R. *et al.* Cholesterol Regulates the Incorporation and Catalytic Activity of Tissue-Nonspecific Alkaline Phosphatase in DPPC Monolayers. *Langmuir* **35**, 15232–15241 (2019).

2. Pei, D. dan *et al.* Contribution of Mitophagy to Cell-Mediated Mineralization: Revisiting a 50-Year-Old Conundrum. *Adv. Sci.* **5**, 1800873–1800885 (2018).

3. Iwayama, T. *et al.* Osteoblastic lysosome plays a central role in mineralization. *Sci. Adv.* **10**, 1–10 (2019).

4. Chaudhary, S. C. *et al.* Phosphate induces formation of matrix vesicles during odontoblast-initiated mineralization in vitro. *Matrix Biol.* **52**–**54**, 284–300 (2016).

5. van Niel, G. *et al.* Challenges and directions in studying cell–cell communication by extracellular vesicles. *Nat. Rev. Mol. Cell Biol.* **23**, 369–382 (2022).

6. Lewin, S., Hunt, S. & Lambert, D. W. Extracellular vesicles and the extracellular matrix: A new paradigm or old news? *Biochem. Soc. Trans.* **48**, 2335–2345 (2020).

7. Rilla, K. *et al.* Extracellular vesicles are integral and functional components of the extracellular matrix. *Matrix Biol.* **75**–**76**, 201–219 (2019).

8. Shapiro, I. M., Landis, W. J. & Risbud, M. V. Matrix vesicles: Are they anchored exosomes? *Bone* **79**, 29–36 (2015).

9. Jeppesen, D. K., Zhang, Q., Franklin, J. L. & Coffey, R. J. Extracellular vesicles and nanoparticles : emerging complexities. *Trends Cell Biol.* **00**, 1–15 (2023).

10. Dixson, A. C., Dawson, T. R., Di Vizio, D. & Weaver, A. M. Context-specific regulation of extracellular vesicle biogenesis and cargo selection. *Nat. Rev. Mol. Cell Biol.* **00**, 1–23 (2023).

11. Nahar, N. N., Missana, L. R., Garimella, R., Tague, S. E. & Anderson, H. C. Matrix vesicles are carriers of bone morphogenetic proteins (BMPs), vascular endothelial growth factor (VEGF), and noncollagenous matrix proteins. *J. Bone*

Miner. Metab. **26**, 514–519 (2008).

12. Minamizaki, T. *et al.* The matrix vesicle cargo miR-125b accumulates in the bone matrix, inhibiting bone resorption in mice. *Commun. Biol.* **3**, 1–2 (2020).

13. Chen, Y. *et al.* Exosome detection via the ultrafast-isolation system: EXODUS. *Nat. Methods* **18**, 212–218 (2021).

14. Zhang, H. & Lyden, D. Asymmetric-flow field-flow fractionation technology for exomere and small extracellular vesicle separation and characterization. *Nat. Protoc.* **14**, 1027–1053 (2019).

15. Kugeratski, F. G. *et al.* Quantitative proteomics identifies the core proteome of exosomes with syntenin-1 as the highest abundant protein and a putative universal biomarker. *Nature Cell Biology* vol. **23**, 631–641 (2021).

16. Bordanaba-Florit, G., Royo, F., Kruglik, S. G. & Falcón-Pérez, J. M. Using single-vesicle technologies to unravel the heterogeneity of extracellular vesicles. *Nature Protocols* **16**, 3163–3185 (2021).

17. Verweij, F. J. *et al.* The power of imaging to understand extracellular vesicle biology in vivo. *Nat. Methods* **18**, 1013–1026 (2021).

18. Wu, H., Friedrich, H., Patterson, J. P., Sommerdijk, N. A. J. M. & de Jonge, N. Liquid-Phase Electron Microscopy for Soft Matter Science and Biology. *Adv. Mater.* **32**, 2001582–2001603 (2020).